

Copyright
by
Gauri Suresh Bhave
2014

The Dissertation Committee for Gauri Suresh Bhawe Certifies that this is the approved version of the following dissertation:

Micro-patterning Colloidal Quantum Dots Based Light Sources for Cellular Array Imaging

Committee:

John X.J. Zhang, Supervisor

Andrew Dunn, Co-Supervisor

Tim Yeh

Pengyu Ren

Haley Tucker

**Micro-patterning Colloidal Quantum Dots Based Light Sources for
Cellular Array Imaging**

by

Gauri Suresh Bhawe, B.E., M.S.

Dissertation

Presented to the Faculty of the Graduate School of
The University of Texas at Austin
in Partial Fulfillment
of the Requirements
for the Degree of

Doctor of Philosophy

The University of Texas at Austin

August 2014

Acknowledgements

This dissertation would not have been possible without the help and support of a long list of people. I would like to start by thanking Dr. John Zhang, my advisor, for his constant support and encouragement. His guidance at difficult times helped me power through the challenges of graduate school. I am grateful for his efforts to provide me a well-rounded experience with exposure to various projects in the lab.

I would also like to thank my committee members, Dr. Andrew Dunn, Dr. Tim Yeh, Dr. Pengyu Ren and Dr. Haley Tucker for helping point out to me the different directions which could be explored during this dissertation.

I would like to thank all my friends who worked with me in the BioMEMS lab. Special thanks to Youngkyu Lee for his help and encouragement throughout this project. He has been a great friend and mentor during the 4 years of my Ph.D. Thanks to Elaine Ng, Yu-Yen Huang and Peng Chen for making the lab a fun place to work. Thanks to Tushar Sharma for being an inspiration and a mentor in the lab and outside too.

Thanks to Dr. Khosrow Behbehani, my advisor at the University of Texas, Arlington. With his enthusiasm and his great effort to explain things clearly and simply, he helped make research fun for me. He has been a mentor and role model for me.

Finally I would like to thank my family for their encouragement throughout this challenging journey. Special thanks to Viraj Gore for his incredible patience and support through all the difficult patches during graduate school.

Gauri Bhawe,
August, 2014.

Micro-patterning Colloidal Quantum Dots Based Light Sources for Cellular Array Imaging

Gauri Suresh Bhawe, Ph.D.

The University of Texas at Austin, 2014

Supervisor: John X.J. Zhang

Co-Supervisor: Andrew Dunn

Lab-on-chip systems have been developed for various applications like point of care diagnostics and compact imaging systems. Compact, on-chip imaging systems face a challenge in the integration of multicolor light sources on-chip. This is because of the unavailability of compact, individually addressable, multicolor light sources on a single planar substrate. Colloidal Quantum Dot based Light Emitting Diodes (QDLEDs), which have found wide appeal, due to their unique properties like their tunable and narrow emission bandwidth and easy fabrication, are ideal for lab-on-chip integration. Among different types of QDLED structures implemented, inorganic QDLEDs have shown great promise. We have demonstrated designs and fabrication strategies for creating QDLEDs with enhanced performance. In particular:

(I) We introduce a sandwich structure with a spin coated inorganic hole transporting layer of nickel oxide underlying the QD layer and with a spin coated zinc oxide electron transporting layer, with patterning of anode and cathode on the substrate. Compared to the use of sputtered thin films, solution processed charge transporting layers (CTLs) improve robustness of the device, as crystalline ZnO shows low CB and VB

edge energy levels, efficiently suppressing hole leakage current resulting in LEDs with longer lifetimes. We also use Atomic Layer Deposition to deposit an additional hole injecting layer to protect the QDs from direct contact with the anode. With this device design, we demonstrate a working lifetime of more than 12 hours and a shelf-life of more than 240 days for the devices. Our solution based process is applicable to micro-contact printed and also spin-coated QD films. QDLEDs with spin-coated CTLs show a lifetime increase of more than three orders of magnitude compared to devices made using sputtered CTLs.

(II) We implement strategies of the enhancement of light extraction from the fabricated QDLEDs. We discuss the integration of a two dimensional grating structure based on a metal-dielectric-metal plasmonic waveguide with the metal electrode of a QDLED, with the aim of enhancing the light intensity by resonant suppression of transmitted light. The grating structure reflects the light coupled with the metal electrode in the QDLED and we found an increase of 34.72% in the electroluminescence intensity from the area of the pattern and an increase of 32.63% from photoluminescence of QDs deposited on a metal surface.

(III) We demonstrate the capability of our fabricated devices as a light source by measuring intensity across stained cells with QDLEDs of two different wavelengths and show the correlation as expected with the absorption profile of the fluorescent dye. We measure the absorption from the biological samples using QDLEDs fabricated with various design modifications, as a quantification of the improvements in device performance, directly affecting to our target application

Table of Contents

List of Tables	x
List of Figures	xi
CHAPTER 1: BACKGROUND AND SIGNIFICANCE	1
1.1 Motivation.....	1
1.1.1. Properties of Quantum Dots.....	4
1.1.2. Applications of QDLEDs.....	6
1.2 Critical Contributions.....	9
1.3 Dissertation Roadmap.....	9
CHAPTER 2: TYPES OF LIGHT EMITTING DIODES	11
2.1 Introduction.....	11
2.2 Review of Light Emitting Diodes	11
2.2.1 Inorganic Light Emitting Diodes	11
2.2.2 Organic Light Emitting Diodes.....	13
2.2.3 Quantum Dot Light Emitting Diodes.....	14
2.3 Colloidal Quantum Dot Based Light Emitting Diodes	16
2.3.1 Properties of Quantum Dots.....	16
2.3.2 Photoluminescence and Electroluminescence	20
2.4 Basic Quantum Dot LED Structure	21
2.4.1 Device Structure Design	21
2.4.2 Quantum Dot Patterning Methods	23
2.5 Summary.....	26
CHAPTER 3: QDLED BASIC DESIGN- FABRICATION AND CHARACTERIZATION	28
3.1 Introduction.....	28
3.2 Device Fabrication.....	29
3.2.1 Fabrication of Anode	30
3.2.2 Fabrication of Hole Transporting Layer	31
3.2.3 Quantum Dot Layer Deposition.....	32

3.2.4 Electron Transporting Layer Deposition	36
3.2.5 Cathode Deposition.....	37
3.3 Device Testing	38
3.3.1 Electroluminescence Testing	39
3.3.2 I-V Characteristics	43
3.3.3 Areas of Device Improvement	44
3.4 Summary	46
CHAPTER 4: QDLED MODIFIED DESIGN- FABRICATION AND CHARACTERIZATION	47
4.1 Introduction.....	47
4.2 Modified Device Design	47
4.2.1 Anode Patterning	48
4.2.2 Hole Transporting Layer.....	49
4.2.3 Quantum Dot Layer	51
4.2.4 Electron Transporting Layer	52
4.2.5 Cathode Patterning.....	53
4.2.6 Summary of Device Design Modifications.....	54
4.3 Modified Device –Testing	56
4.3.1 Electroluminescence Testing	56
4.3.2 Device Characterization.....	58
4.4 Device Comparisons	58
4.4.1 Comparisons of Device Intensity.....	59
4.4.2 Comparisons of I-V curves	62
4.4.3 Comparisons of Device Lifetimes	64
4.5 Summary	65
CHAPTER 5: STRATEGIES FOR ENHANCEMENT OF LIGHT EXTRACTION	66
5.1 Introduction.....	66
5.2 Surface Roughening.....	67
5.2.1 Theory	67
5.2.2 Experimental Results	68
5.3 Plasmonic Grating pattern.....	71

5.3.1 Design of Plasmonic Grating Pattern.....	72
5.3.2 Simulation Results	73
5.3.3 Fabrication	75
5.3.4 Photoluminescence Experiments	77
5.3.5 Wavelength Selectivity	79
5.4 Integration of Plasmonic Gratings with QDLEDs.....	82
5.4.1 Design Changes in QDLED.....	82
5.4.2 Fabrication of Integrated Device	83
5.4.3 Electroluminescence Experiments.....	84
5.5 Summary	87
CHAPTER 6: IMAGING OF BIOLOGICAL SAMPLES	88
6.1 Introduction.....	88
6.2 Imaging of Cancer Cells	88
6.2.1 Experimental Conditions	89
6.2.2 Imaging with Photoluminescence	92
6.2.3 Imaging with Electroluminescence.....	94
6.3 Comparisons of Imaging Results.....	97
6.4 Summary	102
CHAPTER 7: CONCLUSIONS AND FUTURE WORK	103
7.1 Conclusions.....	103
7.2 Future Work.....	106
References.....	107

List of Tables

Table 3.1: Bandgap energy of Quantum dot particles	39
Table 5.1: Increased intensity from grating structure for various individual emission wavelengths.....	81

List of Figures

Figure 1.1: Schematic of lab-on-chip systems (a) current lab-on-chip technology, (b) envisioned QDLED integrated system.....	2
Figure 2.1: Colloidal Quantum Dots made of CdSe/ZnS(core/shell) (a) shows size dependence of emission wavelength from QDs (b) Photoluminescence from QDs of different wavelengths (sizes) []	16
Figure 2.2: Absorption vs. fluorescence of quantum dots with different emission wavelengths [].....	17
Figure 2.3: Schematic showing structure of core: shell Quantum Dots []	18
Figure 2.4: Schematic showing differences in energy bandgap structure of core: shell Quantum Dots and bulk semiconductor material []	19
Figure 3.1: (a) Schematic of cross-section of control device and (b) Energy band diagram of control device	29
Figure 3.2: Schematic of patterned ITO anode structure (top view)	30
Figure 3.3: Schematic of patterned ITO anode structure with patterned NiO (top view)	32
Figure 3.4: Experimental setup for QD monolayer formation (a) Schematic of setup indicating the Teflon ring , the convex water surface pinned by the Teflon ring and the colloidal quantum dot suspension pipetted on the water surface. (b) Picture of actual setup with quantum dots excited by ultraviolet LED. Emission wavelength of QDs used is 580nm.	34
Figure 3.5: Micro-contact printing of quantum dot film (a) Schematic of micro-contact printing procedure (b) Picture of actual setup showing the PDMS stamp and the sample on which QD film is transferred.....	35

Figure 3.6: Photoluminescence image of patterned micro-contact printed QDs (EM 600nm) excited with a UVLED.	36
Figure 3.7: Schematic of patterned ITO anode structure with patterned NiO, QDs and ZnO:SnO ₂ (top view)	37
Figure 3.8: Schematic of patterned ITO anode structure with patterned NiO, QDs, ZnO:SnO ₂ and Ag(top view)	38
Figure 3.9: Electroluminescence of basic QDLEDs, (a) Electroluminescence from 580nm QDLED taken with 10X magnification and 60s exposure time (b) Electroluminescence from 600nm QDLED with taken with 10X magnification and 60s exposure time	41
Figure 3.10: Electroluminescence characteristics of QDLEDs. Spectra measured during electroluminescence of 580nm and 600nm QD LEDs (exposure time 300s). Inset shows electroluminescence image taken with microscope at 10X magnification (scale bar is 200μm) with exposure time 60s.....	42
Figure 3.11: I-V curves for 580nm and 600nm QDLEDs showing turn-on voltage	43
Figure 4.1: Comparison of NiO film uniformity. (a) Sputtered film (b) Spin coated and annealed film.....	50
Figure 4.2: Spin coating of quantum dots. (a) Schematic of procedure used for spin coating. (b) QD profile after spin coating measured using AFM.	52
Figure 4.3: Schematic of comparison between control device and modified device structure. (a)Schematic of control device structure, (b) Schematic of modified device structure, (c) Energy band diagram of modified device structure.....	55

Figure 4.4:	Electroluminescence of modified QDLEDs, (a) Electroluminescence from 580nm QDLED taken with 10X magnification and 60s exposure time (b) Electroluminescence from 600nm QDLED with taken with 10X magnification and 60s exposure time	57
Figure 4.5:	Comparison of emission spectra. (a) Maximum intensity from spectra for 600nm emission wavelength devices of control and modified design types. Inset shows the two LEDs used for obtaining spectra. (b) Maximum intensity from spectra for 580nm emission wavelength devices of control and modified design types. Inset shows the two LEDs used for obtaining spectra	60
Figure 4.6:	Comparisons of QDLED emission. (a) Emission profile across 600nm QDLEDs, (b) Emission profile across 580nm QDLEDs. All images at 10X magnification and 60s exposure time. Insets are images of particular QDLEDs used for measurement shown in the figure.....	61
Figure 4.6:	Comparisons of QDLED I-V curves. (a)I-V curves for QDLEDs fabricated using basic device design (b) I-V curves for QDLEDs fabricated using modified device design. Bars show turn-on voltage for the particular device.....	63
Figure 5.1:	Images showing excessive emissions from the edges of the electrode (a) Electroluminescence of 600nm QDLED at 60s exposure time (b) Electroluminescence of 580nm QDLED at 60s exposure time	67
Figure 5.2:	Schematic showing the difference between light from a flat surface Vs a roughened surface	68

Figure 5.3:	Electroluminescence from QDLED with roughened electrode (a) Brightfield image of QDLED electrode with roughened areas highlighted (b)Electroluminescence showing higher intensity from areas corresponding to the roughened electrode areas highlighted.....	69
Figure 5.4:	Intensity plots of electroluminescence from electrode surface roughening (a) Intensity plot from a specific area of electrode brightfield image (b) Intensity plot electroluminescence image	70
Figure 5.5:	Schematic of designed Plasmonic grating structure showing specific calculated design conditions	73
Figure 5.6:	Simulation results from Plasmonic grating structure. (a) Results from a QD source placed close to a plain metal surface. (b) Results from a QD source placed close to a MDM surface with Plasmonic grating pattern.	74
Figure 5.7:	SEM images of fabricated plasmonic grating structure at two magnifications (11.5kX and 86.4kX).....	76
Figure 5.8	Photoluminescence images of grating structure (a) 10X magnification 60s exposure (b) 20X magnification 60s exposure (c) 40X magnification 60s exposure.....	78
Figure 5.9:	Light transmission spectra from plasmonic grating structures	79
Figure 6.1:	Schematic of experimental setup for imaging of cells using QDLEDs.	89
Figure 6.2:	Brightfield image of cultured and stained MDA 231 cells []	90
Figure 6.3:	Absorption (top) and Transmission (bottom) characteristics of HEMA 3 dye [].	91
Figure 6.4:	Setup for photoluminescence imaging of stained cells.....	92

Figure 6.5: Excitation of same region using two sources (a) 580nm (b) 600nm	94
Figure 6.6: Imaging of cells with electroluminescence from modified QDLED structure (a) Images with RGB CCD (580nm top and 600nm bottom) (b) Images with monochromatic CCD (c) Intensity profile across the same cell with 580 and 600nm light sources.	96
Figure 6.7: Imaging of cells with electroluminescence from two QDLED structures (a) Images with RGB CCD (basic design top and modified device bottom) (b) Images with monochromatic CCD (c) Intensity profile across single cells imaged with basic and modified devices	98
Figure 6.8: Intensity profiles of a cell imaged with electroluminescence from QDLED with plasmonic structure (a) Cell imaged at 10X magnification and 300s exposure time (b) Cell imaged at 10X magnification and 300s exposure time. Insets show images with RGB CCD at specified magnifications	100
Figure 6.9: Electroluminescence Images of cells using QDLED with integrated plasmonic structure at 580nm, and 300s exposure time (a) 10X magnification, (b) 20X magnification	101

CHAPTER 1: BACKGROUND AND SIGNIFICANCE

1.1 MOTIVATION

Microfluidic lab-on-chip systems have gained great importance in the last few years. The advantageous properties of these systems such as their compactness, usefulness in point-of-care applications and low cost, among others, have brought research in lab-on-chip systems to the fore [1]. On-chip imaging systems have been recently brought forward but still face some major challenges. Great progress has been made in on-chip bright field imaging with both lensless systems and with image processing techniques [1, 2, 3, 4]. Although many disadvantages of current systems impede wide implementation, a major obstacle in the development of on-chip hyperspectral systems is the availability of miniature, narrow band light sources [5,6]. Current lab-on-chip systems still rely on the use of off-chip, bulky light sources for multicolor imaging, which obviates their advantages of point-of-care applicability, small size and low cost [7, 8, 9,10,11,12]. Figure 1.1 (a) shows current on-chip imaging technology.

For the designing of a multicolor lab-on-chip imaging system, the light source becomes an important consideration. To improve the performance of the system, some parameters that require consideration are, the bandwidth of the light source, distance between sample and light-source and intensity of light-source among others. Commercially available semiconductor Light Emitting Diodes (LEDs) have been previously used for imaging in miniature systems but present some problems. A major drawback of such LEDs is the unavailability in many wavelength bands since the wavelength depends on the energy band gap structure. This necessitates the use of filters

and other additional elements to obtain the required wavelength band for imaging, thus increasing the cost and bulk of the miniature system.

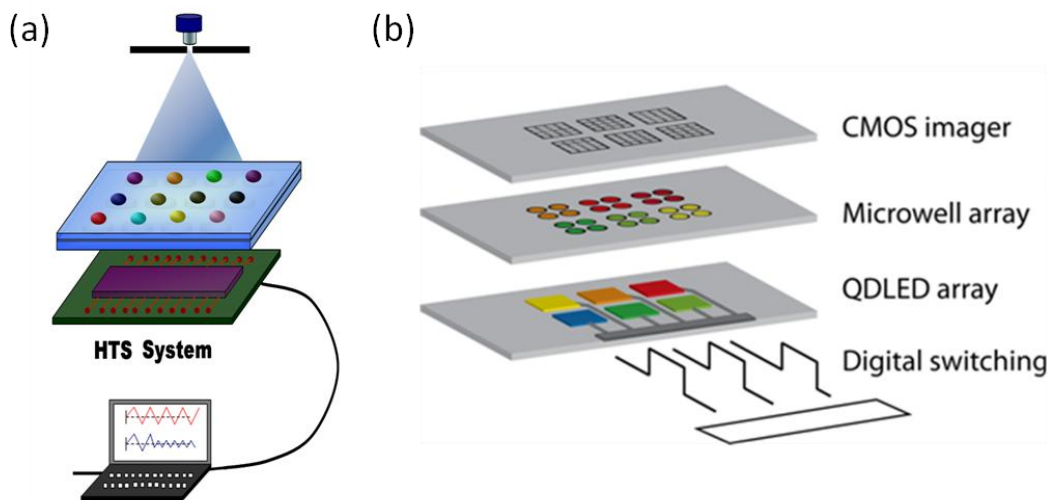


Figure 1.1: Schematic of lab-on-chip systems (a) current lab-on-chip technology, (b) envisioned QDLED integrated system

Colloidal quantum dots (QDs) have, in recent times, been used as lumophores in light emitting devices. Quantum Dot Light Emitting Devices (QDLEDs) have found wide appeal, especially in display applications. The properties of QDs like their tunable and narrow emission bandwidth and easy fabrication make them an attractive choice for flat-panel displays and lighting applications [13,14,15,16,17,18]. These unique properties of QDs can also be applied in imaging of biological samples.

The specific properties of quantum dots are especially suited for integration with applications of interest described previously. Figure 1.1 (b) shows a schematic of an on-chip multicolor imaging system with integrated QDLEDs as light source. The properties of QDs as spectrally pure, efficient emitters can be leveraged for various lighting applications. In size, QDs typically range between 3nm to 12 nm in diameter. Since the

electronic structure of QDs depends heavily on quantum size effects, the property of narrow-band emission, which can be useful for many applications, can be tuned by controlling the size of QDs during synthesis. This narrow bandwidth emission and high luminescence quantum yield make QDs suitable for LED applications [19, 20, 21].

Typically colloidal quantum dot based light emitting diodes have been made as a sandwich structure. Previously QDLEDs have been made using organic charge transport layers. Despite the high quantum efficiencies observed in the diodes, these organic based light emitting structures are susceptible to atmospheric conditions, moisture, thermal and electrochemical degradation [22, 23]. To overcome this drawback, the next generation of QDLEDs was built by sandwiching a layer of colloidal quantum dots between Indium Tin Oxide and metal electrodes. These types of LEDs showed limited electroluminescence. The low efficiency in these structures was due to quenching of QDs, plasmon modes in metal electrodes and imbalances in charge injection. To avoid these issues, intermediate inorganic electron and hole transporting layers were introduced. QDLEDs were made with NiO as the hole transporting layer (HTL), between the ITO anode and the QD layer. An amorphous ZnO layer was used as the electron transporting layer (ETL) between the metal cathode and the QD layer [24, 25, 26, 27, 28, 29, 30]. On application of voltage, excitons are formed near the quantum dot region whereby light emission is observed from the nanoparticles.

In our device, we have used colloidal QDs as light emitters in an inorganic light emitting device. We control the light emitting region of the device by patterning of the light emitting layer by (a) micro-contact printing or (b) patterning of electrodes. Using techniques compatible with standard silicon manufacturing processes, we are able to create multicolor light sources of controllable area on a single substrate. These

individually addressable sources can be excited in close proximity for imaging of biological samples.

The ease of fabrication and processing of colloidal quantum dots through microcontact printing and further integration with metal oxides, opens up the possibilities for creating nanophotonic microsystems with mass reproducibility and enables robust and tunable imaging, sensing and display applications. Here we describe the fabrication of QDLEDs with a basic structure for biological imaging applications. We investigate strategies for the improvement of performance of QDLEDs. We specifically focus on improvements in lifetime and intensity of device which are important for our target application. We also use our QDLEDs to image stained cancer cells to demonstrate the applicability of our QDLEDs in lab-on-chip nanophotonic systems for biological imaging.

1.1.1. Properties of Quantum Dots

Increasing efforts in the fabrication of QDLEDs have been seen for applications such as displays and commercial lighting. The advantages of using quantum dots in these applications lie in their properties of rendering improved color saturation to thin film displays and high color rendering index to white lighting. Since the electronic structure of QDs depends heavily on quantum size effects, the property of narrow-band emission, which can be useful for many applications, can be tuned by controlling the size of QDs during synthesis. QDs with emission in the visible wavelengths can be synthesized with materials such as CdS or ZnS.

Colloidal QDs usually have a passivating layer of ligands which make them solution processable. This property facilitates a large number of deposition techniques such as spin coating, microcontact printing and inkjet printing making fabrication of

LEDs easier. During synthesis, the QDs can be made compatible with either aqueous solutions or with organic solvents. Because of their inorganic semiconductor cores, QDs are more stable than organic dyes and highly resistant to photobleaching. They show a small Stokes shift which makes them an ideal choice for photoluminescence. Unlike organic dyes, they can be excited by a wide absorption band, including visible wavelengths. Due to these properties, QDs are widely applied in photoluminescence applications.

Photoluminescence of QDs can be used for certain types of applications such as staining of biological markers, where photoluminescence properties of QDs can solve issues such as requirement of high intensity emission and in cases where the size of the optical system required for imaging is not of particular importance. A UV source of excitation can be used for excitation of QDs and combinations of filters can be used to focus on emissions from a single color of QD emissions. However since all QDs are excited by UV wavelength, it is not possible to have individually addressable multicolor QDs on a single substrate without the use of emission filters. This type of design would take away from lab-on-chip systems, some of their key advantages of low cost, small size and easy handling.

Hence, some key applications benefit from the electrical excitation of colloidal QDs. For applications requiring creation of nanophotonic microsystems with mass reproducibility, creation of micron scale light sources with pure color emissions and for high throughput applications, it is important to fabricate structures to facilitate electrical excitation of colloidal QDs. The individual addressability of these devices eliminates the need for filters and electrical excitation eliminates the use of excitation light source and filters. The current QDLEDs however, face many challenges like QD charging, QD

luminescence quenching in thin films, plasmon modes in metal electrodes and degradation of QDs due to exposure to environmental factors.

Considering these factors, design of QDLEDs with a long working life and high emission intensity at low voltage and current levels becomes important. Robust structures and long lifetimes are important for point-of care applications where easy handling and reusability are important considerations. High intensity of QDLEDs improves the signal-to-noise ratio, improving the efficacy of the system. These are some of the important issues that need to be considered during the design and fabrication of a QDLED.

1.1.2. Applications of QDLEDs

Site-controlled patterning of light emitting diodes has importance in a number of applications such as MEMS and multicolor excitation sources in micro-total analysis systems (μ -TAS). Combination of filter cubes or laser sources are typically used for standard fluorescence microscopes, which are not suitable for easy-to-use on-site reduced cost diagnostic tools. We have developed QD-LEDs that are planar and easy to integrate to on-chip systems compared to commercial systems. The light emitting area in these diodes can be defined by a combination of (a) micro-contact printing and (b) patterning the cathode of the device. Multicolor LEDs on a single substrate offer a unique capability to excite cells with individual excitation sources in a single substrate for on-chip multicolor imaging.

Integration of LEDs for biomedical applications has been demonstrated previously by incorporating Organic LEDs [31, 32, 33, 34, 35, 36]. Integrated OLEDs are placed on the rear side of the glass substrate and a microfluidic channel made out of polydimethylsiloxane (PDMS) on the front side. The emission wavelength of the OLED

is 520 nm and has a relatively wide peak of 70 nm. Visual inspection of excitation of fluorescent dye Rhodamine B was demonstrated [37].

One application in which QDLEDs can be used is continuous monitoring of cultured cells. During the testing of effects of various drugs on cultured cells, standard 96-well plates are used. In such situations continuous monitoring of cells is useful. In such situations it is useful to have individually addressable, multicolor light sources for each well. Figure 1.3 shows the schematic for a lab-on-chip system for the imaging of cells in a microwell array system [38].

Multispectral imaging of cells has shown great promise. Recent studies have shown that separate data can be obtained using light sources of different wavelengths and the specific spectral signature obtained from biological samples can be used for identification of for various biomarkers[39]. As discussed earlier, the full width half maximum of the emission wavelength of QDLEDs is narrow on the order of 15-20 nm. This gives good control on the emission wavelength and light purity for spectroscopic measurement in the visible wavelength region. These diodes have a capability of multicolor excitation on as single chip. Each individual excitation can be easily controlled due to the patterning capability of the top electrode, thus making the integration of QDLEDs ideal for on-chip spectroscopic imaging.

This dissertation presents three specific aims towards the achievement of the goals described above. In the first aim, we focused on design of QDLEDs. The goals to be achieved were to design robust QDLEDs with a long lifetime which was the basic requirement from the light source to be integrated in lab-on-chip systems. The other requirements to be achieved were the capability of fabricating multicolor QDLEDs on single substrate with a controlled area of emission. We demonstrated fabrication of QDLEDs with a marked improvement in operational and storage lifetimes as compared to

currently available QDLEDs. This was achieved by using combinations of materials and fabrication techniques to optimize the charge carrier concentration to achieve highest efficiency from QDs and also to protect the QDs from environmental factors which play an important role in reducing the lifetime of QDLEDs. We also demonstrated the control of the area of emission by exploring both, different ways of QD deposition and control of electrode deposition to define the active area of emission.

Second, we demonstrated increased intensity of QDLEDs by employing strategies for enhancement of light extraction LEDs. We employed two specific strategies, namely surface roughening of electrodes and integration of plasmonic patterns with the metal cathode of the QDLED to cause reflection of Plasmon modes transmitted along the metal cathode. We showed an increase in intensity corresponding to the patterned surface in both photoluminescence and electroluminescence from QDLEDs. We quantified the increase in intensity obtained across various wavelengths of QDs, thus demonstrating the wavelength selectivity of the designed plasmonic pattern.

Third, we demonstrated the applicability of our QDLEDs by imaging stained cancer cells. We imaged cells using the different stages of the device and used the imaging capability to quantify the improvements in the design of our device. Since the final application of our QDLEDs is expected to be as a light source in imaging applications, we used our devices to obtain preliminary data of imaging stained cells and identified parameters which could be quantified for performance comparisons at each stage of design and fabrication modifications in our QDLEDs.

1.2 CRITICAL CONTRIBUTIONS

This dissertation presents three specific critical contributions to field of fabrication of QDLEDs as light sources for biological imaging. First, we developed a design for fabrication of QDLEDs on glass substrate with long life spans, without special storage or encapsulation conditions. The improvement in working and shelf life of the device was achieved simply through changes in the materials used and fabrication methods applied. We developed a fabrication method that was silicon compatible and easy to fabricate. The methodology was also kept compatible with both microcontact printing and spin coating of QDs to offer flexibility in the fabrication of multicolor or single color QDLEDs on one substrate.

The second contribution was in the improvement of light extraction from the QDLEDs. We showed the integration of a plasmonic grating pattern with the fabricated QDLED and demonstrated a marked increase in the intensity of light obtained from the device. The plasmonic grating pattern is designed to reflect Plasmon waves travelling along the metal electrode of the LED, resulting in increase in the extracted light intensity. We also demonstrated the wavelength specific nature of the plasmonic grating structure. Thus we can design the structure for the specific wavelength of interest.

Third, we demonstrated the used of our fabricated multicolor LEDs for imaging of biological samples. We showed the usefulness of multicolor, individually addressable light sources on a single substrate. Our QDLEDs can be integrated with lab-on-chip systems for spectroscopic measurements.

1.3 DISSERTATION ROADMAP

The motivations for the dissertation and current challenges in on-chip imaging are introduced in Chapter 1. To achieve the goal of integrating multicolor light sources for

on-chip imaging, in Chapter 2 is presented, a review of commercially available LEDs and colloidal quantum dot based light emitting diodes technologies currently under research. Comparisons of the advantages and disadvantages of various light sources and the rationale of the chosen approach are subsequently presented. Based on the requirements of the target application, the design, fabrication and characterization of the basic QDLED structure are presented in Chapter 3. This is the initial device design. Changes made in the design of the device structure including materials used and fabrication methods applied to overcome drawbacks found upon testing the basic device are described in Chapter 4. Quantitative comparisons of emission and storage lifetimes and intensities between the modified and basic design are presented. Chapter 5 focuses on the improvement in intensity of the modified design. Strategies for enhancement of light extraction from the QDLEDs are introduced. The design of the plasmonic pattern based on analytical and simulation results and its integration with our QDLED structure is presented. Comparisons of light intensity obtained from QDLEDs with and without integration of surface roughening and patterning strategies are also discussed. Following the discussion on improvements in QDLED performance based on device lifetimes and intensities, the application of QDLEDs as multispectral light sources for imaging of biological samples is presented in Chapter 6. Finally, Chapter 7 summarizes the dissertation and presents future research directions.

CHAPTER 2: TYPES OF LIGHT EMITTING DIODES

2.1 INTRODUCTION

Light emitting diodes (LEDs) emit light when activated by the recombination of electrons and holes within a basic pn-junction diode [40]. LEDs can be classified into two categories: (a) inorganic based light emitting diodes and (b) organic based light emitting diodes. LEDs have vast applications in full color displays for televisions, cell phones, flashlights, etc. [40]. LEDs have many advantages over incandescent light sources like higher efficiency, lower power consumption, longer lifetimes and smaller size.

We first review the commercially available LEDs which are of two types, inorganic LEDs and organic LEDs. We then introduce colloidal quantum dot based LEDs which can also be classified based on the use of organic and inorganic materials. Through these discussions, we describe the choices of materials and films used in the design of our QDLEDs.

2.2 REVIEW OF LIGHT EMITTING DIODES

2.2.1 Inorganic Light Emitting Diodes

Inorganic LEDs are made from crystalline semiconductor materials. The semiconducting material is doped with impurities to create a p-n junction. Upon application of a voltage, current flows from the anode to the cathode. Electrons and holes flow into the junction and when they combine, the electron falls to a lower energy level

and releases the excess energy in the form of a photon. This is the radiative nature of electron-hole combination.

The wavelength of the light emitted in this case, depends on the energy band gap of the materials forming the p-n junction, since this defines the amount of energy released in the form of a photon. Some materials, like silicon and germanium, are indirect band-gap materials. In such materials non-radiative recombinations are dominant. Radiative recombination lifetimes are on the order of milliseconds. This leads to very low efficiencies, especially at room temperature. All these factors limit the pure wavelengths of light that can be obtained from inorganic LEDs. Materials used to fabricate LEDs have a direct band gap with energies corresponding to near-infrared, visible or near-ultraviolet wavelengths.

Compound semiconductor materials like gallium arsenide, gallium phosphide and indium phosphide are used to make the p-n junction. These compound semiconductors are classified according to the valence bands occupied. III-V semiconductor materials are generally used to make LEDs. The wavelength of light obtained from the LEDs is designed by selecting specific materials. Pure gallium arsenide emits in the infra red region. Other materials commonly used are aluminum gallium arsenide (AlGaAs) for visible red region, gallium phosphide for green region and aluminum indium gallium phosphide for the yellow and orange region.

Silicon is an indirect band gap material. The radiative band-to-band transitions are rare. These materials have radiative recombination lifetime on the order of milliseconds. As a consequence, nonradiative recombination at the defects is dominant. This leads to very low efficiencies, especially at room temperature. A number of different methods have been used to investigate emission from silicon namely, bulk silicon light emitting

diodes, rare earth doped nanocrystalline silicon, SOI based LEDs and porous silicon based LEDs [41].

The advantages of inorganic LEDs are high efficiency, low turn-on voltage, high emission intensity and long lifetimes. There are however some inherent drawbacks due to the nature of operation of inorganic LEDs. LEDs of different emission wavelengths cannot be easily made. Certain wavelengths are produced using either combinations of LEDs emitting primary colors or by the use of a phosphor material in combination with a blue or UVLED to achieve desired wavelength. Using this method, it is not possible to achieve saturated, pure, single wavelengths emissions in all regions of the visible spectrum. The average Full Width Half Maximum (FWHM) for a commercially available inorganic LED is 70~90nm. Another issue faced by these types of systems is that differences exist in the FWHM and efficiency based on the emission wavelength.

2.2.2 Organic Light Emitting Diodes

LEDs in which the emissive layer is composed of an organic compound are called Organic Light Emitting Diodes (OLEDs). The basic structure of OLEDs consists of a layer of certain types of organic materials between two electrodes. The organic materials used are electrically conductive with conductivities ranging from highly conductive to highly resistive. These materials are considered to be organic semiconductors. Different strategies are applied to fabricate OLEDs.

The most basic structure of polymer OLED consists of a layer of organic material between two electrodes. Other strategies consist of designs with two or more polymer layers to improve the efficiency of the device. Materials and layers are chosen to improve charge injection from electrodes or to block the charge from reaching the

opposite electrode. Since silicon has an indirect band-gap nature, it is difficult to get good light emission from silicon. To overcome this drawback, organic LEDs have been combined with silicon substrate [42].

OLEDs are cheaper to produce as compared to traditional inorganic LEDs. OLEDs have found wide applications in cell phones, television displays, digital cameras, etc. [43]. OLEDs have the advantage of good color, brightness, contrast, power efficiency and fast response time. They do not require backlight since each pixel can be controlled individually. This makes it possible to have thinner and more compact OLEDs. OLEDs however face some problems such as instability and lower carrier mobility.

One of the biggest technical issues faced by OLEDs is that of limited lifespan. The lifespan of such devices is limited by the rate of degradation of organic materials. Nonradiative recombination centers and luminescence quenchers accumulate, over time in the emissive layer of the OLED. This results in degradation of the emissive layer. Besides this type of electrochemical degradation, the organic emitters are also susceptible to environmental factors like moisture and thermal conditions.

Due to these drawbacks, organic emitters are gradually being replaced with semiconductor nanocrystals. Nanocrystal emitters have the advantages of well defined and tunable quality of emission along with different emission colors, electron affinities and ionization potentials.

2.2.3 Quantum Dot Light Emitting Diodes

The structure of Quantum Dot Light Emitting Diodes (QDLEDs) is very similar to the structure of OLEDs. The emissive organic layer in the OLED structure is replaced by a layer of QDs. Initial QDLEDs consisted of a basic structure of QDs between the two

electrodes. Improvement in the efficiency of QDLEDs has been achieved over time by the addition of Electron and Hole Transporting Layers (ETL and HTL) between which the QD layer is sandwiched. When an electric field is applied to this structure, electrons and holes move into the quantum dot layer and recombine, resulting in emission of photons.

Compared to traditional inorganic LEDs and OLEDs, QDLEDs display some inherent advantages like better saturation of colors, smaller Full Width Half Maximum (FWHM) value of about 20~30nm. QDLEDs can be fabricated into compact systems. Due to the capability of QDLEDs of working without backlight, they have the possibility of fabricating flexible devices and fabricating multicolor QDLEDs on a single substrate. However QDLEDs face some disadvantages such as low efficiency and lifetime.

QDLEDs are of two basic types a) QDLEDs with organic materials for charge transport layers and b) QDLEDs with inorganic materials for charge transport layers. For the first type in which organic charge transport layers are used, QDLEDs show relatively higher efficiency and have a simpler device design and fabrication. However they face problems like lower maximum current density and device instabilities. To overcome these disadvantages, QDLEDs with inorganic charge transport layers were designed. These devices show better stability but there is a loss of efficiency due to QD damage during deposition of overlying inorganic layers.

2.3 COLLOIDAL QUANTUM DOT BASED LIGHT EMITTING DIODES

2.3.1 Properties of Quantum Dots

Quantum dots are semiconductor materials whose excitons are confined in all three dimensions [44]. They have properties that are in between bulk semiconductors and discrete molecules. The emission wavelength of the particle is controlled by the size of the nanoparticles of the same material (Figure 2.1). Quantum dots have been synthesized to emit light at wavelengths ranging from ultraviolet to infrared. These particles have typical photoluminescence with a full width half maximum (FWHM) of 30 nm or less (Figure 2.2). This narrow spectral distribution indicates the color purity of the emitted light.

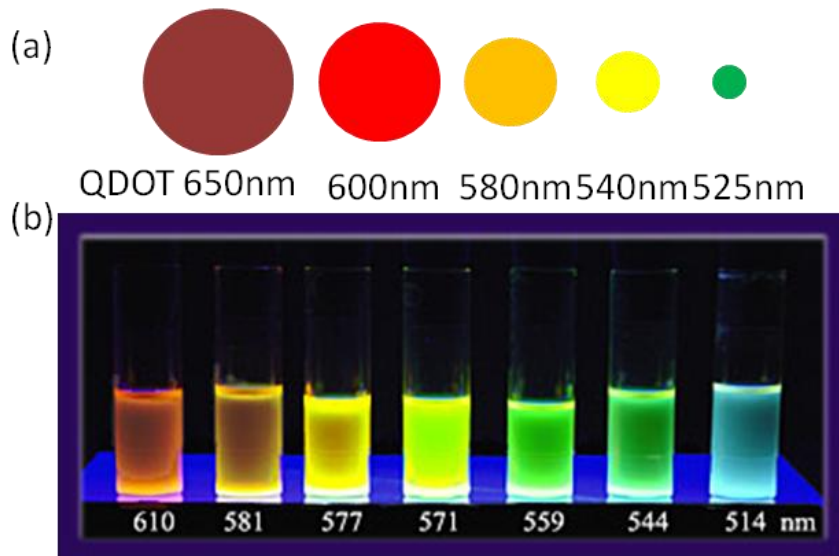


Figure 2.1: Colloidal Quantum Dots made of CdSe/ZnS(core/shell) (a) shows size dependence of emission wavelength from QDs (b) Photoluminescence from QDs of different wavelengths (sizes) [45]

Quantum Dots are currently fabricated using two techniques. These two types of QDs are: (a) Epitaxial and (b) Colloidal. Epitaxial quantum dots are formed by depositing a semiconducting material on a substrate by using Molecular Beam Epitaxy (MBE). The strain causes the top material to buckle and form quantum dots by the Stranski Krastanow growth method [46]. Synthesis of colloidal quantum dots involves the injection of precursors into the organic solvents at high temperatures [47]. The temperature activates nucleation of small crystallites that continue to grow from the unreacted precursors until stopped by cooling. The size of the QDs fabricated using this method can thus be finely controlled, by controlling the process time during synthesis. This process results in monodisperse solution. Colloidal quantum dots are preferred over epitaxial quantum dots, due to their low cost, ease of fabrication and integration.

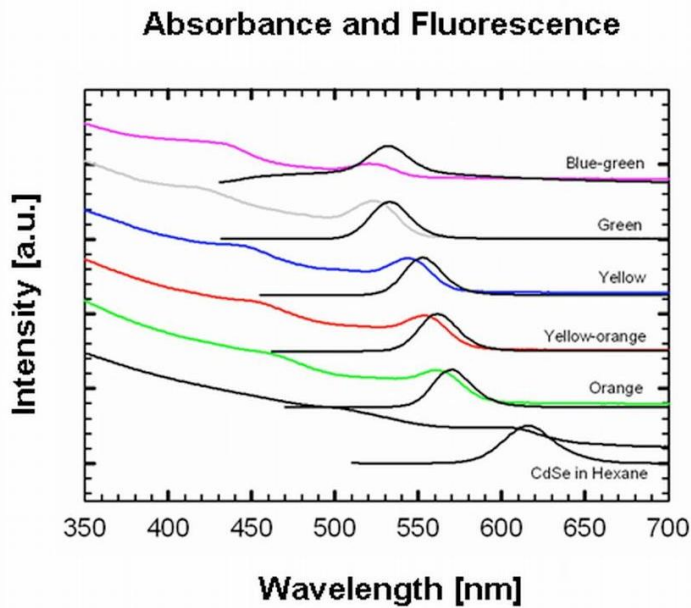


Figure 2.2: Absorbance vs. fluorescence of quantum dots with different emission wavelengths [45]

In our experiments, we use the core-shell type of colloidal quantum dots with an organic capping layer. Core and shell structures are typically composed of type II-VI, IV-VI and III-V semiconductors. We will focus our discussion more on the Cadmium selenide (CdSe): Zinc Sulfide (ZnS) core: shell quantum dots that we use in this thesis. Organic capping is typically provided to prevent the aggregation or precipitation of quantum dots (Figure 2.3). Organic compounds such as thiols, trioctylphosphine oxide oleic acids have been used to create organic capping.

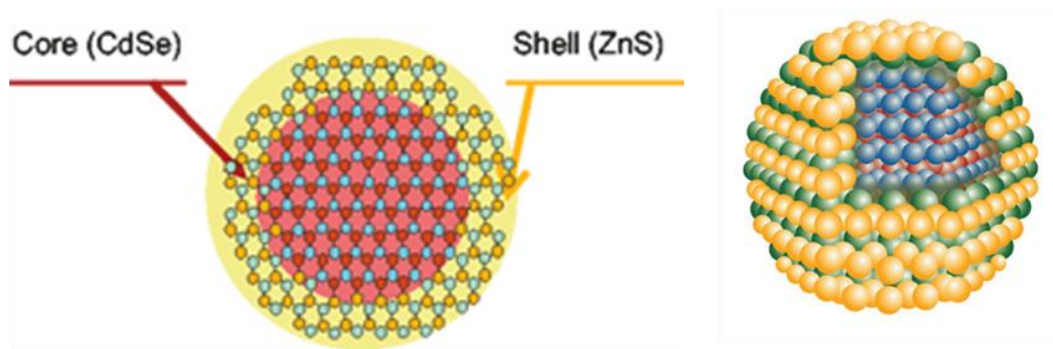


Figure 2.3: Schematic showing structure of core: shell Quantum Dots [45]

Core-shell QDs are divided into three types based on the relative conduction and valence band edge alignment of the core and shell. The types are: (a) Type I, (b) Reverse Type I and (c) Type II. In Type I, the bandgap of the core is smaller than that of the shell. Due to this, the conduction and valence band edges of the core lie within the bandgap of the shell, confining the electrons and holes in the core. In the Reverse Type I configuration, the bandgap of the core is wider than the shell and the valence and conduction band edges of the shell lie within the band edges of the core. In the Type II configuration, the valence and conduction band edges of the core are both either lower or higher than the band edges of the shell.

Quantum Dots have properties between those of bulk semiconductors and single molecules. When the size of a semiconductor crystal becomes small enough that it approaches the size of the Exciton Bohr Radius, then the electron energy levels can no longer be treated as continuous. The energy levels must be treated as discrete, such that a small and finite separation between energy levels is present. This situation of discrete energy levels is called quantum confinement, and under these conditions, the semiconductor material ceases to resemble bulk, and instead can be called a quantum dot (Figure 2.4).

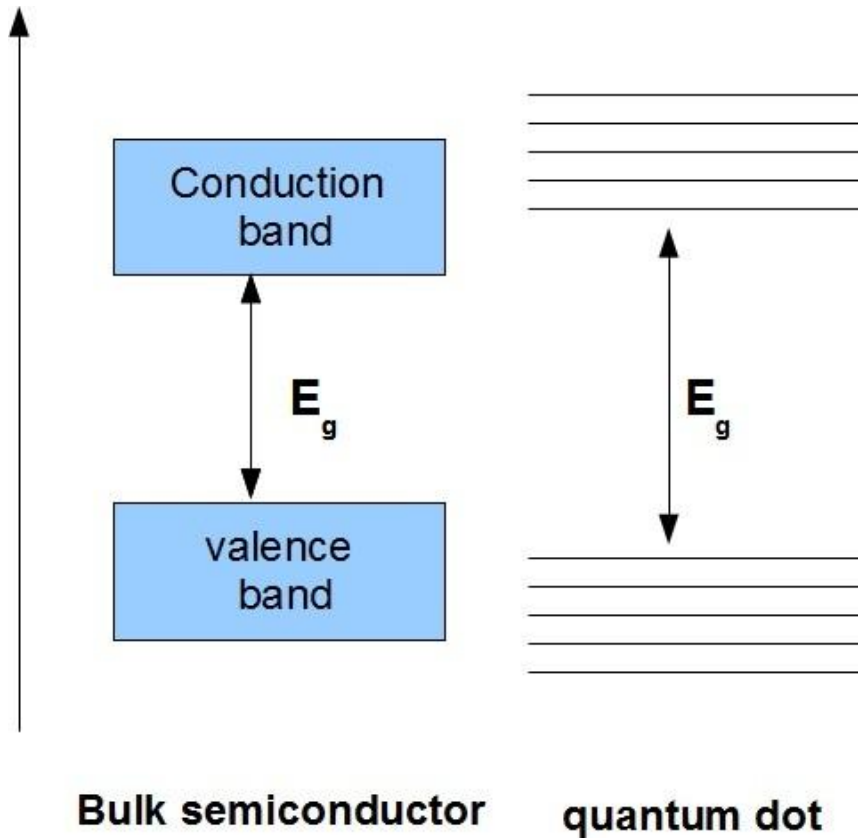


Figure 2.4: Schematic showing differences in energy bandgap structure of core: shell Quantum Dots and bulk semiconductor material [45]

Quantum Dots can be excited in two ways to achieve fluorescence from them, namely (a) Photoluminescence and (b) Electroluminescence. In photoluminescence, QDs are excited by light of a lower wavelength and red shifted emission of the emission wavelength corresponding to the quantum dot size is obtained. In electroluminescence, electric field is applied to a layer of quantum dots to obtain emission of photons.

2.3.2 Photoluminescence and Electroluminescence

Photoluminescence occurs in quantum dots when a light of lower wavelength, thus higher energy excites a quantum dot. The diameter of quantum dots is smaller than the size of its exciton Bohr radius which leads to quantum confinement. Fluorescence occurs when an excited electron relaxes to ground state, combining with a hole. In photoluminescence the initial energy required to move the electron to a higher energy state is provided by a photon of higher energy striking on the quantum dot. The red shifted emission wavelength thus depends on the band gap energy, the confinement energies of the electron-hole pair and bound energy of the exciton. The emission energy thus depends on the size of the quantum dot.

In electroluminescence, the excitement energy for moving an electron to a higher energy level is provided by the recombination of electrons and holes, in the vicinity of the quantum dot, due to the application of an electric field.

2.4 BASIC QUANTUM DOT LED STRUCTURE

2.4.1 Device Structure Design

As described in an earlier section, the structure of QDLEDs is similar to the basic structure of OLEDs. The organic layer in OLEDs is replaced with a layer of QDs. When an electric field is applied across the device, the electrons and holes move to the QD layer, which is sandwiched between the anode and cathode, and is captured in the QD, where they recombine to emit a photon. To improve the efficiency of the QDLED and to address the challenge of bringing together the electrons and holes in a small region of the QD layer, Hole Transporting and Electron Transporting Layers (HTL and ETL) were added to the structure. ETL and HTL effectively bring together the electrons and holes in the small region of the QD layer and suppress the dissipation and escape of photons. A single layer of QDs is used as the emissive layer, to allow electrons and holes to be directly transferred from the surfaces of the ETL and HTL, to provide high recombination efficiency.

The choice of materials for the ETL and HTL depends upon a number of conditions, including the application and desired qualities of the QDLED. Organic, inorganic or a combination of the two materials can be used. Depending on the use of organic or inorganic materials, injection and transport of either holes or electrons is favored. This results in electron-hole combination, either closer to the cathode or to the anode, which can lead to the quenching of produced excitons. To prevent this, a number of strategies are used. In some cases where organic materials, which favor hole transport are used, an extra hole-blocking layer is introduced. Other strategies include the optimization of HTL and ETL through changing of thin-film thickness and fabrication techniques to balance the charge carrier and transport capacities of the two layers.

The choice of HTL and ETL materials significantly affects the other layers of the QDLED structure. When organic materials are used to form the ETL and HTL, the fabrication of these layers is usually done by spin coating of the Charge Transport Layers (CTLs). This imposes certain constraints on the materials that can be chosen and also the fabrication methods used to deposit the underlying and overlying layers. Some solvents can affect the underlying electrode during deposition and if baking is required, this can affect the resistance of the underlying layer. The deposition of QDs also faces some constraints when the CTLs are organic layers since organic solvents have to be deposited before and after the deposition of the QDs which can disturb the QD layer.

When inorganic materials are chosen to be used as the CTLs, the properties of inorganic thin films can affect the performance of the QDLED structure. Different approaches to thin film deposition have to be explored to avoid pin-holes and other defects in CTLs to protect QDs from environmental contact and also from direct contact with the electrodes. During deposition of the layer over the QDs, some metal oxide deposition techniques requiring high temperature cannot be used, to avoid degradation of the QD layer. The charge transport capabilities of the ETL and HTL have to be finely tuned to enable the recombination of holes and electrons in the QD layer as recombination in other layers reduces efficiency. Other factors which affect the choice of CTL materials and fabrication methods are the ease of handling and fabrication compatibility, optical and electronic properties of thin films and physical properties such as uniformity of film obtained, control over thickness etc.

The choice of the cathode and anode used depends on various desired properties. Usually Indium Tin Oxide (ITO) is used as an anode material for fabrication of a QDLED on a glass substrate. This is because of the hole injection capabilities of ITO in addition to ITO being optically transparent in the visible wavelength range, allowing the

passage of the QD emission through the anode and glass substrate. In some other designs, doped silicon is used as an anode and in this case the cathode is kept transparent to obtain the light emissions. A metal like Aluminum or Silver is usually used to form the cathode due to its electron injecting capacity. The choice of metal is made depending on the desired fabrication method compatible with the underlying layer, desired lifetime and thickness.

Quantum dots are chosen based on the desired wavelength, emission intensity and deposition method to be used, which also depends on the other materials used in the structure design. A number of methods have been studied and developed for the deposition of QDs onto different substrates.

2.4.2 Quantum Dot Patterning Methods

Deposition of Quantum Dots to create LEDs forms a defining step in QDLED device design and performance. Several approaches have been explored which have certain advantages depending on the desired application of the QDLED. Some factors however are common across the different deposition strategies. For high QDLED efficiency, it is desirable to deposit a monolayer or bilayer of QDs across the QDLED surface. High uniformity without defects is desired.

Some standard methods of QD deposition, which have been implemented to create quantum dot thin films are, phase separation, spin coating, Langmuir Blodgett method and microcontact printing.

(a) Phase Separation

Phase separation is usually used as a method of quantum dot deposition in cases where organic materials are used as charge transporting layers. In this method, the organic layer and QDs are spin coated at the same time. During the spin coating process, the QDs separate from the small molecules and form a monolayer on top of the organic top surface. Devices fabricated using this method have shown an efficiency of 2% [48]. This method however places some constraints on the organic material that can be used, since the organic material is required to be compatible with quantum dots. Another constraint of this method is that the quantum dots cannot be patterned on the substrate while depositing.

(b) Spin Coating

Spin coating of quantum dots in chloroform solution can be used in the cases of inorganic charge transport layers and has also been shown to work on a hydrophobic thermally cross-linked hole transport layer [49]. The devices showed an efficiency of 1.6% in this method. One condition while using this method of quantum dot deposition is that the charge transport layer underlying the quantum dot layer must remain unaffected by chloroform which is used as a solvent. Patterning of multicolor quantum dots on a single substrate cannot be done using this method.

(c) Langmuir Blodgett Method

In this method, Metal organo-chemical vapor deposition was combined with colloidal quantum dots. A Langmuir Blodgett film of quantum dots was sandwiched between a p-type MOCVD GaN layer grown on sapphire and n-type GaN layer grown using epitaxy as demonstrated by Achermann, et. al. [50].

(d) Micro-contact Printing

In this method patterning is done using conformal contact of inked PDMS on flat substrates. In the case of QDLED fabrication, micro-contact printing can be used for deposition of quantum dots. This method allows for patterning of quantum dots on non-planar surfaces and this is its main advantage over methods like photolithography, inkjet printing, nano-imprinting and soft lithography.

Although micro-contact printing techniques have been widely applied towards deposition of various particles, this method is of particular interest in our application due to some of its inherent advantages. In this technique, a polydimethylsiloxane (PDMS) stamp is used to transfer films of quantum dots onto the substrate. This methodology enables contact of the stamp over controllable areas of the substrate, making it possible to pattern films in nanometer, micrometer and even millimeter ranges, providing great flexibility in device size. This method has the advantages of low cost, high resolution and large area of operation [51, 52, 53].

Use of PDMS stamps has some drawbacks. Non-polar solvents cannot be used in combination with PDMS since they cause swelling of the PDMS stamp, resulting in a change in shape and size of the stamp. This property of PDMS does not allow for the direct use of colloidal quantum dots in chloroform or toluene in combination with the PDMS stamps. Alternate methods like modifying the PDMS surface by coating Parylene-

C using Chemical Vapor Deposition (CVD) or inkjet printing of quantum dots onto the PDMS surface have been tried to avoid or minimize the contact between PDMS and solvent. These methods are complicated and result in wastage of a significant amount of material [54, 55, 56].

We use a method previously developed in our lab, where colloidal quantum dots re-suspended in hexane and 1,2-dichloroethane, are used in a Langmuir Schaffer technique to create thin films. The thin films of quantum dots are then picked up by PDMS stamps and are micro-contact printed on to the hard substrate [20, 21].

2.5 SUMMARY

In this chapter we discussed the various types of light emitting devices, including traditional inorganic LEDs, organic LEDs and quantum dot based LEDs. Traditional LEDs have the advantages of low cost, high intensity and long lifetime, however they lack the capability of single wavelength emission and are not available at all wavelengths in the visible range. This is because in these types of LEDs, the material defines the emission wavelength. This drawback makes them unsuitable for our desired application.

In the case of organic LEDs, they have some advantages over traditional LEDs like compact size and possibility of flexible devices however they face drawbacks like relatively short lifetime, large emission bandwidth and degradation over time. Due to these, we opt for colloidal quantum dot LEDs for our application. QDLEDs can be fabricated at very compact sizes and emission wavelengths with narrow bandwidth can be achieved over the entire visible spectrum.

We also discussed strategies for device design, including materials and conditions for each layer in the sandwich structure of the QDLED including an overview of various

techniques that can be used for quantum dot deposition. The next chapter will discuss our specific device design and fabrication.

CHAPTER 3: QDLED BASIC DESIGN- FABRICATION AND CHARACTERIZATION

3.1 INTRODUCTION

In this chapter, we introduce the design and fabrication of a colloidal quantum dot based light emitting device (QDLED) structure with inorganic charge transport layers (CTLs). Such a device was first introduced in 2006 by Caruge, Halpert and Bulovic [57]. The QDLED structure is based on a glass substrate with a combination of NiO as HTL and ZnO:SnO₂ as the ETL. An ITO anode and silver cathode constituted the device structure. Bilayers of colloidal quantum dots were deposited using spin coating techniques to form the emissive layer of the device. These devices overcome some major drawbacks faced by devices with organic CTLs like limited lifetime and deposition of QDs by phase separation.

We modified the structure described, to be compatible to our application by introducing the deposition of quantum dots using micro-contact printing techniques and by patterning of electrodes thus allowing for the fabrication of multicolored QDLEDs on a single substrate with a finely defined area of electroluminescence. Having the capability of fabricating multicolor QDLEDs on a single substrate along with a defined area of electroluminescence is critical for our application and this contributes to making use of inorganic CTLs important for our device.

We use this structure as the basis of our experiments and will refer to it as the control device in this thesis. In this chapter we discuss the design and fabrication of this control device. We will also discuss the testing of the device and the analysis of improvements required in the device to make it compatible to our application.

3.2 DEVICE FABRICATION

A sandwich structure was fabricated with a layer of colloidal quantum dots sandwiched between inorganic charge transporting layers. The QDLED is fabricated on a glass substrate and Indium Tin Oxide (ITO) is used as an anode. Nickel Oxide is used as the hole transporting layer and is deposited on top of the ITO anode. On top of this, the quantum dot layer is deposited using two different techniques of micro-contact printing and spin coating. On top of the quantum dot layer, a thin film of zinc oxide: tin oxide is deposited which acts as the electron transporting layer. Silver is used as the top electrode (cathode). Figure 3.1 (a) shows the schematic of the cross-section of the device and (b) shows the energy band diagram which dictates the flow of electrons and holes through the device.

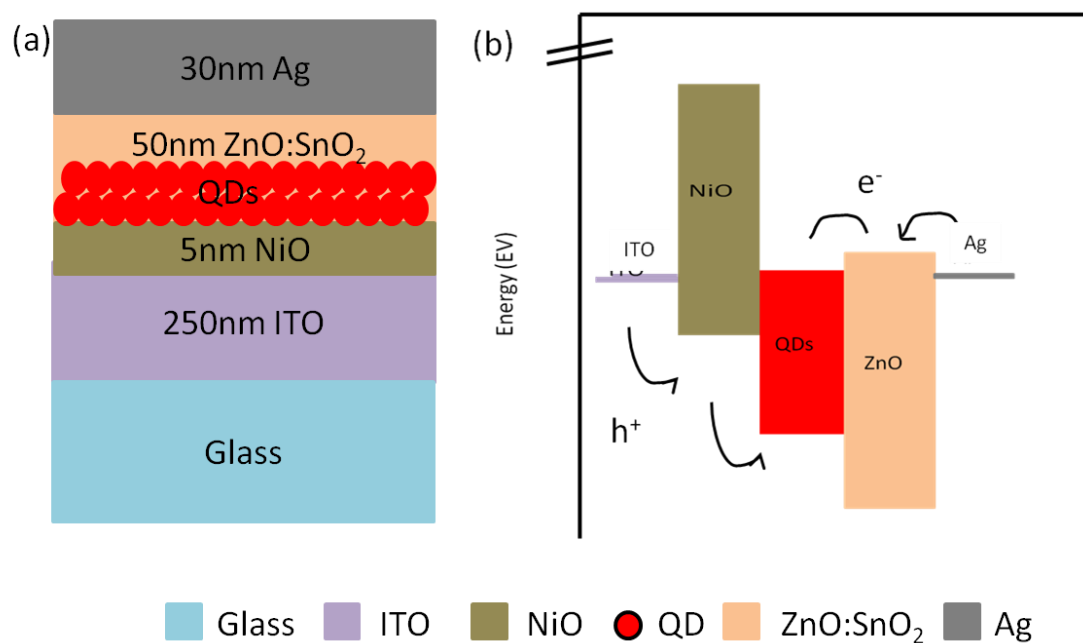


Figure 3.1: (a) Schematic of cross-section of control device and (b) Energy band diagram of control device

3.2.1 Fabrication of Anode

The flat glass substrate was cleaned by the three step process of rinsing with acetone followed by methanol and water rinse. A 250nm thick ITO layer was sputtered on the glass substrate using DC sputtering at the rate of 30A/s. Patterning of anode was done using photolithography technique. A negative photoresist (AZ 2590) was spin coated on top of the ITO layer. An absorbing chrome photomask was used to pattern the anode and the sample was exposed to UV-radiation. The sample was developed by washing in developer. ITO was then etched after post baking at 90C for 10minutes. For ITO etching a 3:1 solution of 37% HCl and HNO₃ was used. The developed sample was washed with the etching agent for 4 minutes. After etching the remaining photoresist was stripped by sonicating the sample in acetone followed by sonication in methanol for 3 minutes each. After stripping of photoresist, the sample was washed and any remaining photoresist was removed by using O₂ plasma. The ITO resistance was then adjusted by annealing at 400C for 60 minutes in the presence of oxygen.

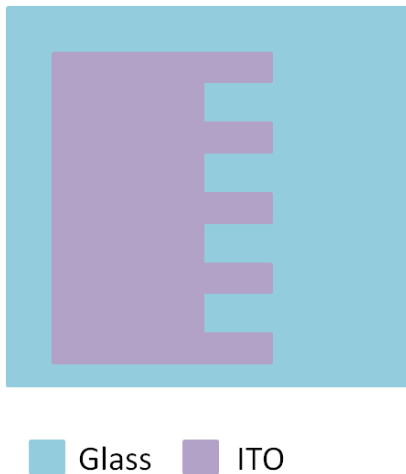


Figure 3.2: Schematic of patterned ITO anode structure (top view)

Annealing of ITO increases the resistance of the film. This is important because we wish eliminate the possibility of device failure by passage of current through pin holes and other defects which might be present in the different layers of the device especially in the QD layer. To avoid this type of failure, it is important to avoid large differences in the resistance of the different layers of the device. We used annealing technique to increase the resistance of the ITO layer and time and temperature of anneal was fixed through experiments. The annealing process was used because it has been shown in literature that upon annealing sputtered ITO also obtains better optical properties due to high refractive index. The optical properties are also of interest to us since the emission for the QD layer has to be obtained through the ITO layer [58].

3.2.2 Fabrication of Hole Transporting Layer

Nickel oxide was chosen to be used as the hole transporting layer due to its suitable band gap structure and hole transport capability. Deposition of this layer was done by using a SEC-1000/SE-1000 e-beam evaporator by CHA Industries, CA. Deposition was done under chamber pressure of 10^{-6} torr. This was followed by annealing in the presence of oxygen to form a NiO layer on top of the ITO layer. We deposited a 5nm thick layer of Ni on top of the ITO anode. The patterning was done using a hard mask, during deposition. To form NiO, the sample was annealed at 400C for 30minutes. The thickness of the Ni layer that can be used, is limited due to the optical properties required. The Ni layer cannot be too thick since it has to be completely oxidized to form a smooth, amorphous layer, which is transparent in the visible wavelength spectrum. Oxidation of the Ni layer by annealing it in the presence of oxygen forms the NiO layer which is transparent. However since this oxidation takes place at a

high temperature, it also affects the resistance of the underlying ITO layer. This limits the temperature and time for which oxidation can be carried out. The thickness is thus limited by the oxidation capability and also by the charge carrier density. In our control device we used a 5nm thickness of NiO layer.

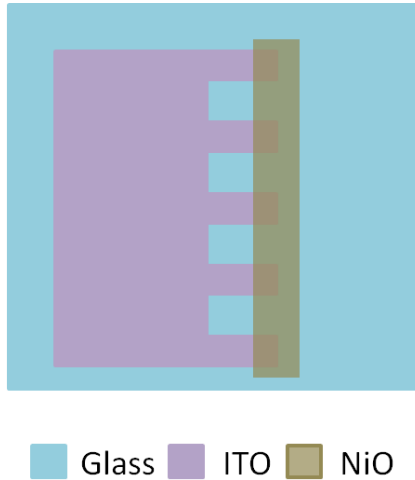


Figure 3.3: Schematic of patterned ITO anode structure with patterned NiO (top view)

3.2.3 Quantum Dot Layer Deposition

We used a process of micro-contact printing of quantum dots in combination with the Langmuir Schaffer technique to create and deposit thin films of quantum dots on the substrate to create the QDLED emissive layer. The procedure followed consisted of several steps described in the following section.

(e) Re-suspension of Quantum Dots

For our device, we used a colloidal suspension, in toluene, of quantum dots of CdSe: ZnS (core: shell) type (Evident Technologies). The quantum dots were precipitated and re-suspended in hexane (Reagent grade-Sigma Aldrich) to remove excess ligands. For micro-contact printing, we prepared a suspension of 15 μ l of CdSe: ZnS particles in a 1:1 (vol.) solvent of hexane and 1,2-Dichloroethane. 200 μ l of each solvent was used and a total of 400 μ l of solvent was prepared.

(f) Film Formation

A film of quantum dots was prepared by using the self-assembly of quantum dots. Self-assembly techniques for formation of monolayers or thin films with multi-layered structure using nanoparticles have been studied in the past [59, 60]. For our experiments, we used a technique of evaporation of suspended nanoparticles on a water surface [61]. We use a modified version of the traditional Langmuir-Schaeffer technique to form a uniform self-assembled film of quantum dots.

A Teflon disk of 20mm inner diameter and 2mm thickness was placed in a Petri dish. Water was pipetted into the Petri dish, such that a convex water surface was formed, pinned by the edges of the Teflon ring. The solvent with the quantum dots was pipette onto the convex water surface. The solvent evaporated, leaving behind a uniform array of self assembled quantum dots formed due to capillary immersion and convective forces. Figure 3.4 shows the experimental setup and quantum dot film formation. After the formation of this film the micro-contact printing step was performed.

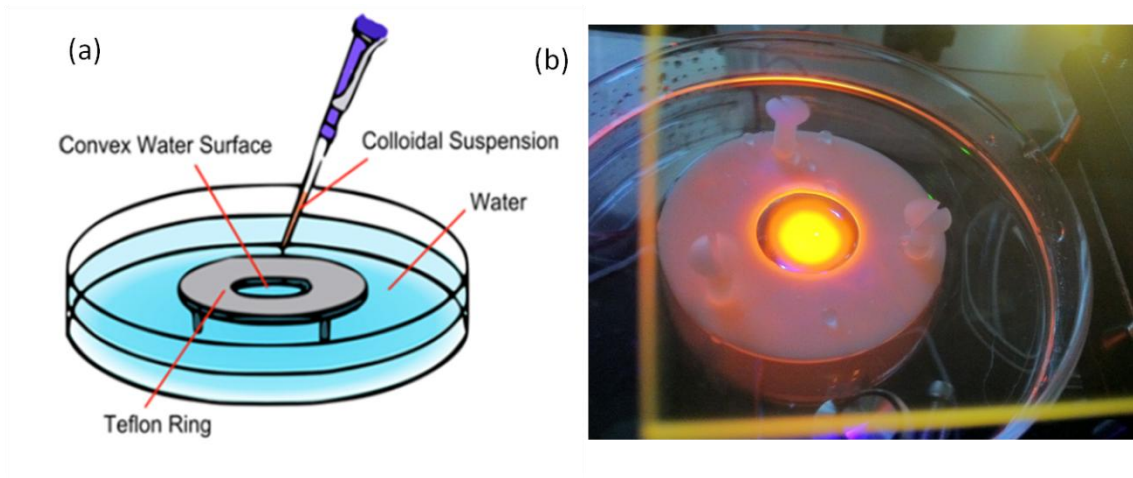


Figure 3.4: Experimental setup for QD monolayer formation (a) Schematic of setup indicating the Teflon ring, the convex water surface pinned by the Teflon ring and the colloidal quantum dot suspension pipetted on the water surface. (b) Picture of actual setup with quantum dots excited by ultraviolet LED. Emission wavelength of QDs used is 580nm.

(g) Micro-contact Printing

Upon formation of the quantum dot film on the water surface, the film was picked up by hydrophobic polydimethylsiloxane (PDMS) stamps and deposited on to the NiO layer. This was repeated with quantum dots of different emission wavelengths. We used quantum dots of two different emission wavelengths, 580nm and 600nm.

The PDMS stamp was fabricated using rapid prototyping technique. SU8 photoresist (Microchem Corp [62]) was patterned photolithographically on a silicon wafer. PDMS (Sylgard 184, Dow Corning Corp [63]), with added curing agent in the ratio of 10:1 was poured over the SU8 master mold. This was cured by baking at 70C for 30 minutes and then peeled off to form stamps [64].

The PDMS stamp was cut into desired shape and size and the stamp was used to pick up the QD film formed on the convex water surface. The inked stamp was then

inverted onto the substrate and gentle pressure was applied to cause transfer of the quantum dot particles from the PDMS stamp to the substrate. Figure 3.5 shows the procedure used for micro-contact printing.

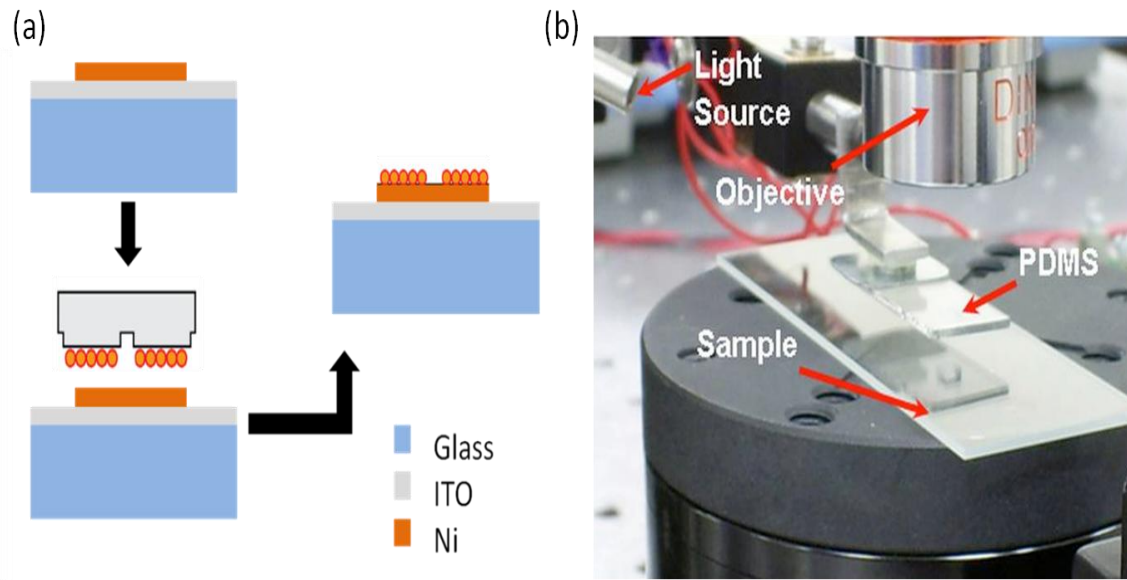


Figure 3.5: Micro-contact printing of quantum dot film (a) Schematic of micro-contact printing procedure (b) Picture of actual setup showing the PDMS stamp and the sample on which QD film is transferred

Patterning was done by repeating this procedure several times, separately for each QDLED corresponding to each electrode. Quantum dots of two emission wavelengths 580nm and 600nm were used to create multicolor QDLEDs on a single substrate. Figure 3.6 shows the image of photoluminescence from a micro-contact printed quantum dot pattern.

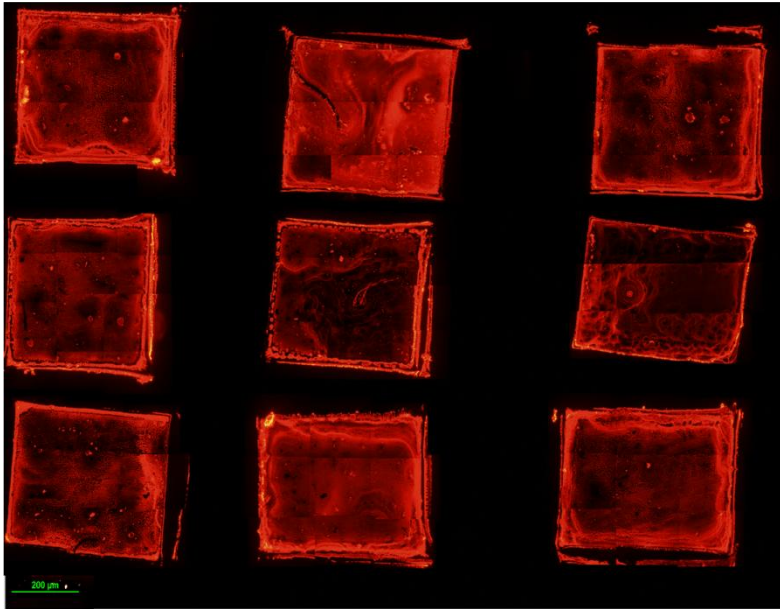


Figure 3.6: Photoluminescence image of patterned micro-contact printed QDs (EM 600nm) excited with a UVLED.

3.2.4 Electron Transporting Layer Deposition

A mixture of ZnO:SnO₂ was used as the Electron transporting layer. This material was chosen because of its compatible band gap structure. This alloy is an n-type semiconductor and its conduction band allows injection of electrons onto the CdSe: ZnS conduction band. The other property of this metal oxide is its ability to form thin amorphous films. We co-sputtered a mixture of ZnO:SnO₂ using RF sputtering process (Edward Auto 500) using a power of 40W at a rate of 0.1A/s. The low rate was maintained to minimize damage to the quantum dot layer. This layer was patterned using a hard mask during deposition. Figure 3.7 shows the patterning of the ETL on our device design.

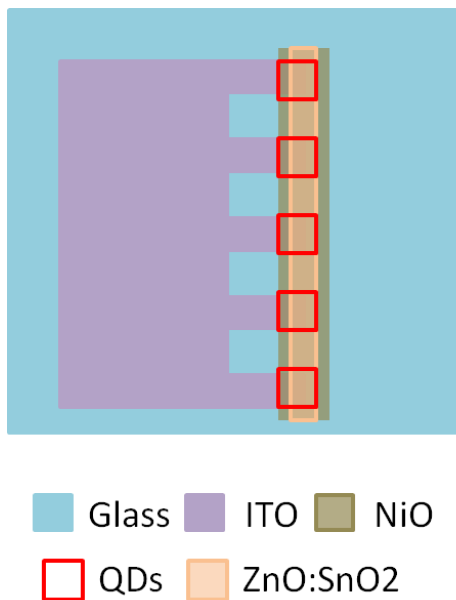


Figure 3.7: Schematic of patterned ITO anode structure with patterned NiO, QDs and ZnO:SnO₂ (top view)

3.2.5 Cathode Deposition

The inorganic QDLED structure has a bottom emission structure. Hence, the layers on top of the quantum dot layer, including the top electrode (cathode) do not have particular requirements for desired optical characteristics. We use an Ag cathode in our structure because of its electron injection capability.

We used e-beam evaporation technique using a SEC-1000/SE-1000 e-beam evaporator by CHA Industries, CA. Deposition was done under chamber pressure of 10^{-6} torr. 30nm thick Ag film was formed. Patterning of cathode was done by using a hard mask during deposition. Patterning of the cathode was done to define the area of electroluminescence. Expected electroluminescence was from the intersection of the anode, the quantum dot layer and the cathode. Figure 3.8 shows the patterning of the

cathode and the design of the entire device, showing multiple devices on a single substrate.

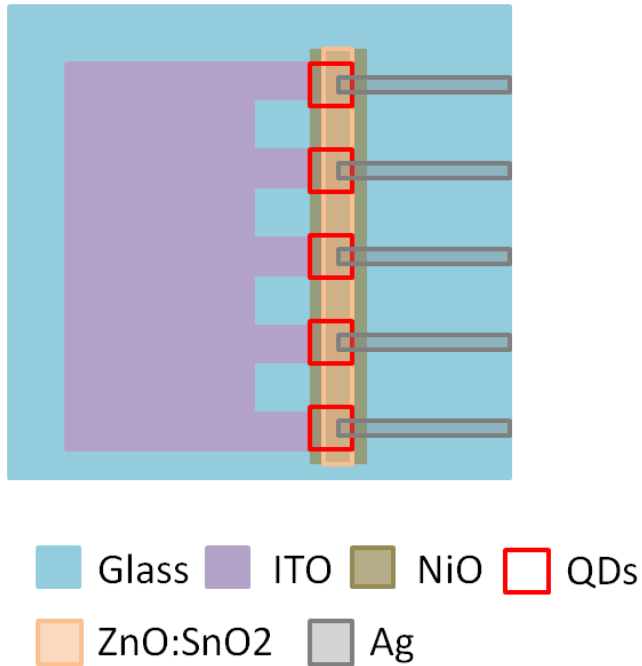


Figure 3.8: Schematic of patterned ITO anode structure with patterned NiO, QDs, ZnO:SnO₂ and Ag(top view)

3.3 DEVICE TESTING

After fabrication, the QDLEDs were tested by applying voltage across the electrodes, to observe electroluminescence. Certain parameters were studied to quantify the performance of our devices and were analyzed to devise changes in the QDLED structure and fabrication to achieve better performance from our devices. In this section we discuss the methods and results of the experiments performed.

3.3.1 Electroluminescence Testing

To test our devices for electroluminescence, we had to apply voltage across the device. For this, multi strand wires were attached, one each to the anode (ITO) and cathode (Ag). Silver paste was used to attach the wires to the two electrodes and to minimize the contact resistance. Voltage was applied in increments of 0.1V and the corresponding current was noted using a LabView program. Electroluminescence was observed through an upright optical microscope at various magnifications. We fabricated QDLEDs with quantum dot layers of two emission wavelengths (580nm and 600nm). The size of the QDLED emission area was defined by, (a) size of micro-contact printed quantum dot pattern and (b) the patterned area of intersection of the anode, quantum dot layer and cathode. We fabricated QDLEDs of average area of $200\mu\text{m} \times 800\mu\text{m}$.

The bandgap energy of quantum dots depends on the size of the quantum dots and thus depends on the emission wavelength of the quantum dots. The bandgap energy of quantum dots corresponding to various emission wavelengths is given in table 3.1.

Wavelength (nm)	Bandgap (eV)
560	2.125
580	2.0
600	1.98
620	1.91

Table 3.1: Bandgap energy of Quantum dot particles

From the table we can see that the bandgap energies of quantum dots increase with decreasing wavelengths. Upon consideration of these values, we chose quantum dots of wavelengths 580nm and 600nm for our experiments since they lie in the visible range and are also require relatively lower energy to activate.

Figure 3.9 shows electroluminescence from QDLEDs at (a) 580nm and (b) 600nm emission wavelengths. These images are taken using 10X magnification and 60s exposure time each. We tested 56 QDLEDs with emission wavelength of 600nm and 35 QDLEDs with emission wavelength of 580nm. Measurements for turn-on voltages, emission wavelengths and lifetimes were made.

From figure 3.9 we observed that the emission is not uniform over the entire area of the fabricated QDLED and depends on various factors such as uniformity of the micro-contact printed quantum dot layer, uniformity of the anode and other layers of the QDLED structure. Another observation over the testing of all the QDLEDs was that in the case of holes or defects in the QD layer, we found emissions from a very small area of the QDLED. We conclude that this occurs due to the large differences in resistance in the different layers of the QDLED. The resistance of the quantum dot layer is much larger than the resistances of the layers surrounding the quantum dot layer. Due to this any holes in the quantum dot layer acted as a short circuit, and all of the current passed through this area causing emissions from the few quantum dots present close to the area of the defect. This resulted in device failure where we obtained no emissions from the remaining area of the QDLED. Apart from this extreme case of QDLED failure, we also found that non-uniformity in the quantum dot layer caused corresponding non-uniformity in the electroluminescence emissions obtained. Over time this led to failure of devices in the devices in which excess current was passing through a particular area of the device.

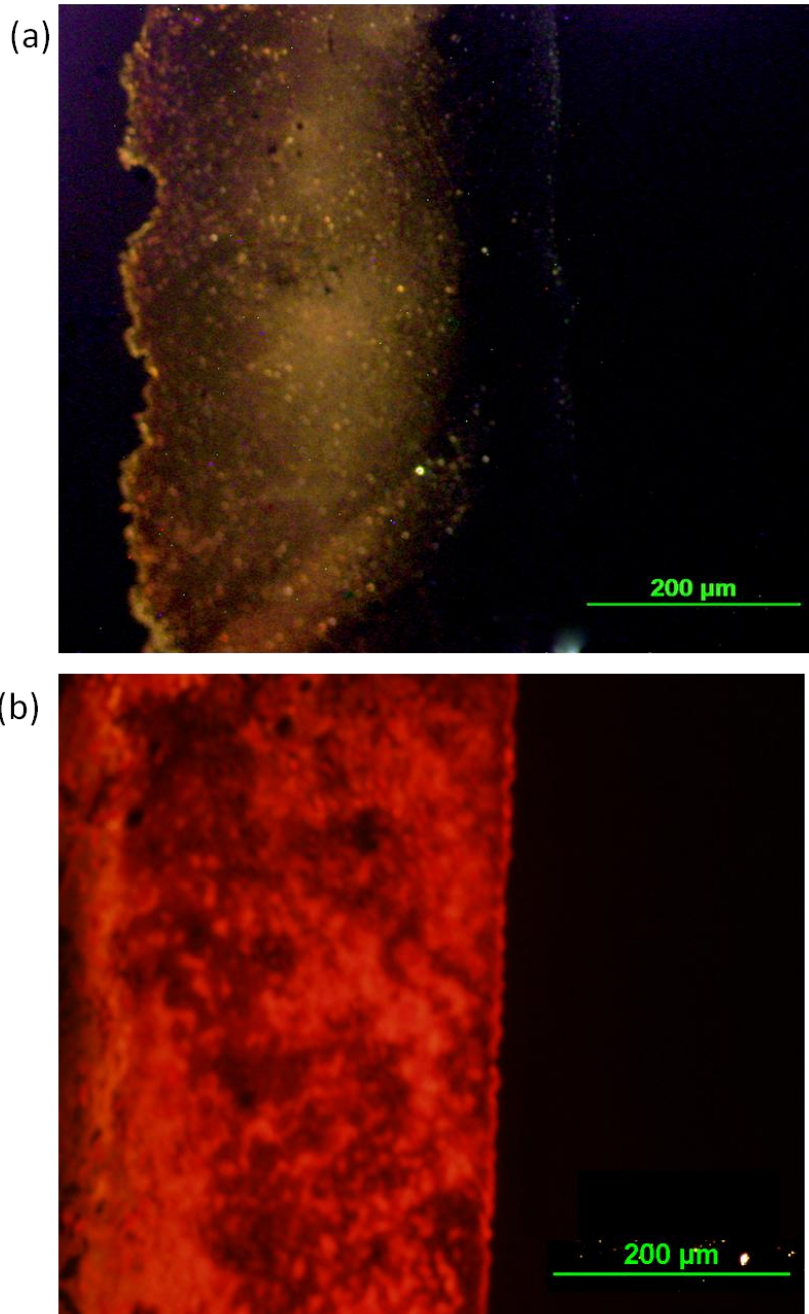


Figure 3.9: Electroluminescence of basic QDLEDs, (a) Electroluminescence from 580nm QDLED taken with 10X magnification and 60s exposure time (b) Electroluminescence from 600nm QDLED with taken with 10X magnification and 60s exposure time

Since the emission from the QDLED is observed through the glass substrate, emissions from the hole transporting layer (HTL) can get added on to the emissions from the quantum dot layer. Emission from other layers can occur due to imbalances in charge carriers, causing the electrons and holes to combine in layers other than the quantum dot layer. To avoid these emissions, the thicknesses of the charge transport layers (CTLs) were fixed through iterative experiments. To obtain the spectra, we used a spectrometer with exposure time of 300 seconds. The Figure 3.10 shows spectra obtained from QDLEDs with 580nm and 600nm emission wavelengths. The inset has an image of a QDLED at 10X magnification with 60s exposure time taken with a RGB CCD.

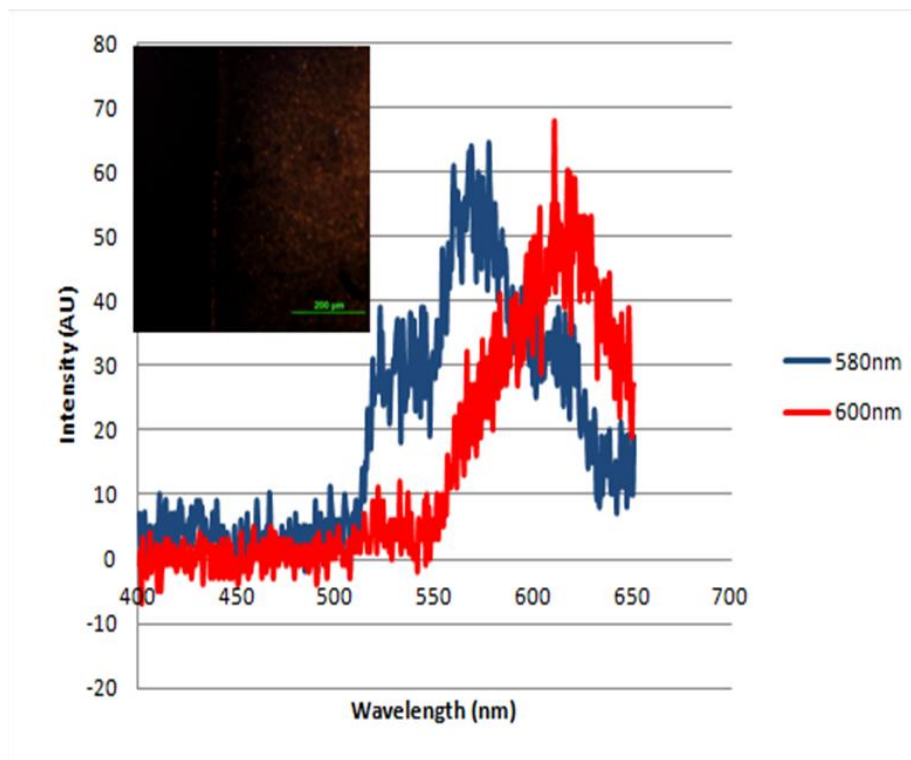


Figure 3.10: Electroluminescence characteristics of QDLEDs. Spectra measured during electroluminescence of 580nm and 600nm QD LEDs (exposure time 300s). Inset shows electroluminescence image taken with microscope at 10X magnification (scale bar is 200μm) with exposure time 60s.

For measurements over all samples fabricated, (n=56 for 600nm wavelength and n=35 for 580nm wavelength), full width half maximum values were found to be ~40nm for 600nm QDLEDs and ~38nm for 580nm QDLEDs. From these values we conclude that we have achieved good charge carrier balance and do not observe very high emissions from any layer other than the quantum dot layer.

3.3.2 I-V Characteristics

While testing our QDLEDs, we noted the current through the device at incremental voltage values. We also noted the turn-on voltages for each device. I-V characteristics of QDLEDs are important for a number of reasons. A high turn-on voltage reduces the working lifetime of the device. High voltages increase the temperature of the device causing breakdown of various layers of the device and also reduce the efficiency of the device. Figure 3.11 shows the I-V characteristics for one pair of 580nm and 600nm QDLEDs tested.

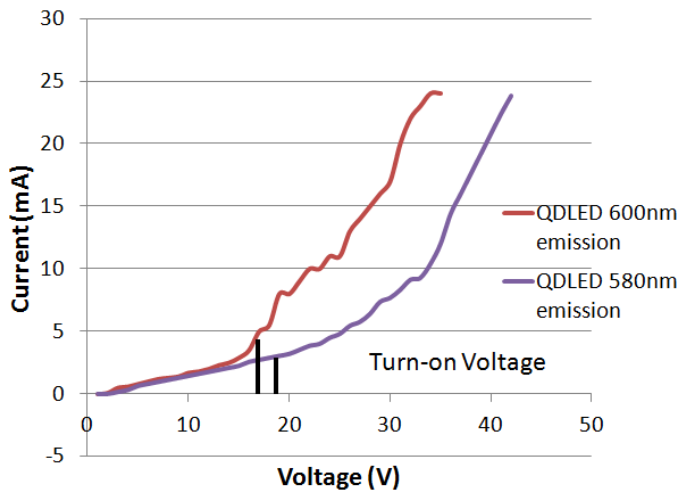


Figure 3.11: I-V curves for 580nm and 600nm QDLEDs showing turn-on voltage

Over the samples tested, we found an average turn-on voltage for 580nm QDLEDs to be 20.4V and that for 600nm QDLEDs to be 18.7V. We expect the voltage for 580nm QDLEDs to be higher than that of 600nm QDLEDs since the energy bandgap for 580nm quantum dots is larger than that for 600nm quantum dots.

Another important characteristic of QDLEDs that we focused on was the lifetime of the device. For the devices tested, we applied voltage in 0.1V increments till the turn-on voltage was reached. After we observed emissions from the device, we applied constant voltage to the QDLED and we found the maximum lifetime of the devices over the entire sample size to be 160 minutes for the 580nm LEDs and 150 minutes for the 600nm LEDs. Device failure was usually a result of electrode damage due to high voltage or due to burning of QDs from direct contact with electrodes.

3.3.3 Areas of Device Improvement

From the experimental results discussed in the section above, we found several areas of improvement which are discussed in this section:

(a) ITO Anode

From the photolithography and wet etching techniques used for patterning the anode, we found some non-uniformity in the ITO pattern. This happens because it is difficult to control the spin-coating and etching time exactly to obtain perfectly uniform patterns. We obtain bevel shaped anode structures which affect the resistance of the anode. The resistance of the anode showed differences at the edges as compared to the resistance over the entire region of the anode. This can cause failure at the edges of the QDLED.

(b) Hole Transporting Layer

Since e-beam evaporation was used to deposit NiO as the hole transporting layer, maximum possible thickness of the HTL is constrained by the optical properties and annealing and oxidation requirement. Excessive annealing can lead to increase in the resistance of the underlying ITO layer and less annealing can lead to incomplete oxidation of the Ni layer, forming pockets of NiO which disrupts both the optical and electrical characteristics of the device. Deposition of thin films less than 10nm in thickness using e-beam evaporation causes pin-hole defects and patches in the film. This leads to uneven hole transport and patches can cause quantum dots to come in contact with the environment and also causes direct contact with the anode. At high turn-on voltages, direct contact of quantum dots with the anode can cause burning and damage of quantum dots. Contact of quantum dots with the environment causes degradation of QDs and leads to reduced lifetime of device.

(c) Electron Transporting Layer

We co-sputtered an amorphous film of ZnO:SnO₂ as the electron transporting layer. This amorphous film is sputtered directly on the QD layer. Quantum dots are damaged during this sputtering and the amorphous layer also causes contact of the quantum dot layer with the environment. This reduces the efficiency and lifetime of the QDLED. Sputtering also causes quenching of the quantum dots, this leads to lower intensity of electroluminescence.

(d) Cathode

In this device silver was used as the material for the cathode and was deposited using e-beam evaporation. Ag is easily oxidized and does not conduct current well after oxidation. This leads to lower lifetime of device.

3.4 SUMMARY

In this chapter we discussed the basic device which was used as a control device to be improved upon during further experiments. The basic device structure used was a modified version of devices presented in literature. We discussed the experimental results obtained from devices with this configuration and upon analysis of the results, enumerated the areas of the device which could be changed to obtain better performance. In the next chapter we will discuss strategies for improvements in this basic design and compare the performance results of the two designs.

CHAPTER 4: QDLED MODIFIED DESIGN- FABRICATION AND CHARACTERIZATION

4.1 INTRODUCTION

In this chapter, we introduce changes in the device design described in chapter 3. We focused on analysis of the experiments performed using QDLEDs fabricated according the basic design and made changes in the design to improve the performance of our QDLEDs. We focused separately on each layer and devised strategies to overcome the drawbacks which were analyzed and presented in the previous chapter.

We also present experiments with the modified device and make quantitative comparisons between performance parameters obtained during experiments with the basic devices and modified devices.

For changes in the device design, we still use the basic sandwich structure of the inorganic QDLED because of the advantages of inorganic charge transport layers discussed earlier [57]. Changes were made in the materials and fabrication techniques used to improve device performance. First, we focus on improvement of device lifetime. We will first describe and characterize the changes made to each layer of the QDLED structure followed by analysis and comparisons of experimental results to quantify the improved performance obtained from our new device design.

4.2 MODIFIED DEVICE DESIGN

Based on our analysis, presented in chapter three, we discuss here the drawbacks of each layer, specific to our target application and describe modifications made to each layer to overcome individual constraints.

4.2.1 Anode Patterning

In the basic QDLED design, the anode was fabricated by deposition of ITO on a glass substrate followed by photolithography and wet etching techniques to pattern the anode. Some of the drawbacks of this method were that the etching rate could not be controlled very closely in the prototype fabrication facility because the concentrations of acids used cannot be exact which leads to differences in etching rates. This resulted in anodes with surface non-uniformities and beveled edges, which caused differences in resistances in the various areas of the anode leading to non-uniform emissions and possible failure of devices due to excessive current and heat passing through a small region of the device.

To overcome these constraints, we replaced the photolithography-wet etching technique. A hard mask was used for patterning during sputtering of the ITO to obtain uniform deposition over the entire anode area. RF sputtering was done using UNIVEX-450 system. Deposition was done at high vacuum of 10^{-6} mbar to obtain uniform sputtering in an Argon environment, with 200W power. Rate of deposition used was 30Å/s to deposit a 250nm thick anode.

To create the hard mask for patterning, we used kapton tape. Kapton tape is compatible with the sputtering chamber and can be used in environments ranging from -196C to +400C. The maximum temperature of the chamber during sputter deposition is expected to be 200C. Kapton tape has a thickness of 0.03mm. This small thickness is advantageous because it allows for a smaller step between the substrate and the mask, resulting in sharper edges of the pattern after deposition. Similar to the first device, ITO resistance was then adjusted by annealing at 400C for 60 minutes in the presence of oxygen [58].

4.2.2 Hole Transporting Layer

In the basic design, NiO hole transporting was fabricated by e-beam evaporation of 5nm thick layer of Ni, followed by annealing in oxygen to form NiO. We enumerated the drawbacks of this method which included (a) constraints on thickness of layer that could be deposited to maintain optical properties of the layer, leading to direct contact of quantum dots with the anode and also with environment decreasing device lifetime (b) Patched Ni layer due to small thickness, which is difficult to control in e-beam evaporation technique even at very high vacuum levels (c) pockets on unoxidized Ni in the NiO layer which leads to non-uniform charge transport causing lower lifetime of device.

In the new design, we tried to address all the drawbacks from the previous device. Changes were made in both the materials and the fabrication techniques used. To overcome the constraint of low thickness, and patched layer due to small thickness, we first replaced the method of NiO layer fabrication. We had two choices for replacing the e-beam evaporation technique, namely, sputtering and spin-coating. We chose to fabricate this layer by spin coating Nickel Acetate tetrahydrate in methanol at 1500 rpm and then annealing at 120C for 90 minutes. The 20nm thick film has been shown to have optical properties which do not affect the device in the visible wavelength range and small thicknesses of 20nm [65].

Spin coating followed by annealing gives a smoother surface with fewer holes and other defects as compared to sputtered films of similar thickness. For this reason, we chose spin-coating followed by annealing as the technique to deposit this layer. Since annealing is done at low temperature of 120C, it does not greatly affect the resistance of the underlying ITO layer. Figure 4.1 shows the comparison between uniformity of

sputtered and spin coated NiO film by comparing Atomic Force Microscopy (AFM) images of two such films deposited on a glass substrate with a patterned ITO layer.

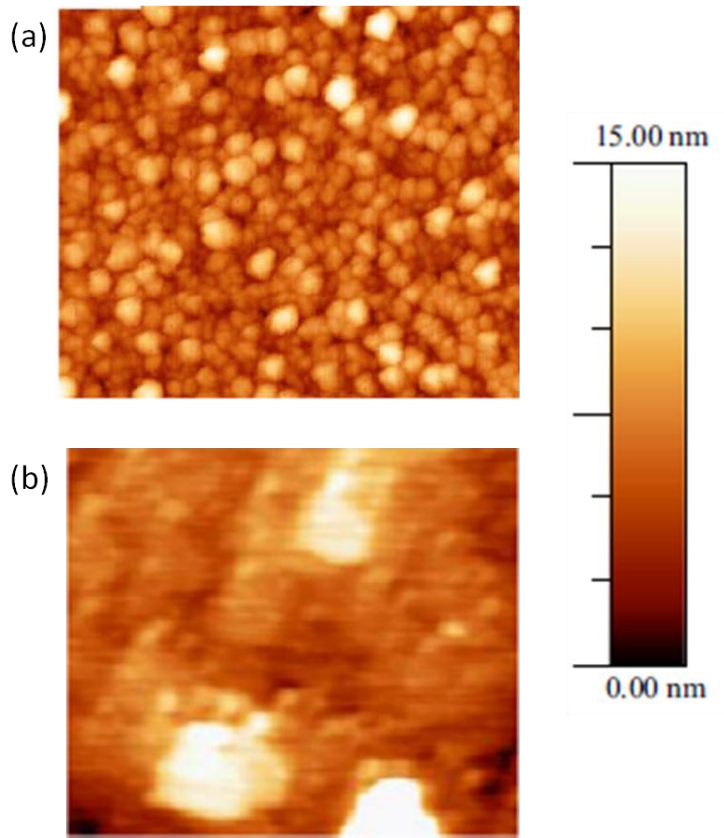


Figure 4.1: Comparison of NiO film uniformity. (a) Sputtered film (b) Spin coated and annealed film

From these AFM images we concluded that spin coating followed by annealing would give much more uniform film with fewer defects and used this method to form the NiO hole transporting layer. Spin-coating is also easier and quicker than sputtering.

The other issue with the earlier method was that of quantum dots coming in direct contact with the anode and also with the environment causing burning and degradation of quantum dots, lowering lifetime. Although this problem was mainly due to defects in the

NiO layer in the basic device structure, we focused on this drawback in order to improve device lifetime. We added an extra layer of Al_2O_3 between the ITO and NiO layers.

The Al_2O_3 was deposited using Atomic Layer Deposition (ALD) technique in which the surface of the substrate is chemically acted upon by the precursor of the metal oxide to be deposited. Due to this, at each pulse, a single atomic layer of the material is deposited on the substrate. This technique deposits a layer over the entire substrate irrespective of the non-uniformities of the substrate. Thus we used Al_2O_3 , deposited using ALD as a protection layer between the ITO and NiO layers. Due to this, even in areas where defects are formed in the NiO layer, quantum dots would not come in direct contact with the ITO layer and the environment. Al_2O_3 has a bandgap structure similar to NiO and can thus act as a hole injection layer. NiO layer is still required as the carrier concentration of Al_2O_3 , is low and using only Al_2O_3 , as the hole transporting layer would reduce the efficiency of the device.

4.2.3 Quantum Dot Layer

In the first design we used micro-contact printing as the method for deposition of quantum dots. This method is important for our target application as we want to create multicolor QDLEDs on a single substrate. Hence we use the same method in our new device design. However, since most literature uses spin coating of quantum dots as the method of deposition of quantum dots, we also apply this method to deposit quantum dots in our device. For the second device we used two methods, micro-contact printing and spin coating to deposit quantum dots. Micro-contact printing is done using the method described in chapter 3.

For spin coating, we re-suspended 5 μ l of quantum dots in 200 μ l chloroform. The solution was spin coated at 2500rpm to form a bilayer of quantum dots on the substrate with patterned ITO, Al₂O₃ and spin coated NiO as the underlying layers. Figure 4.2 (a) shows the schematic of the procedure of spin coating and (b) shows the QD profile after spin coating measured using AFM.

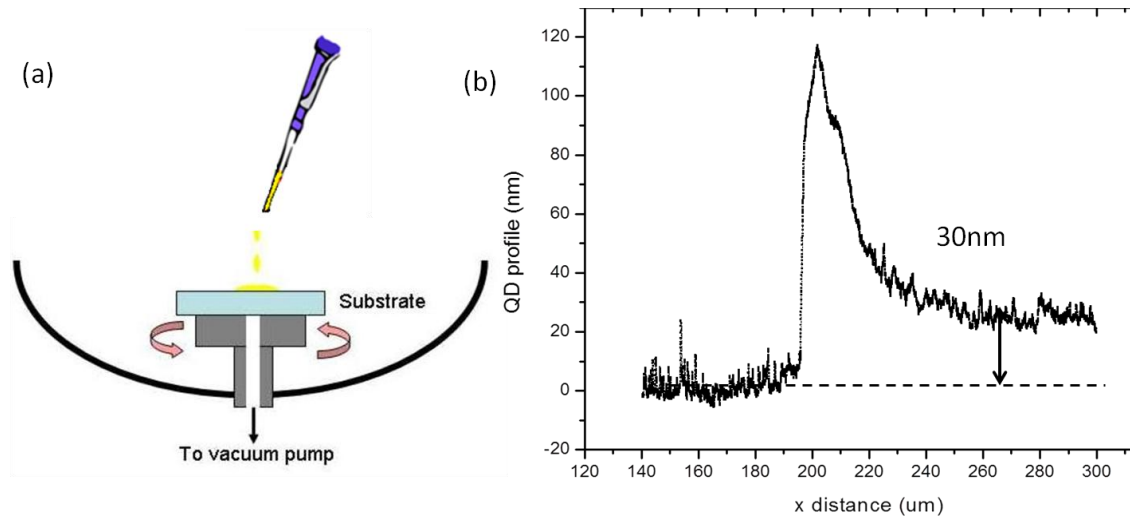


Figure 4.2: Spin coating of quantum dots. (a) Schematic of procedure used for spin coating. (b) QD profile after spin coating measured using AFM.

4.2.4 Electron Transporting Layer

In the basic structure design we used a co-sputtered a layer of ZnO:SnO₂ as the Electron Transporting Layer (ETL). The amorphous ETL though effective in electron transport, does not protect the underlying QD layer from environmental factors, such as contact with oxygen. The quantum dot layer also gets affected during the sputtering of the metal oxide film overlying the quantum dot layer. This results in shorter lifetimes of QDLEDs [66].

To overcome these drawbacks, we introduced a device structure using a spin coated ZnO nanoparticles film as the ETL. The ZnO nanoparticles film offers the advantage of efficient electron transport and is more robust and easier to process as compared to sputtered metal oxide films of comparable thickness [66].

For the deposition of the ZnO layer, we used n-Butanol as the solvent. N-Butanol has a solvent polarity of 4. Due to the strong forces between the HTL and the QDs, the spin coating of the ZnO nanoparticles in n-butanol solvent does not affect the QD layer formed on substrate. Spin coating of the ZnO layer offers a number of advantages over sputtering or thermal annealing of metal oxides as the ETL. The solution processed ZnO nanoparticles film shows good electron mobility of $\mu_e \sim 1.3 \times 10^{-3} \text{ cm}^2/(\text{V s})$. The crystalline ZnO film shows low CB and VB edge levels of -4.02 and -7.47eV. The solution processed layer is more robust than a sputtered thin film with less possibility of pin holes in thin films. This avoids direct contact between the cathode and the QD layer.

The fabrication procedure followed was determined by an iterative experimental process in combination with results from similar experiments in literature [66]. 2% weight solution of ZnO nanoparticles (size: 10nm) was prepared in n-Butanol. The solution was sonicated for 10 minutes and then spin coated on top of the QD layer at 2000rpm for 60 seconds to form a 50nm thick film. The sample was then baked at 90C for 10 minutes to remove the solvent.

4.2.5 Cathode Patterning

In our basic device structure we used e-beam evaporation to deposit Ag electrodes which were patterned using a hard mask. Some drawbacks of this method are the subjection of the substrate to high temperature during e-beam evaporation and

oxidization of the Ag cathode causes lower lifetimes. To overcome this drawback, we substituted the cathodes by using sputtered Aluminum thin films patterned using hard mask. Aluminum shows better qualities as a cathode and helps in improving the lifetime of the device.

4.2.6 Summary of Device Design Modifications

For the entire device, the following changes were made in every layer:

- (a) Anode: Sputtering of ITO using hard mask for patterning.
- (b) Hole Transporting Layer: Al_2O_3 layer deposited using ALD, followed by spin coating and annealing of NiO layer.
- (c) QD Layer: deposited using micro-contact printing/ spin coating
- (d) Electron Transporting Layer: Spin coating of ZnO nanoparticles in n-butanol.
- (e) Cathode: Al sputtered and patterned using a hard mask

Figure 4.3 shows the comparison between the device structure used for the basic device and the modified device structure. Energy bandgap diagram of the new device structure is also shown to explain the flow of holes and electrons.

Schematics of the basic control device structure and the new device structure are shown to summarize the device design modifications discussed in this section. In the next section we discuss the experiments performed and the results obtained from this modified device design.

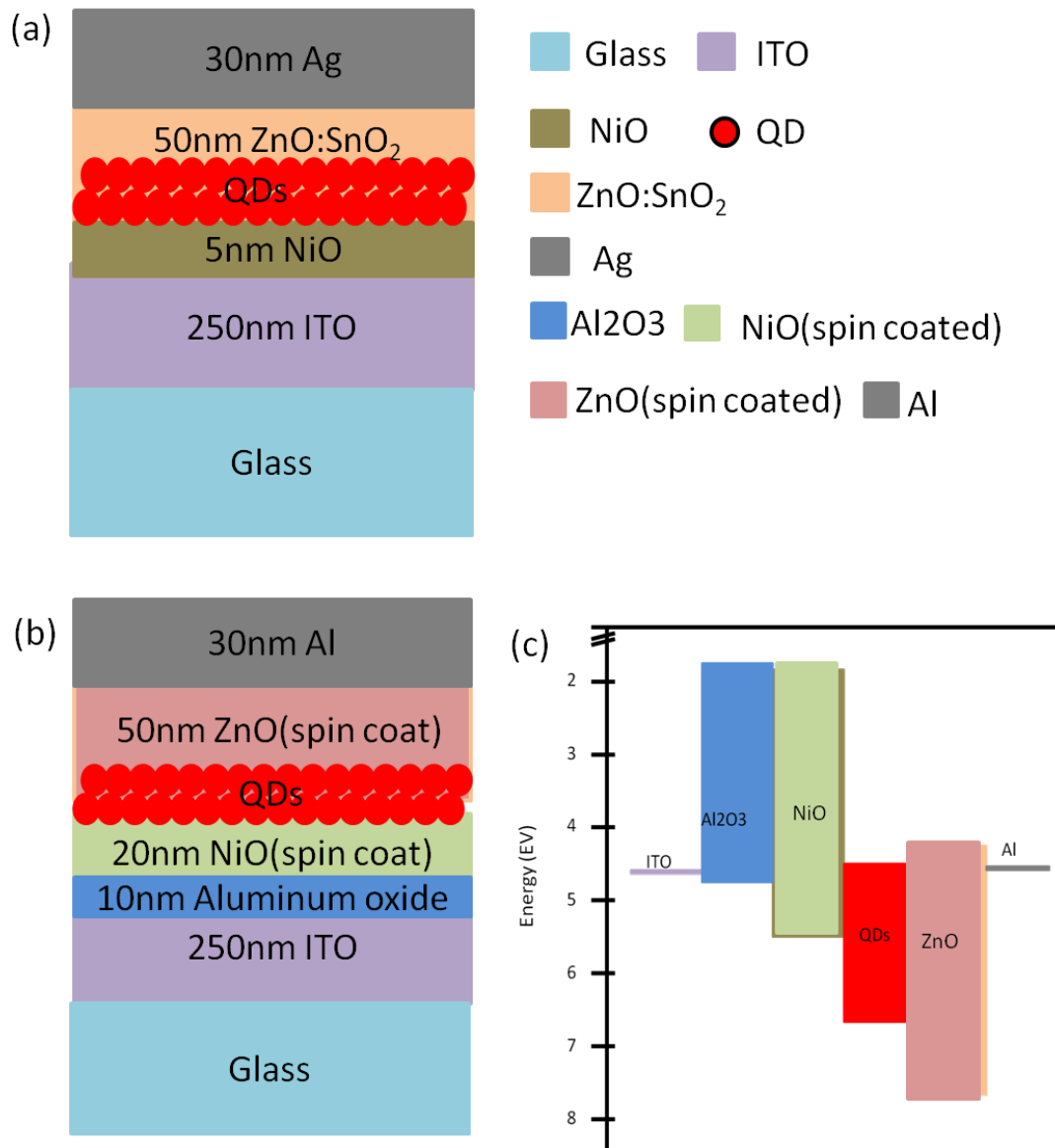


Figure 4.3: Schematic of comparison between control device and modified device structure. (a) Schematic of control device structure, (b) Schematic of modified device structure, (c) Energy band diagram of modified device structure.

4.3 MODIFIED DEVICE –TESTING

After fabrication of the modified QDLEDs, the devices were tested by applying voltage across the electrodes to observe electroluminescence. We quantified the performance of the QDLEDs using the same parameters that were used while testing the QDLEDs with the basic device structure. In this section, we discuss the results obtained upon testing of the modified QDLEDs.

4.3.1 Electroluminescence Testing

To test the electroluminescence performance of the modified QDLEDs, we followed a procedure identical to the testing of the basic sample devices. We attached multi strand wires, one each to the anode (ITO) and cathode (Al). Silver paste was used to attach the wires to the two electrodes and to minimize the contact resistance. Voltage was applied in increments of 0.1V and the corresponding current was noted using a LabView program. Electroluminescence was observed through an upright optical microscope at various magnifications. We fabricated QDLEDs with quantum dot layers of two emission wavelengths (580nm and 600nm). QDLEDs were fabricated using both micro-contact printing and spin-coating methods of QD deposition. We fabricated QDLEDs of $\sim 200\mu\text{m} \times 800\mu\text{m}$ in size which were patterned by patterning of anode and cathode. Figure 4.4 shows electroluminescence from QDLEDs at (a) 580nm and (b) 600nm emission wavelengths. These images are taken using 10X magnification and 60s exposure time each. We tested 20 QDLEDs with emission wavelength of 600nm and 35 QDLEDs with emission wavelength of 580nm. Measurements for turn-on voltages, emission wavelengths and lifetimes were made.

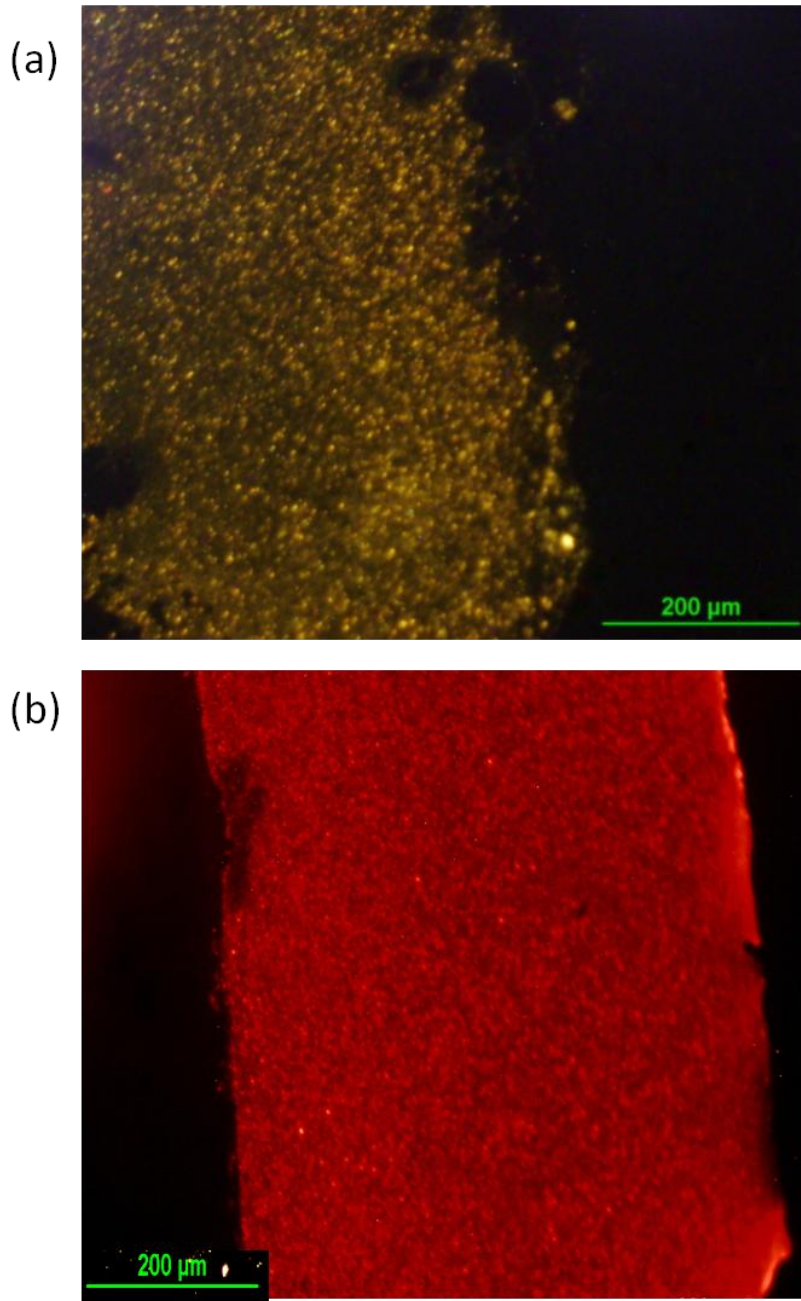


Figure 4.4: Electroluminescence of modified QDLEDs, (a) Electroluminescence from 580nm QDLED taken with 10X magnification and 60s exposure time (b) Electroluminescence from 600nm QDLED with taken with 10X magnification and 60s exposure time

4.3.2 Device Characterization

We first measured the spectra obtained from the electroluminescence to verify that no emissions from other layers of the QDLED are affecting the performance of our devices. For the devices fabricated with emission wavelength of 600nm, we found a maximum at 606nm and a full width half maximum of ~43nm on an average (n=30 QDLEDs). For the devices fabricated with emission wavelength of 580nm, we found a maximum at 590nm and a full width half maximum of ~40nm on an average (n=20 QDLEDs).

We also measured the turn-on voltages for all the devices fabricated and saw an average turn-on voltage of 8.2V for the 600nm wavelength QDLEDs and an average turn-on voltage of 9.7 V for 580nm emission wavelength QDLEDs.

The third characteristic measured was the lifetime of the fabricated devices. Voltage was applied in increments of 0.1V till the turn on voltage was reached. Upon observing emissions from the QDLED the applied voltage was kept constant. We tested for a maximum of 12 hours of continuous operation of the QDLED with no damage. After this the device was stored at room conditions without encapsulation or any special packaging and the LEDs were found to be operational for up to 8 months after fabrication.

4.4 DEVICE COMPARISONS

After testing both the designs, namely the control sample QDLED and the modified QDLED, we compared the performance of the two types of devices. Comparisons of the three parameters made were intensity, turn-on voltage and device lifetime.

4.4.1 Comparisons of Device Intensity

We expected a marginally higher intensity from our modified structure due to multiple reasons. The layer overlying the quantum dot layer was a spin coated ZnO nanoparticles film and not a sputtered film; we expected the ZnO nanoparticles film to offer an advantage of better electron transport. Also the spin coating technique is expected to avoid the damage caused to the quantum dot layer during sputtering, thus avoiding quenching of QDs

Also the spin coated NiO film provides higher transparency in the visible region as compared to the e-beam evaporated, annealed film. This leads to higher extraction of emission from the QD layer thus indirectly increasing the emission intensity observed.

The differences in intensities of the two device structures fabricated were measured using two methods. In the first method, comparisons were made between the maximums of the spectra obtained from the two devices. For this we measured the spectra from all the fabricated devices. The spectra with the highest observed maxima from each group (control samples and modified devices) were chosen and compared. Figure 4.5 shows these comparisons for each wavelength between two devices. Inset for each spectrum comparison shows the two specific QDLEDs which were used to obtain the specific spectra compared.

Difference between the maximum intensity points on the spectra of the two devices was compared and percentage increase in intensity was calculated. We found a 17% increase in maximum intensity in the 600nm QDLEDs with modified design and a 22% increase in 580nm QDLEDs with modified design as compared to the corresponding QDLEDs fabricated using the control structure design.

Intensity comparisons were also made by using image processing methods. The same two sets of QDLEDs were used to calculate the intensity. Images of the QDLEDs

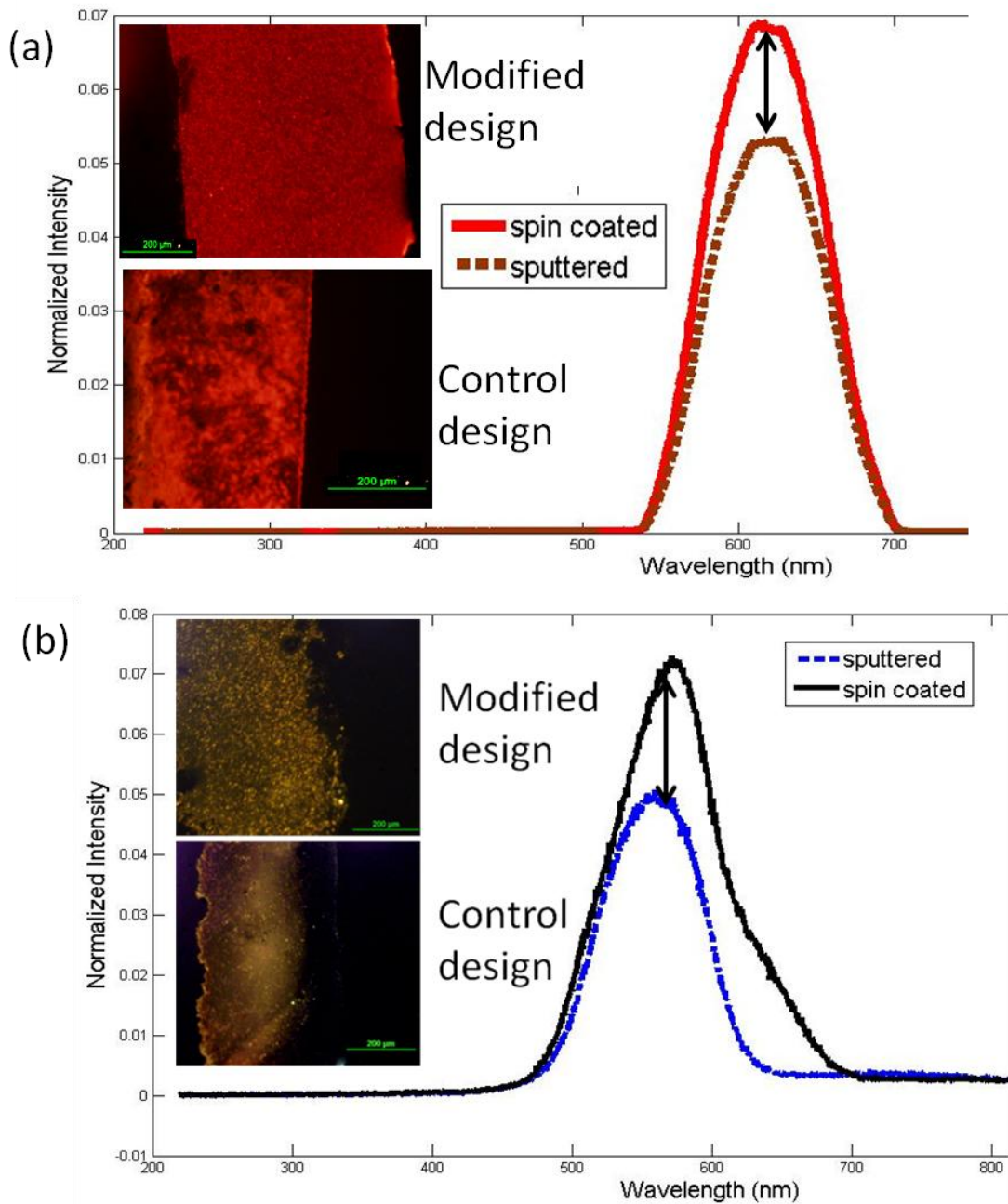


Figure 4.5: Comparison of emission spectra. (a) Maximum intensity from spectra for 600nm emission wavelength devices of control and modified design types. Inset shows the two LEDs used for obtaining spectra. (b) Maximum intensity from spectra for 580nm emission wavelength devices of control and modified design types. Inset shows the two LEDs used for obtaining spectra

were taken at 10X magnification and 60 seconds exposure time each. One line across each QDLED was chosen and intensity profile was plotted. The profile was plotted using MATLAB and comparison was done between the average intensities of the two LEDs. Figure 4.6 shows the QDLEDs and comparisons of intensities.

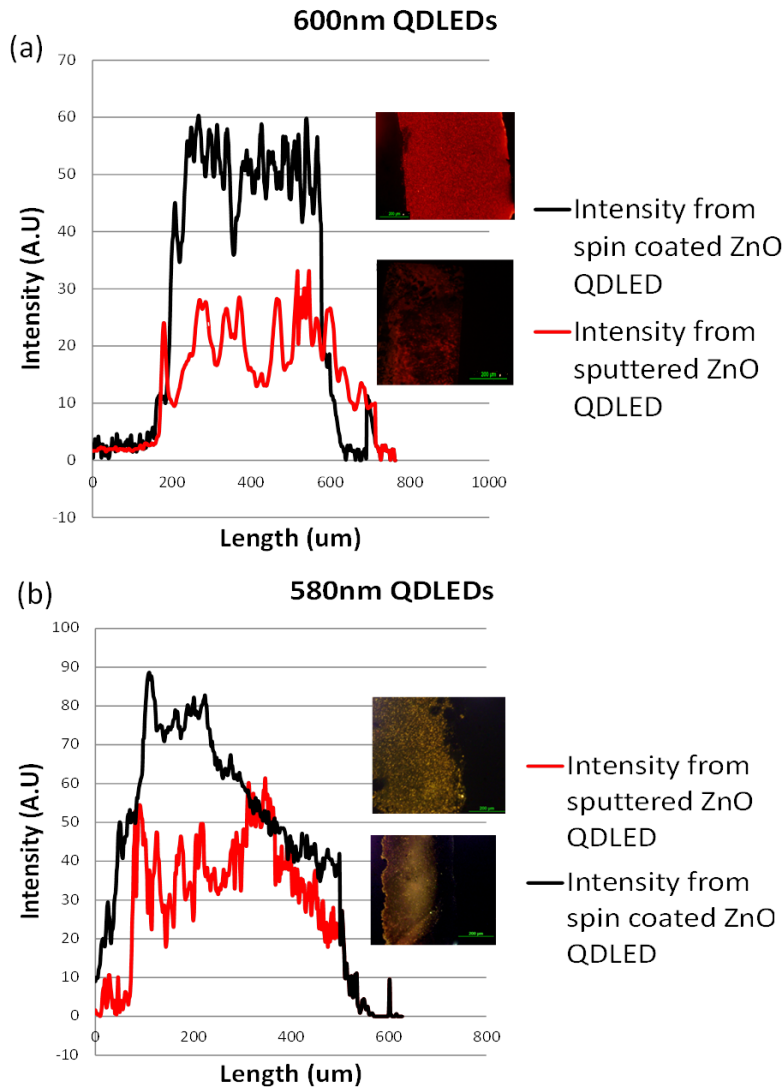


Figure 4.6: Comparisons of QDLED emission. (a) Emission profile across 600nm QDLEDs, (b) Emission profile across 580nm QDLEDs. All images at 10X magnification and 60s exposure time. Insets are images of particular QDLEDs used for measurement shown in the figure.

From these measurements, we found an increase of ~18% in intensity of the QDLEDs with the modified design as compared with QDLEDs with the control sample design structure for QDLEDs with 600nm emission wavelength and a 15% increase in intensity for the QDLEDs with 580nm emission wavelength. These values are reasonably close to the values obtained from comparisons of the spectrum measurements from the same LEDs. From these analyses we conclude that as expected, we obtain a marginal increase in intensity from the modified structure

4.4.2 Comparisons of I-V curves

Upon testing of the new device design, we expected a lower turn-on voltage as compared with the original devices, based on a number of modifications implemented. First, the replacement of the thin, e-beam evaporated Ni layer (5nm) followed by annealing, which resulted in patches of film with pockets of NiO, with thicker (20nm) NiO spin coated film was expected to provide better charge transport capability. Another reason for expected lower turn-on voltage was the use of spin-coated ZnO nanoparticles film in the place of sputtered film. ZnO nanoparticles film has been shown to have better charge transport capabilities and also does not affect the quantum dot layer by quenching that occurs during sputtering [66].

From the tested QDLEDs we found average turn-on voltages of 9.7V for the 580nm wavelength QDLEDs and an 8.2V for 600nm emission wavelength QDLEDs. This is about 9V lower than the average turn-on voltages of 18.7V for 600nm and 20.4V 580nm QDLEDs fabricated using the control sample design. Figure 4.7 shows the comparisons between the turn-on voltages for the two groups of devices

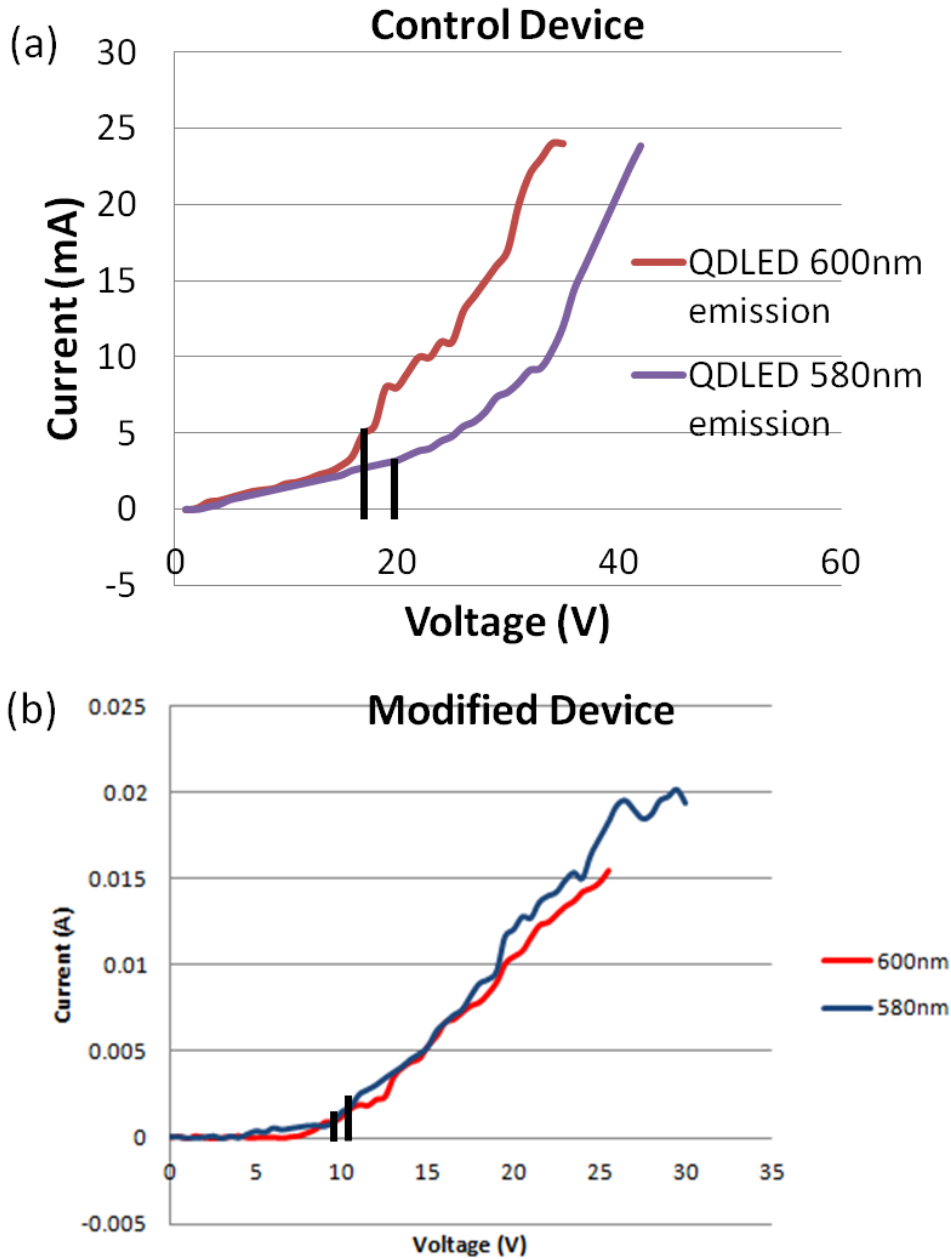


Figure 4.6: Comparisons of QDLED I-V curves. (a) I-V curves for QDLEDs fabricated using basic device design (b) I-V curves for QDLEDs fabricated using modified device design. Bars show turn-on voltage for the particular device

4.4.3 Comparisons of Device Lifetimes

The modifications in our device structure were focused on improving the life times of the device. We expected the modification in the device structure and fabrication methods to eliminate the possible reasons for early device failure.

By using a ZnO nanoparticles spin coated layer for the ETL, we eliminated the amorphous ZnO:SnO₂ sputtered film used in the previous structure. By this we reduce the chances of pin holes and defects in the film leading to better protection of the quantum dot layer from the environment and also from direct contact with the cathode. This reduces rate of degradation of quantum dots leading to longer lifetimes. Spin coating also protected the quantum dots from quenching and degradation which can occur during sputtering.

The addition of the Al₂O₃ layer deposited using ALD and the spin coated NiO layer also helped in increasing the lifetime of the devices. The Al₂O₃ layer ensures that the quantum dots do not come in direct contact with the ITO anode thus reducing damage due to burning of quantum dots. Since we use a NiO film which can be spin coated, a much thicker film (20nm as compared to the previous 5nm) can be used which leads to fewer defects and better protection of the quantum dot layer. Thus the two spin-coated layers of the HTL and ETL encapsulate the quantum dot layer, drastically reducing the environmental damage and degradation of quantum dots and improving the device lifetimes.

We found a dramatic increase in the lifetime of our devices as the modified devices showed more than 12 hours of continuous emissions and could be stored, unencapsulated, at room conditions for 8 months and showed electroluminescence after this storage time as compared to the maximum of 160minutes of continuous electroluminescence obtained from our basic device design.

4.5 SUMMARY

In this chapter we discussed the modifications made to the device structure to improve device performance. . We discussed the experimental results obtained from devices with this modified configuration and compared it with results obtained from our basic design device. We found improvements in three basic areas, a marginal increase in intensity obtained from the QDLEDs, lower average turn-on voltages resulting in better efficiency and a dramatic increase in the lifetime of the devices. In the next chapter we will focus on enhancement of light extraction from the modified devices.

CHAPTER 5: STRATEGIES FOR ENHANCEMENT OF LIGHT EXTRACTION

5.1 INTRODUCTION

In the previous chapter we discussed the improvements achieved in the performance of QDLEDs by implementation of specific modifications to the basic device structure. Specifically we found an increase in device lifetime greater than three orders of magnitude. This improvement was one of the critical factors in the applicability of our QDLEDs in lab-on-chip systems. Another parameter that is important for our application is the intensity of light emission obtained from the QDLEDs. With the modified design we found an average increase in intensity of $\sim 17\%$. However, the QDLEDs designed still face some issues of loss of light energy due to various factors.

One channel of energy loss was due to coupling of Plasmon waves with the metal electrode in the QDLED device structure. This results in waves travelling along the surface of the electrode and being dissipated at the edges, thus reducing the energy obtained at the region of interest, which is the direction perpendicular to the electrode. Figure 5.1 shows examples of electroluminescence from our modified QDLEDs where higher emission can be observed at the edges of the electrodes. Some of the strategies proposed to enhance the light emission obtained from LEDs include substrate modification, incorporation of scattering medium, micro lenses, nanogratings microstructures and so on.

In this chapter we discuss two strategies to enhance the light intensity extracted from the fabricated QDLEDs namely, electrode surface roughening and integration of plasmonic structures with the QDLEDs.

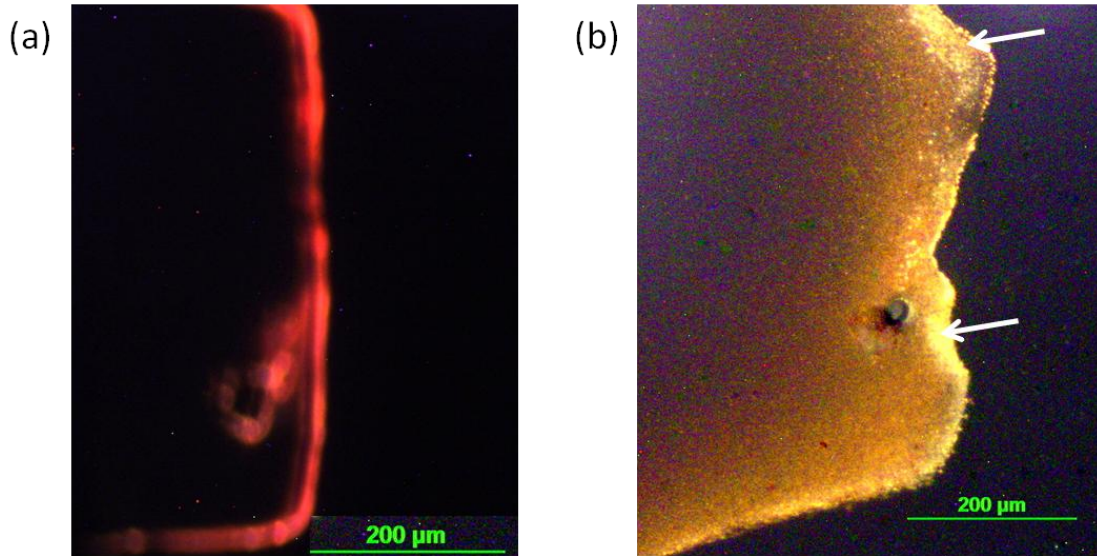


Figure 5.1: Images showing excessive emissions from the edges of the electrode (a) Electroluminescence of 600nm QDLED at 60s exposure time (b) Electroluminescence of 580nm QDLED at 60s exposure time

5.2 SURFACE ROUGHENING

5.2.1 Theory

Surface plasmons are the quanta of surface-charge-density oscillations. Metals support surface plasmons of low energy which can be excited by light. Since one electrode (cathode) of our QDLED structure is metallic and is very close to the QD layer, some of the electroluminescence obtained from the QDLED can be lost as a Surface Plasmon (SP) wave. This energy can be scattered and obtained as light intensity from the opposite end of the LED.

There are many different strategies that can be explored to obtain this result. Surface texturing of the electrodes is one method to improve the intensity obtained from

the LEDs. Figure 5.2 shows the mechanism of scattering observed from a roughened surface [67].

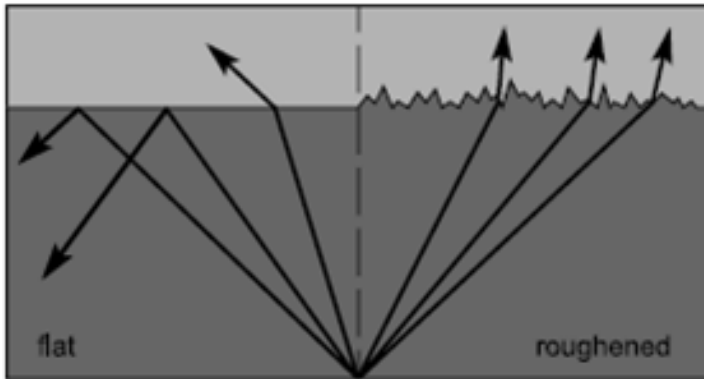


Figure 5.2: Schematic showing the difference between light from a flat surface Vs a roughened surface

A number of surface roughening schemes have been applied to increase the intensity obtained from traditional inorganic LEDs. Nano roughened surfaces prepared by plasma etching showed a significant increase in output power [67]. Other schemes included incorporation of gold and silver nanoparticles in the electrode layer to create a rough surface between the metal electrode and the emissive layer.

5.2.2 Experimental Results

As an initial strategy towards the enhancement of light intensity obtained from the fabricated QDLEDs, we applied the surface roughening strategy which has previously been applied with traditional inorganic LEDs. We modified the QDLED fabrication procedure to create surface roughening of the metal (Al) cathode. This was done by modifying the fabrication of the spin-coated ZnO electron transporting layer. As

discussed in chapter 4, we spin coated a layer of ZnO nanoparticles (10nm diameter) in n-butanol as solvent as the electron transporting layer. This layer formed a thin film between the emissive QD layer and the metal cathode. To introduce surface roughening, we introduced clusters of ZnO nanoparticles in the electron transporting layer, thus causing roughening of the overlying aluminum cathode. Figure 5.3 shows electroluminescence enhancement from one such QDLED with roughened metal surface.

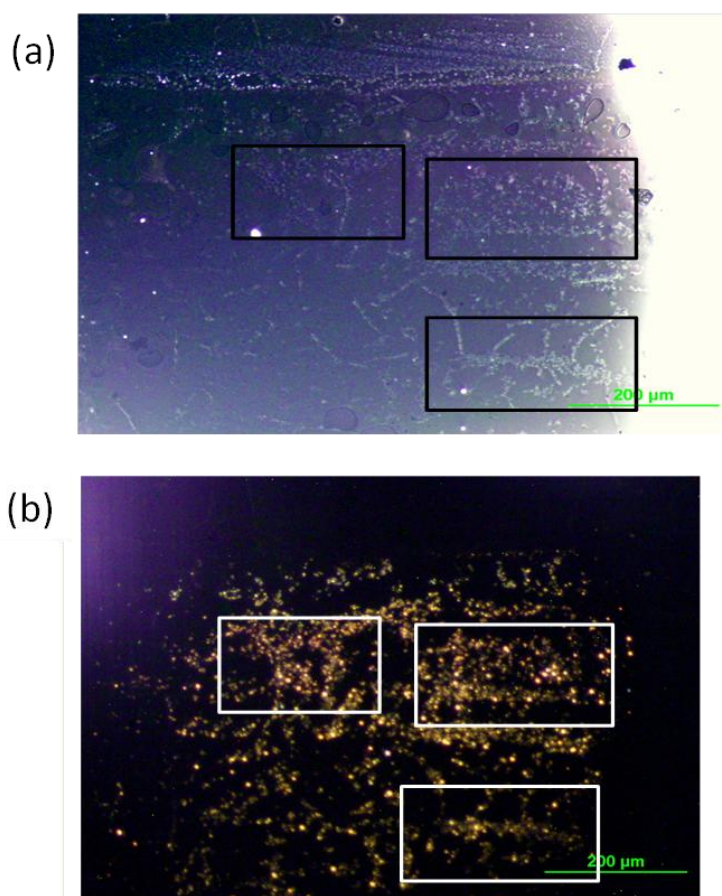


Figure 5.3: Electroluminescence from QDLED with roughened electrode (a) Brightfield image of QDLED electrode with roughened areas highlighted (b) Electroluminescence showing higher intensity from areas corresponding to the roughened electrode areas highlighted

From figure 5.3 we can see that the highlighted areas in the brightfield image which show the roughened electrode surface, match with the increased intensity of electroluminescence observed from the same area. We calculated the intensities of particular areas of both the brightfield image of the electrode and the electroluminescence image using MATLAB. Figure 5.4 shows the comparison of the intensities of one such area.

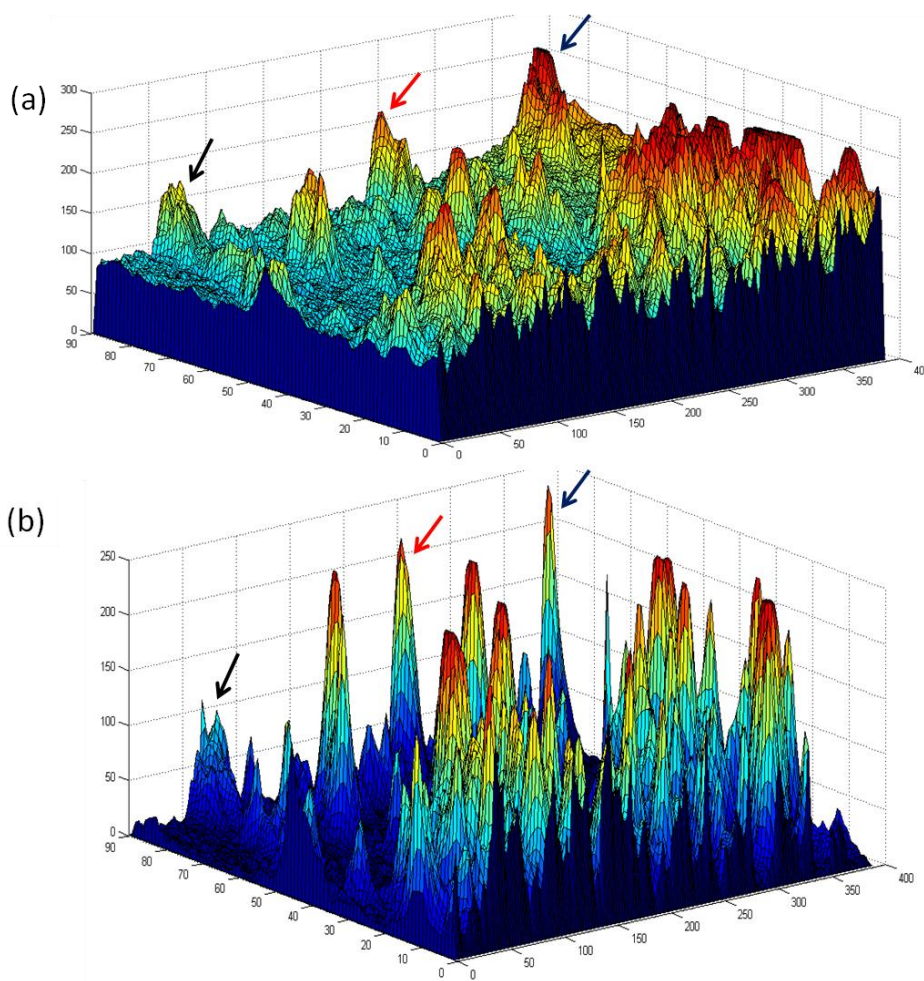


Figure 5.4: Intensity plots of electroluminescence from electrode surface roughening (a)
Intensity plot from a specific area of electrode brightfield image (b)
Intensity plot electroluminescence image

From the figure 5.4 we can see a co-relation between the intensity peaks obtained from the bright field image and from the electroluminescence image. From the figure 5.4(a) the peaks in intensity correspond to the ZnO nanoparticles clusters which cause roughening of the surface of the electrode. Thus from the electroluminescence intensity plot, we see a co-relation between the roughening of the metal electrode and increased electroluminescence intensity.

However, this method of surface roughening faces some problems which limit its applicability in our QDLEDs. It is difficult to create clusters of nanoparticles over large areas of the QDLED resulting in non-uniform intensity. Clusters of ZnO cause areas of excessive charge transport compared to the remaining area of the QDLED. This can result in device instabilities and reduced lifetime. To overcome these drawbacks, we investigate the integration of plasmonic grating patterns with our QDLEDs.

5.3 PLASMONIC GRATING PATTERN

The resonant response of diffraction gratings is usually associated with sharp field variations over a narrow frequency or angular band. Since the first observation [68] and confirmation [69, 70] by Wood and Rayleigh, these phenomena have been widely studied by many researchers, including Fano [71] who offered a breakthrough in the theoretical understanding of these resonant anomalies. The widely accepted mechanism on which they are based, as pointed out by several seminal papers [71, 72], consists in the complex field interaction of guided modes supported by periodic gratings. The accurate prediction of the dispersion of these modes has been greatly simplified with the advent of rigorous vector models, and the concept of coupled resonances [73,74] has become a topic of interest, envisioning new applications of optical gratings. Recent studies [75. 76, 77, 78,

79] have shown the potential of local oscillators arrays coupled with the impinging light, and some of them have reported significant suppressed transmission [68, 69, 70, 78, 79] at resonance, despite their thin features

5.3.1 Design of Plasmonic Grating Pattern

The design of the pattern used for integration of our QDLEDs was based on a number of considerations based on our QDLED design. We designed a two-dimensional grating structure based on metal-dielectric-metal (MDM) plasmonic waveguide structure. By realizing coupled resonance modes in this easily modeled geometry, we showed that an effective control of resonant suppression of transmitted light could be achieved. Depending on the resonance mode and its resulting standing wave, the designed mechanism is highly selective to the frequency of operation.

We design a structure with, periodic gratings of periodicity p and slit width w_s . In this configuration, we assume that the slit width w_s and dielectric thickness t_D are small compared to the wavelength of operation λ , and that the metal thickness t_M is significantly thicker than the skin depth at the frequency of operation, conditions that ensure the propagation of only one fundamental mode in the MDM waveguide formed by the two perforated metal screens. The frequency bandgap of resonant suppression of transmitted light can be achieved by designing the adjustment of values for w_s , t_D , and t_M .

For our application, we required highest resonant suppression at 580nm since we fabricated QDLEDs with emission wavelength of 580nm emission wavelength. From analytical calculations, we defined the parameters of the grating designed. We defined the slit width to be 70nm, the thickness of the metal to be 50nm and thickness of dielectric

layer to be 50nm. Figure 5.5 shows the schematic of the designed plasmonic grating structure.

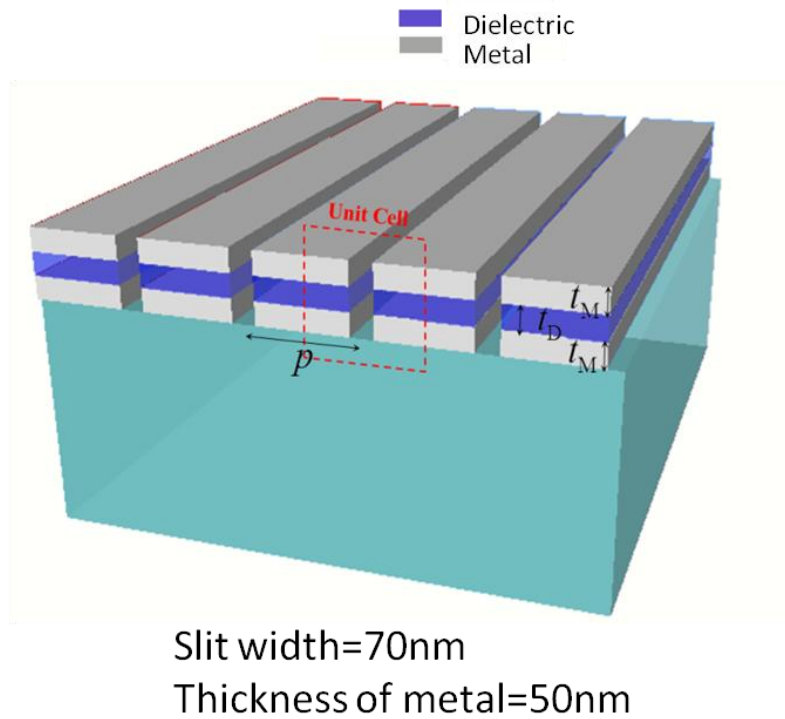


Figure 5.5: Schematic of designed Plasmonic grating structure showing specific calculated design conditions

5.3.2 Simulation Results

With the design described in the previous section, simulations were performed to calculate the expected increase in observed light intensity due to the reflection of transmitted Plasmon waves. For the simulation, we considered a point source of light (QD) placed close to a metal surface. We show simulation results first from a quantum dot source close to a plain metal surface which represents our current QDLED structure.

The simulation results can be seen in Figure 5.6. As we can see a major part of the QD emission is seen to be lost through the Surface Plasmon waves transmitted along the plain surface of the metal (electrode) Figure 5.6 (b) shows simulations for a QD source placed close to a MDM surface with the patterned plasmonic grating structure. From the simulation results we can see a marked increase in the intensity observed in the direction perpendicular to the metal surface. From the simulation results we expect an increase in intensity of $\sim 40\%$, observed in the direction perpendicular to the metal surface.

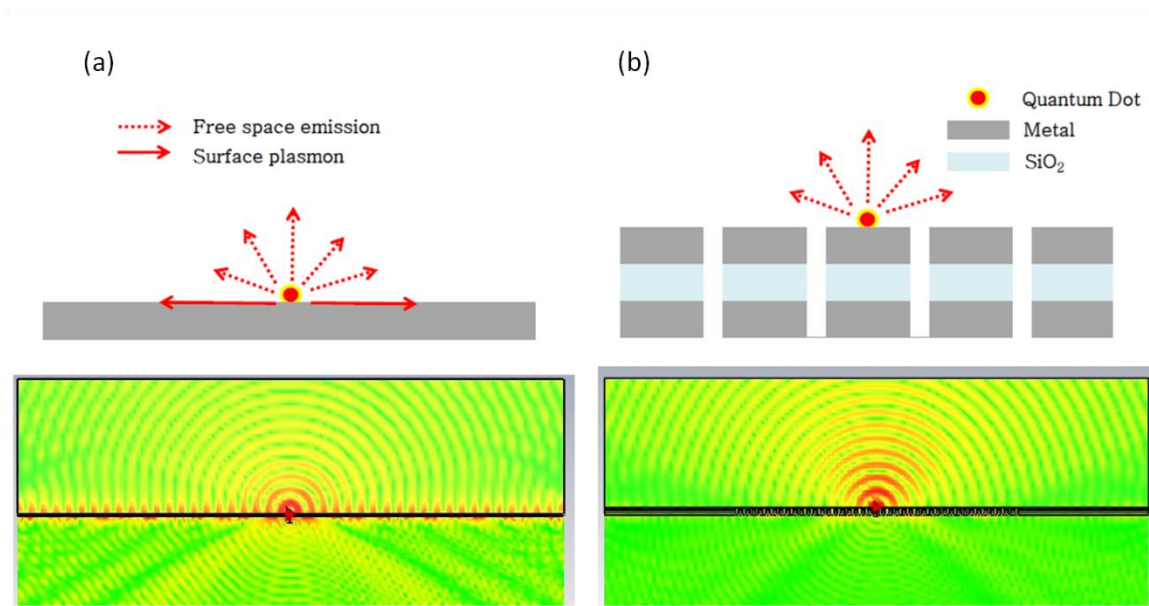


Figure 5.6: Simulation results from Plasmonic grating structure. (a) Results from a QD source placed close to a plain metal surface. (b) Results from a QD source placed close to a MDM surface with Plasmonic grating pattern.

5.3.3 Fabrication

We first fabricated the plasmonic grating structure for photoluminescence experiments with quantum dot light sources. A structure was fabricated by sputtering of Al-ITO-Al (MDM) layers of 50nm thickness each on a glass substrate. For sputtering of Al and ITO, the UNIVEX-450 sputter system was used. Al was deposited using DC sputtering in an Argon environment at a high vacuum of 10^{-6} torr. The deposition rate used was 10A/s. ITO was deposited using RF sputtering in the presence Argon gas at 10^{-6} torr chamber pressure. A deposition rate of 10A/s was used. The entire structure was fabricated on a glass substrate. The three layers were deposited successively without removing the sample from the vacuum chamber.

The grating pattern was fabricated on this structure by using focused ion beam (FIB) milling technique. For this, the FEI x835 dual beam system consisting of a Gallium source for ion beam deposition and also including electron beam imaging capability was used. The total area of fabricated pattern was $\sim 25\mu\text{m} \times 15\mu\text{m}$. Figure 5.7 shows Scanning Electron Microscopy (SEM) images of the fabricated pattern at different magnifications. The images show the milled pattern. At a higher magnification, slit width can be measured to be $\sim 70\text{nm}$ as required by the design. The slit width and depth of pattern is controlled during fabrication by the dwell time of the focused ion beam at each point of the pattern. Longer exposure of the sample to the ion beam causes damage to the sample. For this reason, the ion beam imaging is switched off during the milling. After the milling of the complete pattern, images are taken with the electron beam imaging system included in the FEI tool.

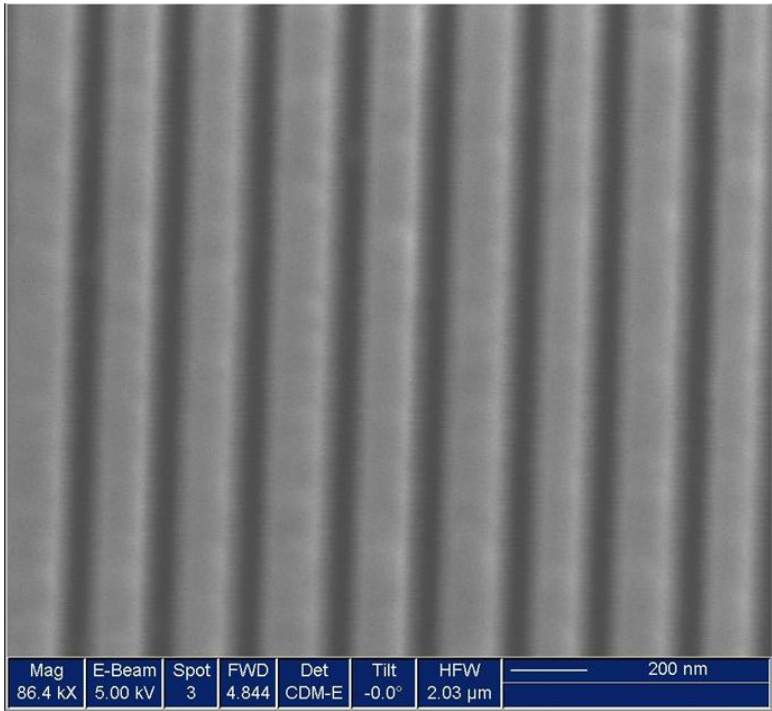
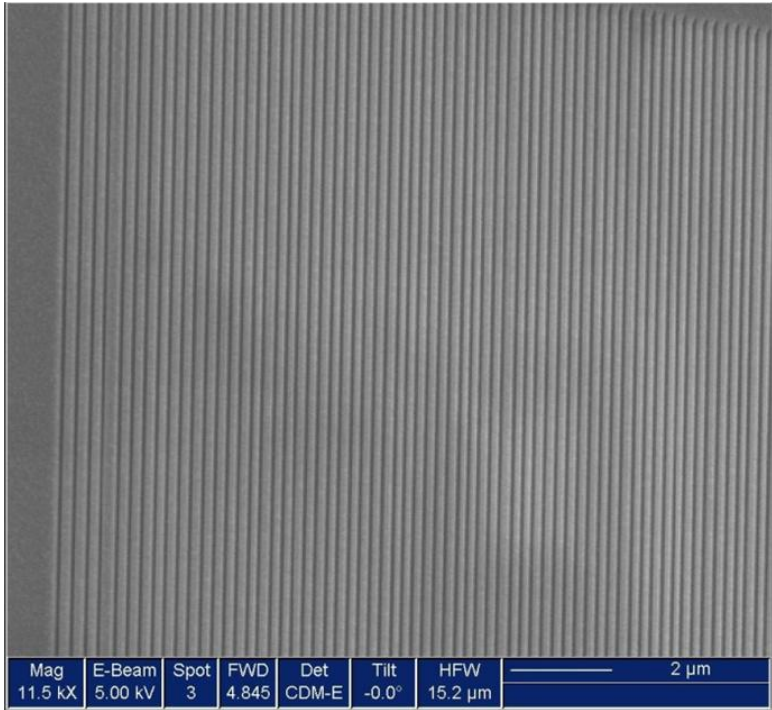


Figure 5.7: SEM images of fabricated plasmonic grating structure at two magnifications (11.5kX and 86.4kX)

5.3.4 Photoluminescence Experiments

To demonstrate the reflection of SP waves from our Plasmonic grating pattern, we first performed experiments using the photoluminescence property of QDs. After the fabrication of the MDM surface and the Plasmonic grating pattern on a glass substrate, a thin film of QDs was deposited on this structure by spin coating CdSe/Zns (core/shell, EM=580nm) QDs suspended in chloroform. 5 μ l of colloidal QDs in toluene were resuspended in 20 μ l of chloroform for this purpose.

This sample was then mounted on a microscope for imaging. The spin-coated QD film was excited using an external UVLED source. A UV filter was used to eliminate stray and reflected UV light from the sample. Images were obtained using various magnifications and exposure times. Figure 5.7 shows QD emission images obtained at various magnifications for the area of the grating structure. We could observe the enhanced emission from the region of the grating structure when compared with the surrounding plain metal surface.

The increase in emission intensity was calculated using MATLAB image processing software. QD emission images were taken for the grating structure at 10X, 20X and 40X magnifications with exposure times of 40s, 50s and 60s each. For each image, the area of the grating structure was selected and average intensity over that area was calculated. For each image, this value was then compared with the maximum intensity from a similar sized area in the same image. A percentage increase in intensity was calculated from this data. An average of the percentage increase from each image was then calculated. Figure 5.8 shows a sample of the photoluminescence images taken to show the increased radiation from the grating structure.

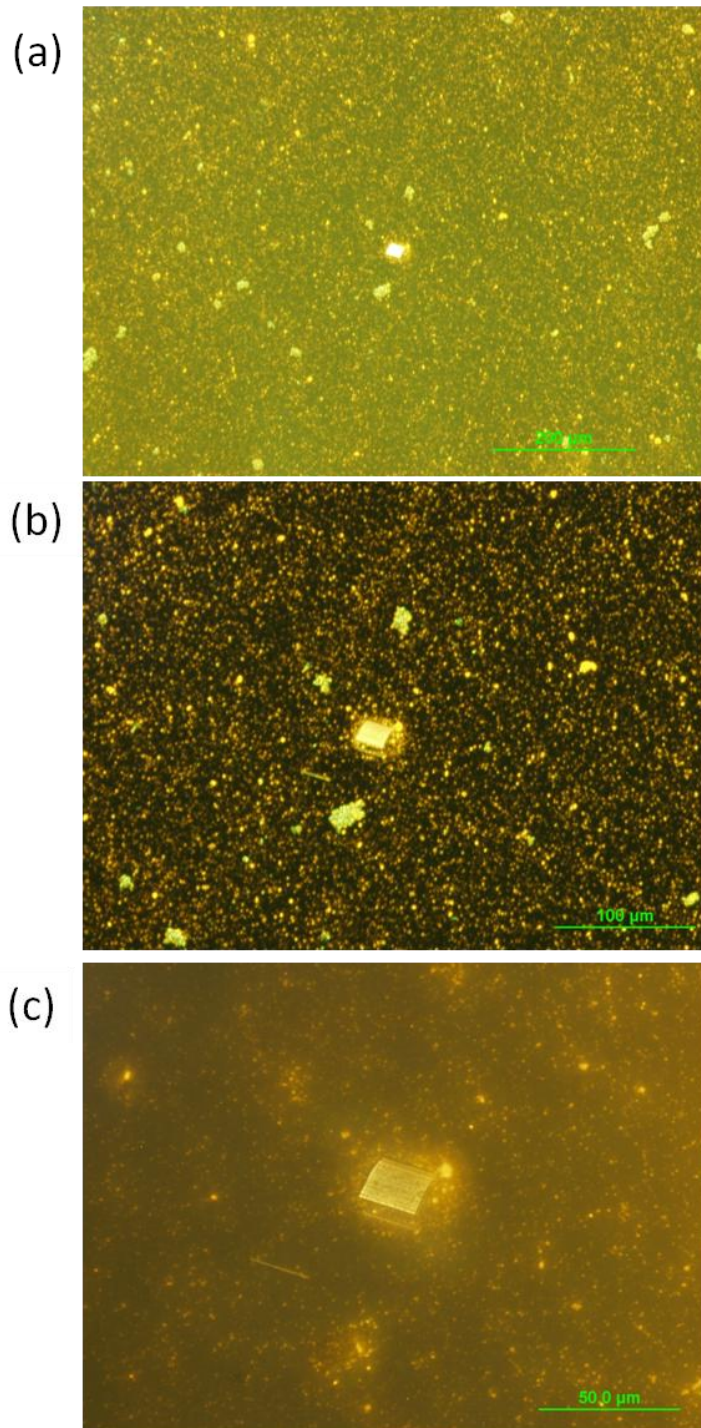


Figure 5.8 Photoluminescence images of grating structure (a) 10X magnification 60s exposure (b) 20X magnification 60s exposure (c) 40X magnification 60s exposure

In Figure 5.8 we can clearly see a higher intensity of emission from the QDs in the area of the grating structure. From the photoluminescence experiments, using QD excitation with a UVLED source, we found an average of 32.63% increase in intensity from the grating structure as compared to the emission from QDs deposited on the plain metal surface.

5.3.5 Wavelength Selectivity

From the theory and simulation results, we expected the plasmonic grating structure to show sharp characteristic bandgap selectivity. Our design was optimized to have the highest suppression of transmission waves at 580nm. Figure 5.9 shows transmission spectra for incident light from two such designed plasmonic grating structures. From the figure we can see that the bandgap can be tailored for specific wavelengths by changing the unit cell dimension p .

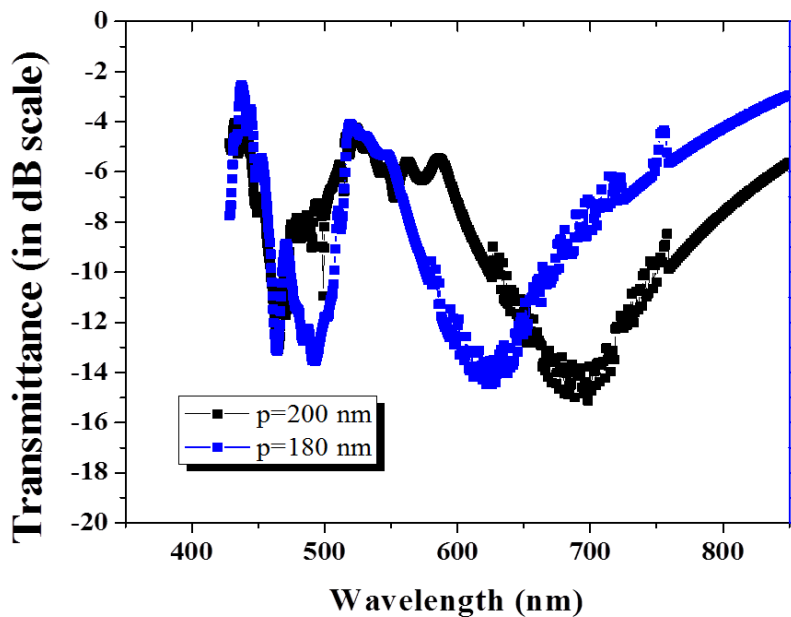


Figure 5.9: Light transmission spectra from plasmonic grating structures

The data in figure 5.9 was obtained by using a wideband light source in combination with a spectrometer. The light was made incident on to the grating structure and the transmitted intensity was measured. From this, we show that dimensions of the grating structure define spectral properties of the device.

To measure the spectral characteristics of our fabricated device, to verify highest transmission at our desired wavelength of 580nm we tested its spectral selectivity as follows. After the fabrication of the plasmonic grating pattern as previously described, we prepared a solution of QDs of various emission wavelengths in chloroform. This mixture of the combination of QDs was spin coated on top of the fabricated device to form a thin film. After this, the sample was mounted on a fluorescence microscope and the QD layer was excited using a UVLED source. Filters corresponding to the individual QD wavelengths in the film were used to obtain images of intensity from the individual components of the various wavelength sources (QDs of various emission wavelengths) present on the grating structure. Images were obtained at various magnifications (10X, 20X and 40X) and different exposure times (60s, 50s and 40s). For each image, intensity of the particular wavelength component at the grating structure area was calculated. Similarly, in each image, another area of highest intensity apart from the area of the grating structure was identified. The intensities of these areas (highest intensity apart from the grating structure) were normalized. These were used as weights while normalizing the intensities of emission from the grating structure. The remaining procedure for each individual emission wavelength was identical to the procedure followed for the photoluminescence imaging. After calculating the increased emission from the grating structure for each individual wavelength, the data was normalized using the weighting parameters previously calculated. Table 5.1 shows the wavelengths of the QDs used; the individual intensity differences obtained and normalized intensities for the

wavelengths used. Figure 5.10 shows the increase in light emission at various wavelengths, due to the grating structure.

Wavelength (nm)	Intensity increase (A.U.)	Normalized Intensity
400	7094.342	0.160318
450	20942.53	0.47326
520	21046.76	0.475616
550	27782.96	0.627841
580	44251.61	1
660	16486.91	0.372572
700	4304.177	0.097266
400	7094.342	0.160318

Table 5.1: Increased intensity from grating structure for various individual emission wavelengths

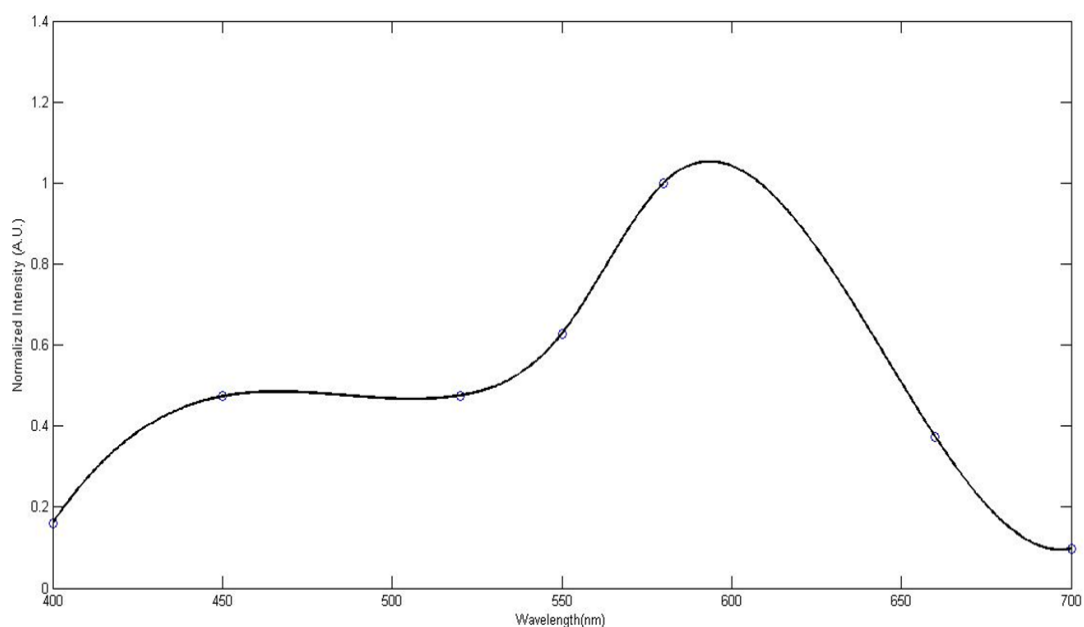


Figure 5.10: Wavelength selectivity of plasmonic grating structure

5.4 INTEGRATION OF PLASMONIC GRATINGS WITH QDLEDs

After the fabrication and testing of the plasmonic grating structures using photoluminescence properties of quantum dots, the next step was the integration of these structures with our QDLEDs to obtain an increased intensity from the QDLEDs. To achieve this result, certain changes had to be made in the QDLED device design to accommodate the integration of a working plasmonic grating device.

5.4.1 Design Changes in QDLED

Since the design of the plasmonic grating structure requires a metal-dielectric metal structure, we added layers of ITO and Al on top of the existing Al cathode to form a MDM structure with each layer of 50nm thickness. The design of the QDLED structure with the added layers is shown in figure 5.11.

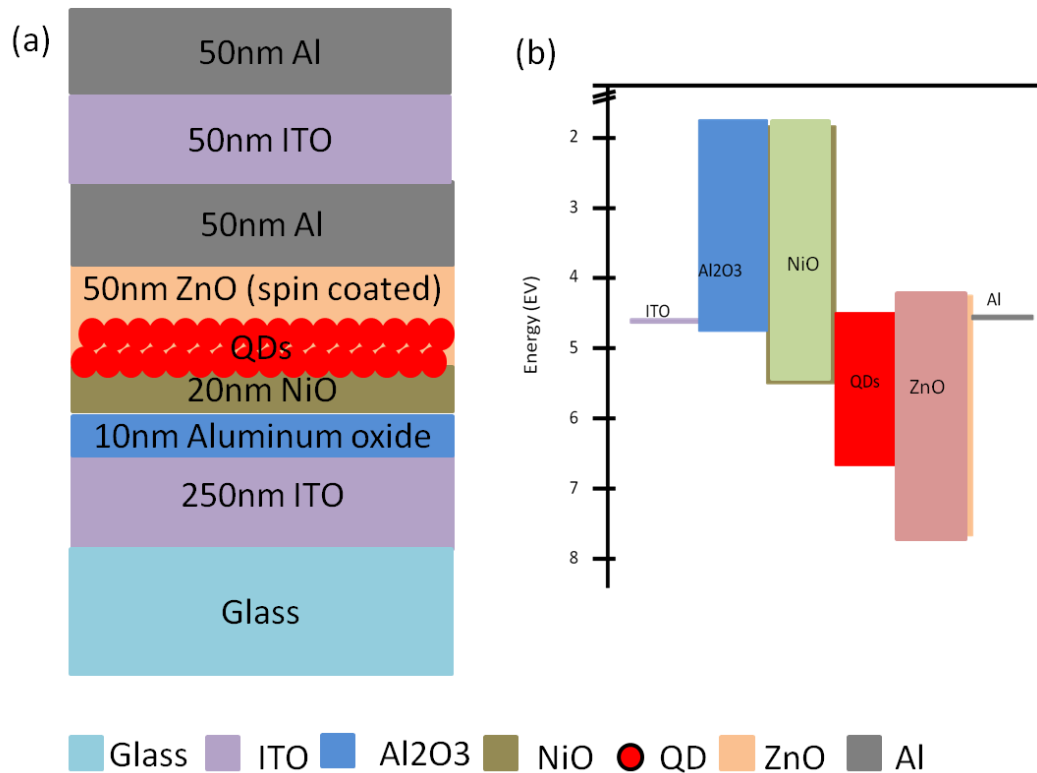


Figure 5.11: Schematic of changes in QDLED structure for plasmonic grating integration (a) Schematic of cross-section of complete QDLED structure (b) Energy band diagram of QDLED

5.4.2 Fabrication of Integrated Device

The first change in the fabrication of the QDLED was the increase in cathode from 30nm to 50nm which was made during sputtering of the Al cathode. Following this, a hard mask was created to create areas on the cathode for electrical contacts. The remaining areas of the cathode were covered by sputtered films of ITO of 50nm thickness followed by another Al layer of 50nm thickness. The fabrication procedure for the remaining layers of the QDLED was identical to the fabrication procedure described in chapter 4. In short, ITO was sputtered on the glass substrate using the RF sputtering at the

rate of 30A/s. A hard mask was used to pattern the ITO electrodes. The sputtered ITO was annealed at 400C for 60 minutes in the presence of O₂. Atomic Layer deposition (ALD) was used to grow a 5nm thick Al₂O₃ layer on top of the ITO. This was done at the rate of 0.92A/cycle at 250C. For the HTL, 20nm thick nickel oxide layer was spin coated at 1500 rpm for 60s. Nickel acetate tetrahydrate was dissolved in methanol at 0.5M concentration and used to spin coat the NiO layer. The sample was annealed for 60 minutes at 120C to form a film with uniform texture.

QDs (Emission Wavelengths: 580nm) were suspended in chloroform and spin coated on top of the NiO layer to form a 30nm thick layer. Spin coating was done at 3500 rpm for 60 seconds. The sample was then baked at 90C for 10 minutes to remove the solvent.

Following this, the solution-processed ZnO layer was deposited. 2% weight solution of ZnO nanoparticles (size: 10nm) was prepared in n-Butanol. The solution was sonicated for 10 minutes and then spin coated on top of the QD layer at 2000rpm for 60 seconds to form a 50nm thick film. The sample was then baked at 90C for 10 minutes to remove the solvent. Aluminum cathodes were patterned using a hard mask and 50nm thick Al was sputtered at the rate of 3A/s.

After the Al-ITO-Al layer fabrication, the plasmonic grating structure was patterned on the QDLED by following the method described in the previous section, using focused ion beam milling technique.

5.4.3 Electroluminescence Experiments

Figure 5.12 shows the experimental setup for the electroluminescence experiments. The QDLED with the integrated plasmonic pattern was mounted on an

optical microscope (Olympus BX-51) with an attached RGB CCD camera. Voltage was applied across the QDLED identical to the procedure followed during the electroluminescence experiments described in the previous chapter.

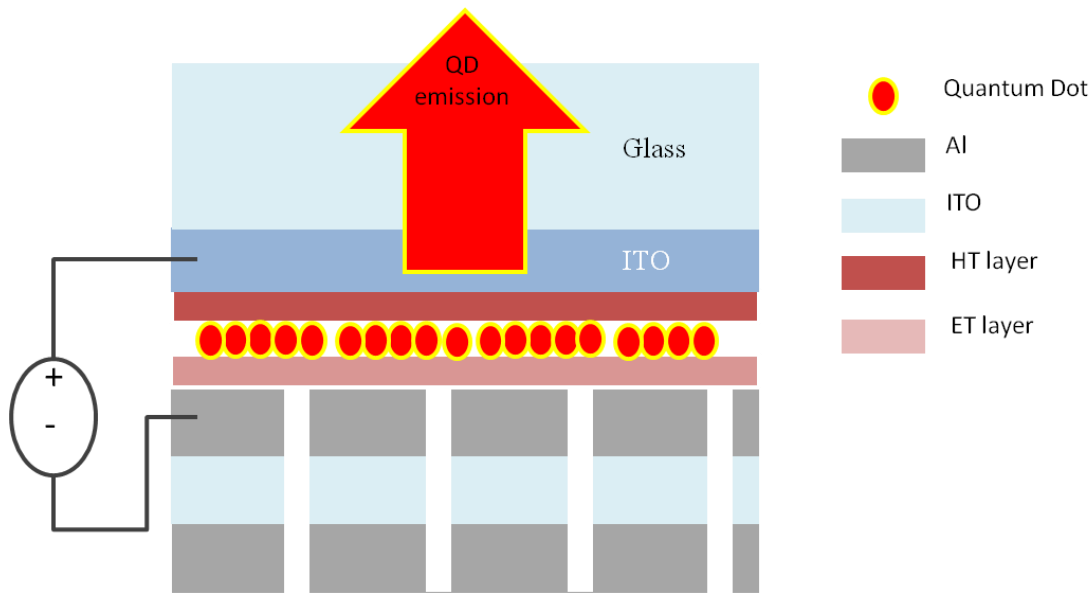


Figure 5.12: Schematic of experimental setup for electroluminescence testing of plasmonic grating structure.

Testing of electroluminescence of the QDLED was first done before the patterning of the plasmonic grating structure. Images were obtained at 60s exposure time and 10X magnification. The intensity from these images was used as the control for calculation of change in intensity upon the integration of the plasmonic pattern. After the fabrication of the plasmonic grating structure, images were obtained under identical conditions of voltage applied (8V), exposure time (60s) and magnification (10X). These electroluminescence results are shown in figure 5.13.

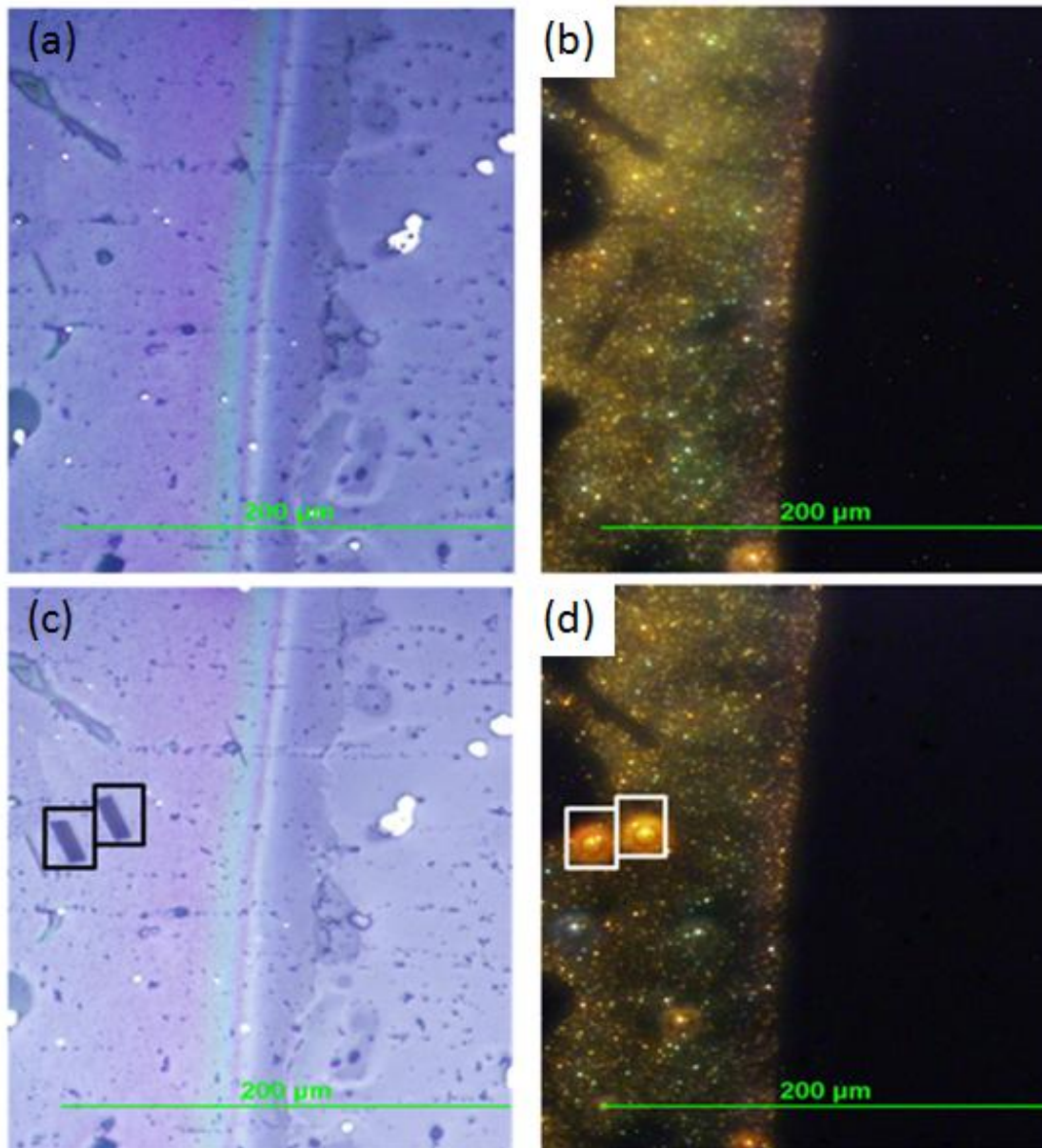


Figure 5.13: Electroluminescence results from patterned grating structure (a) Brightfield image of QDLED before patterning. (b) Electroluminescence image of QDLED before patterning of grating structure (c) Brightfield image of QDLED showing patterned integrated grating structures (highlighted) (d) Electroluminescence image of QDLED showing increased intensity of electroluminescence from areas of patterned grating structure (highlighted).

From Figure 5.13 we can see a significant increase in the electroluminescence intensity after integration of the plasmonic grating structure as compared to the electroluminescence intensity from the same area of the QDLED prior to the plasmonic patterning.

The percentage increase in intensity was calculated by using MATLAB. Intensity from the same area of the QDLED was measured before and after the patterning of the plasmonic grating structure and the difference in intensity was calculated. We found an increase in intensity of 34.72% due to the patterning of the grating structure.

5.5 SUMMARY

In this chapter we discussed two strategies to enhance the intensity of emissions obtained from our QDLEDs. The first strategy of surface roughening presents an easy, quick way of increasing the emission intensity. However this strategy could not be finely tuned or controlled. The second strategy involved integration of a plasmonic grating pattern with our QDLED to suppress SP waves resulting in higher emissions in the direction perpendicular to the metal electrode. We discussed the fabrication procedure and changes in the QDLED device structure. We presented results from experiments performed and calculated an average increase of 34.72% in the intensity of electroluminescence and an increase of 32.63% in the photoluminescence intensity from QDs. In the next chapter we will discuss the application our devices as light sources for cellular imaging.

CHAPTER 6: IMAGING OF BIOLOGICAL SAMPLES

6.1 INTRODUCTION

In this chapter we demonstrate the capability of our multicolor QDLEDs fabricated on a single substrate, to be used as a light source in lab-on chip type imaging systems for imaging of biological samples. For this purpose, we show results from imaging of stained cells with our fabricated devices as the light source.

We use the different types of devices fabricated, including QDLEDs with the basic design discussed in chapter 3, QDLEDs with the modified design discussed in chapter 4 and QDLEDs with integrated plasmonic grating structures to image cells. We quantify the imaging capabilities of these different designs to show the improvement in imaging quality achieved from modifications in the device structure.

We show the capability of our LEDs to image cells and detect morphological characteristics of cells. In order to show the excitation capability of our device, we integrated our planar QDLEDs with a cancer cell line. Excitation from QDLEDs with two different emission wavelengths allowed us to determine nucleus-to-cytoplasm ratio, one of the key characteristic properties of cancer cells.

6.2 IMAGING OF CANCER CELLS

Figure 6.1 shows a schematic of the setup used for imaging cells using electroluminescence from QDLEDs. Multicolor (EM 580nm and 600nm) fabricated on a single substrate were placed under a microscope and a stained cancer cell sample is placed over the QDLEDs and is observed using the microscope. We imaged MDA MB-231 breast cancer cells stained with HEMA-3 dye in our experiments.

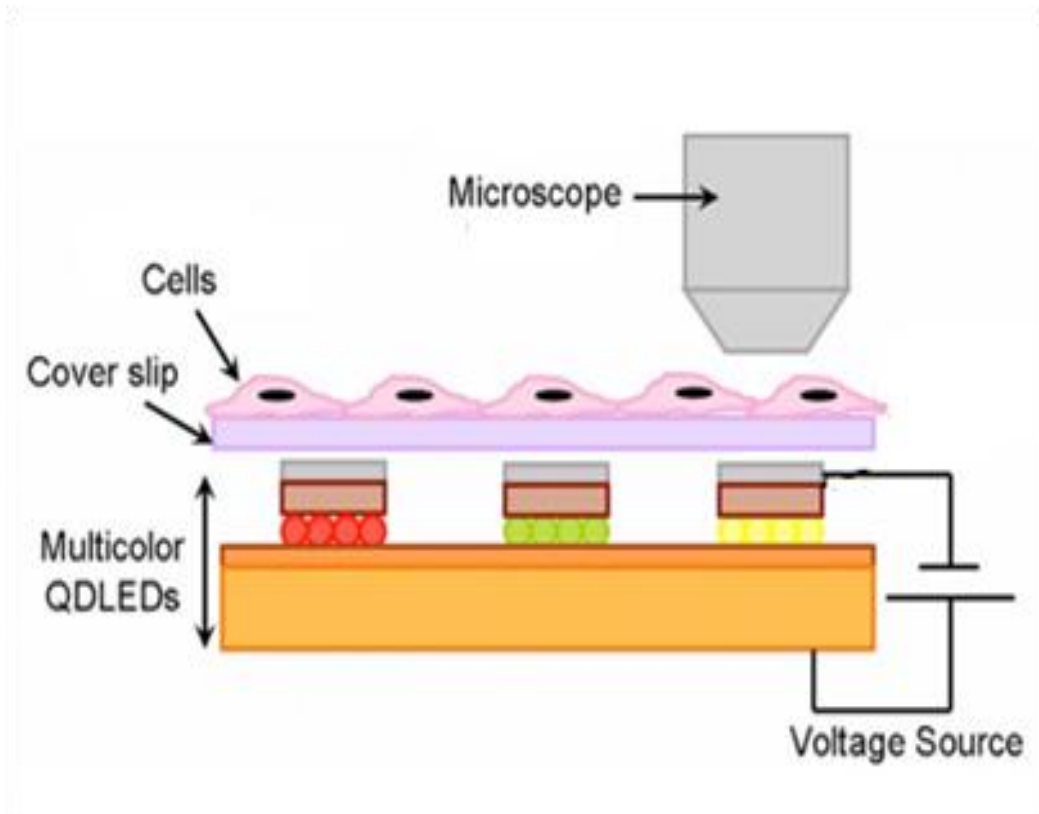


Figure 6.1: Schematic of experimental setup for imaging of cells using QDLEDs.

6.2.1 Experimental Conditions

We used breast cancer cells as the imaging samples. MDA-MB 231 cell line was derived from a female patient with breast cancer [80] at the MD Anderson Cancer Center, and has been shown to be highly metastatic in mice [81,82]. This cell line has been used in a large number of breast cancer studies [83]. Breast cancer is the most common cause of cancer death in women. It has been shown that early detection can lead to increased survival rates and early screening enables studying the dependence of survival rates on stage of diagnosis. We used the MDA-MB 231 as the primary cell line to observe

absorption at two different wavelengths (580nm and 600nm) when stained with HEMA 3 dye. The MDA-MB 231 cells were maintained in a cell culture medium and cleaned coverslips were placed in the petri dish for cell culture. These cells were then stained with HEMA 3 dye to stain the nucleus and cytoplasm. A brightfield image is shown in figure 6.2

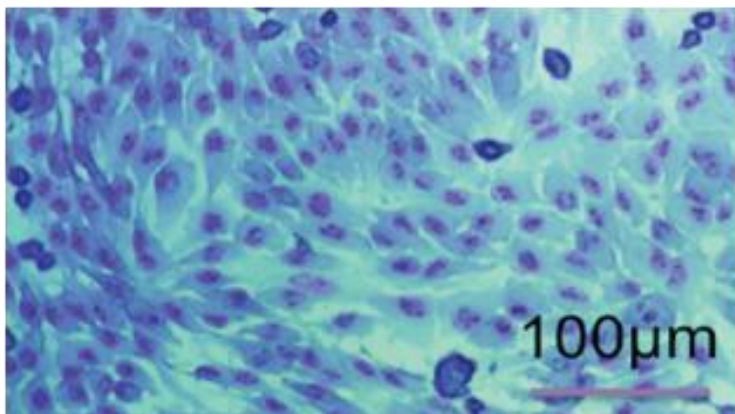


Figure 6.2: Brightfield image of cultured and stained MDA 231 cells [41]

We chose HEMA 3 dye to stain our sample cells. HEMA 3 stain is a modified quick Wright-Giemsa staining method [84]. The staining process takes 30 seconds and the samples are air dried. Typically, cell samples on glass slides are first dipped into methanol which is the fixative for 5 seconds. After that, the sample is dipped into a mixture of sodium azide, potassium phosphate monobasic, sodium phosphate dibasic, eosin Y and water for 5 seconds. This stains the cytoplasm and collagen part of the cell. Following this, the sample is dipped into a combination of azure A, sodium azide, potassium phosphate monobasic, sodium phosphate dibasic, methylene blue and water for 5 seconds. This stains the nucleus of the cell [41].

The absorption and transmission spectrum of the HEMA3 dye measured using UVVIS system is shown in figure 6.3.

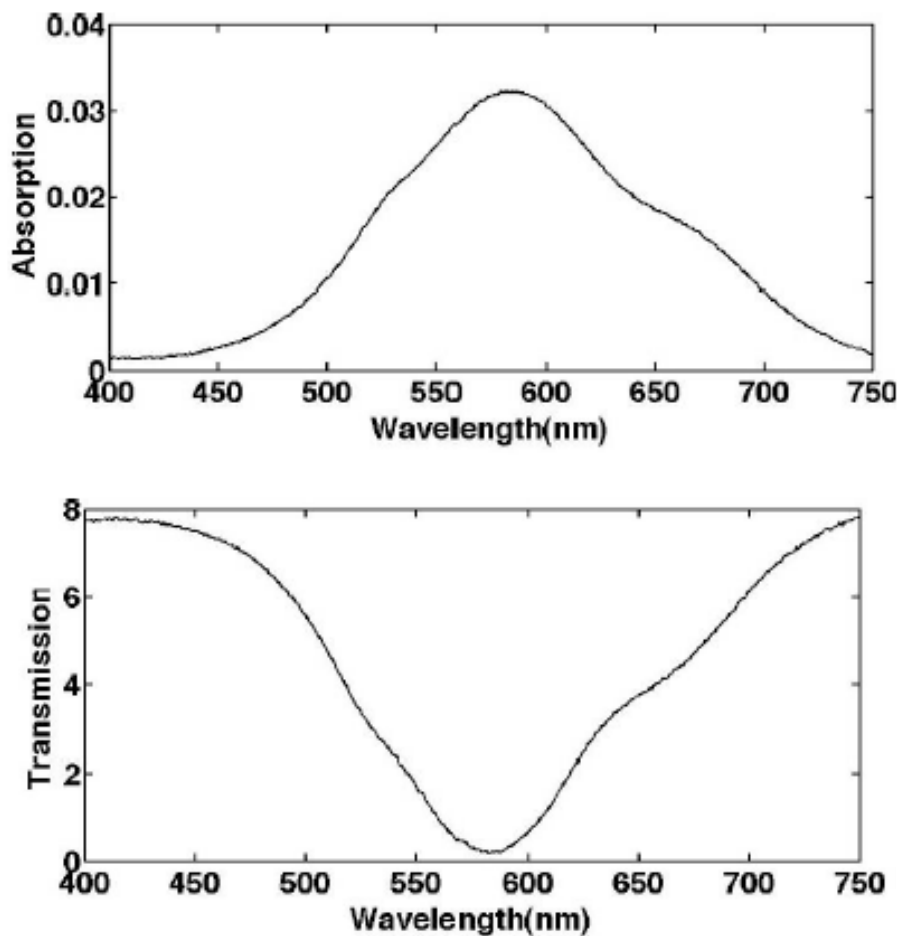


Figure 6.3: Absorption (top) and Transmission (bottom) characteristics of HEMA 3 dye [41].

From the figure 6.3, we can see that the absorption spectrum of the HEMA-3 dye is from 540nm-620nm with a peak at 580nm.

For imaging of cells using electroluminescence of QDLEDs, we used cells cultured on cover slips. Due to this the cells to be imaged could be kept very close to the

QDLED source. The distance between the sample and the diode was maintained within $100\mu\text{m}$. We excited the sample cells at two wavelengths 580nm and 600nm. We expected the nucleus to absorb the 580nm excitation indicating decrease in intensity at the nucleus as compared to the 600nm source. Using multispectral data for imaging single cells we can determine the nucleus to cytoplasm ratio which can be used to determine the developmental stage of cancer cells. We performed imaging experiments to show the efficacy of the various designs of our QDLEDs.

6.2.2 Imaging with Photoluminescence

As control experiments, we first performed imaging experiments by using the photoluminescence from QDs. Figure 6.4 shows an image of the setup used for photoluminescence of QDs used for cell imaging.

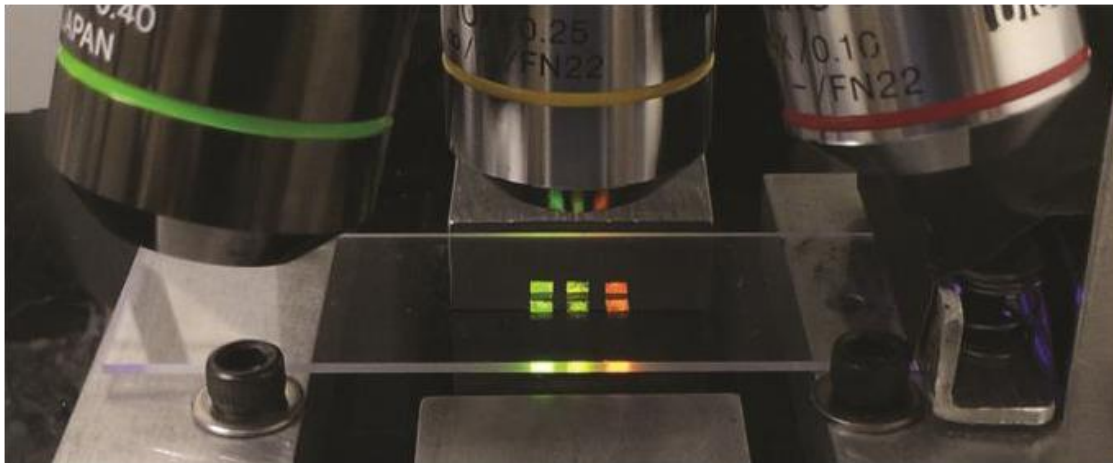


Figure 6.4: Setup for photoluminescence imaging of stained cells.

On a cleaned glass slide, films of QDs (EM=580nm and 600nm) were transferred using micro-contact printing technique described in chapter 3. A UV light with the

emission wavelength peak at 365 nm from a high-power LED (200mW) was focused and introduced inside a glass slide. An evanescent field was induced on the glass slide surface due to the total internal reflection of the transmitted UV light. The QD films were excited using this field. Since the UV evanescent field on the glass slide decays quickly in the near-field and does not transmit energy in the far-field, the UV light intensity observed with the microscope was negligible compared to that of the excited QDs.

The coverslip with the stained cell samples was placed on top of the QD films. This resulted in a very small distance (thickness of coverslip < 150 μ m.) between the light source (excited QDs) and the sample. Images were acquired using Olympus BX-51 microscope without the use of any filters.

Images were taken with both RGB CCD and monochromatic CCD at the two wavelengths in the visible region. The nucleus-cytoplasm ratio was measured which is one of the important factors in cancer cell identification and characterization. Cancer cells tend to have larger nucleus/cytoplasm ratio than other cells. This criterion is often applied in computer based cancer cell analysis such as the study of cellular response to drugs.

Figure 6.5 shows images of HEMA 3 stained cells obtained by using UV excitation of QD films as a light source (a) shows an image obtained with a 580nm QD emission wavelength and (b) shows an image obtained with 600nm QD emission wavelength. Images are at 10X magnification.

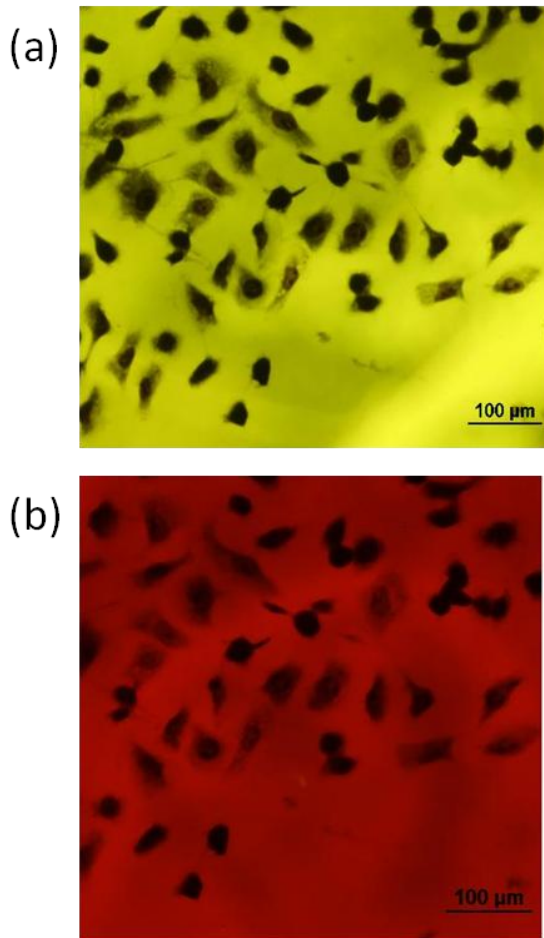


Figure 6.5: Excitation of same region using two sources (a) 580nm (b) 600nm

From Figure 6.5 we observed higher absorption of the 580nm source by the nuclei of the stained cells. This was expected as the absorption characteristics of the HEMA 3 stain show a peak at 580nm

6.2.3 Imaging with Electroluminescence

After successfully imaging cancer cells using photoluminescence from quantum dots, the next experiment was to use electroluminescence from QDLEDs to image stained cancer cells. The fabricated QDLED structure was mounted under the microscope and

voltage was applied across the device. The coverslip with stained cells was placed over the working region of the QDLED. The focus of the microscope was adjusted to observe the stained rather than the QD emission. In this case there was a greater distance between the light source and the stained cell sample. This was because we observed electroluminescence of the QDLEDs through the 20nm NiO layer, the 250nm ITO layer and the glass substrate (1 mm thickness). The stained cells on the coverslip (150 μm) are placed on top of this glass substrate. Due to this added distance between the light source and the sample, when the microscope is focused on the coverslip, we could not observe any specific patterns or defects in our QDLED sources due to the limited depth of focus at higher magnification. This also limited the magnification which could be used to image the cells since the intensity of light reaching the cells was not enough to obtain images at a very high magnification.

We used all the different types of QDLEDs fabricated, namely, QDLEDs with basic sputtered design, QDLEDs with modified spin coated design and QDLEDs with integrated plasmonic grating structure to obtain images of cells. Figure 6.6 shows cell images obtained with QDLEDs fabricated using the modified spin coated device structure with emission wavelengths of 580nm and 600nm. Images are obtained using both RGB and monochromatic CCDs. The transmission intensity across cells was measured using both the emission wavelengths. Intensity of transmission was measured using ImageJ image processing software. As expected, according to the transmission characteristics of the HEMA 3 stain we found maximum absorption of the 580nm light by the nucleus and lower absorption of the 600nm light source.

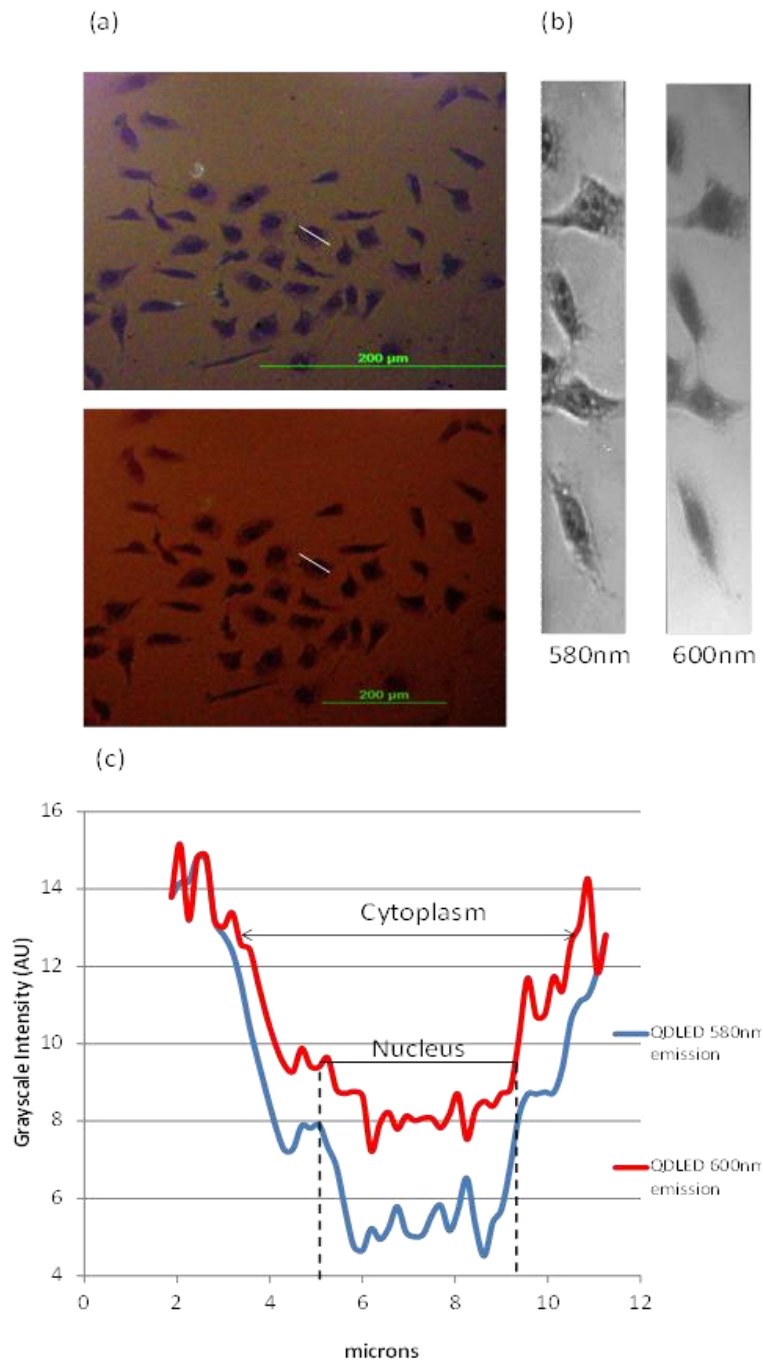


Figure 6.6: Imaging of cells with electroluminescence from modified QDLED structure (a) Images with RGB CCD (580nm top and 600nm bottom) (b) Images with monochromatic CCD (c) Intensity profile across the same cell with 580 and 600nm light sources.

The shape of the nucleus is clearly shown in the image with 580nm illumination. The profile with 600nm is unclear and boundary lines are hidden in the noise level. On the other hand, excitation with QD600 is suitable for observation of the inside of the nucleus. The two types of QD light sources can be therefore used for imaging different cellular structures. RGB images were taken with 300s exposure time at 10X magnification and the monochromatic images were taken at 900s exposure time at 10X magnification for each image.

6.3 COMPARISONS OF IMAGING RESULTS

We used the capability of our devices in the imaging of cells as a parameter to define the efficacy of our devices. For testing this, we imaged the HEMA 3 stained cells using devices fabricated using each of our structure designs described in the previous chapters. The ratio between the absorption of the excitation light by the nucleus and that by the cytoplasm for a particular wavelength (eg. 580nm) is defined by the signal to noise ratio, which depends on the intensity of the light source.

Following this, comparisons between two light sources can be made by comparing the data obtained from cell imaging, using the two devices as excitation light sources for the cell imaging. A higher intensity difference is obtained between the cytoplasm and nucleus in a case where a higher intensity of light is obtained from the QDLED. This directly affects analysis as the sizes of the nucleus and cytoplasm become easier to measure, resulting in easier identification of cancer cells based on nucleus and cell morphology. Figure 6.7 shows images of cells taken with the basic QDLED design and the modified QDLED design. Comparison of the intensity profiles of cell images obtained with both types of QDLEDs is shown.

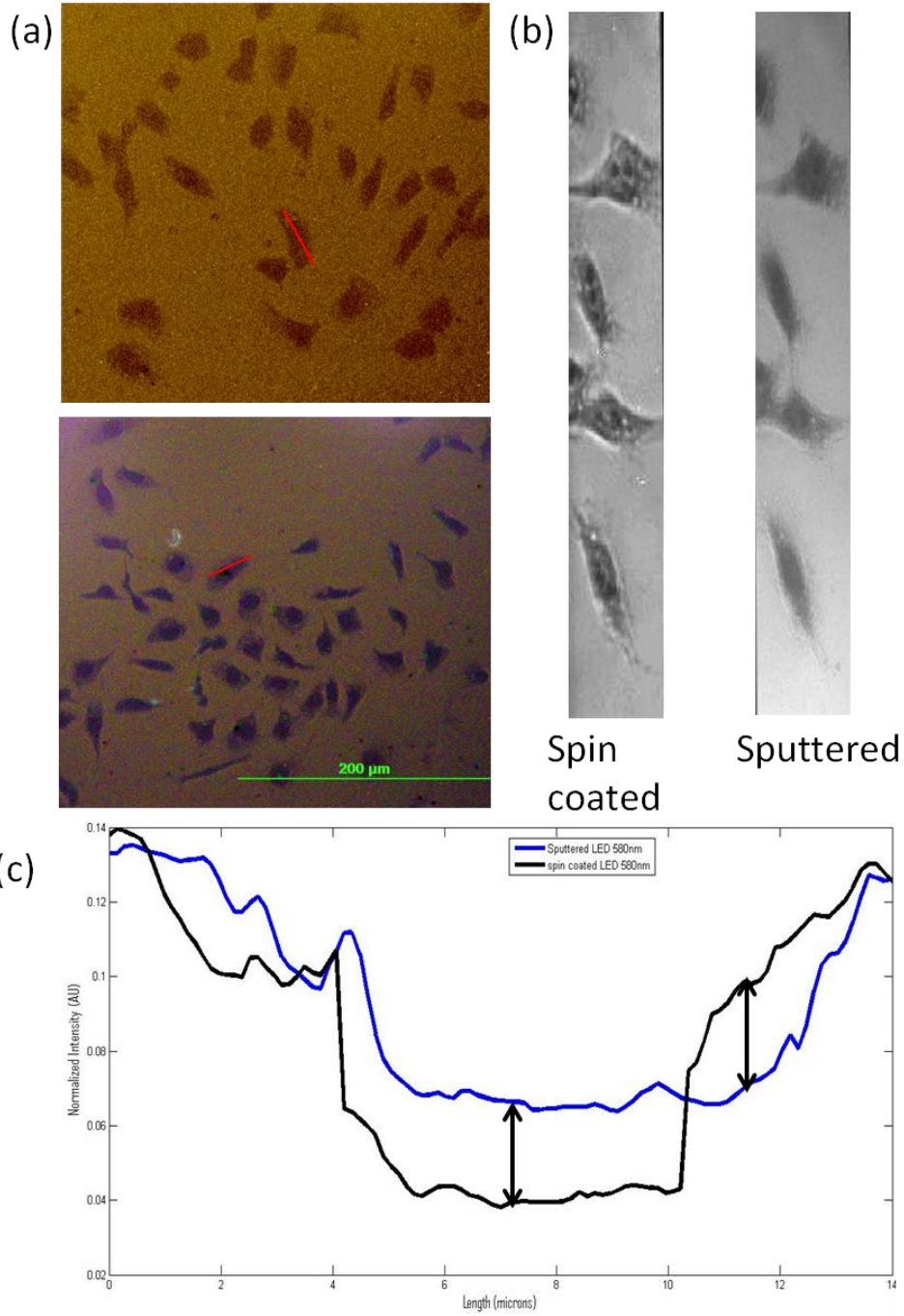


Figure 6.7: Imaging of cells with electroluminescence from two QDLED structures (a) Images with RGB CCD (basic design top and modified device bottom) (b) Images with monochromatic CCD (c) Intensity profile across single cells imaged with basic and modified devices

From figure 6.7 we saw that a higher contrast was achieved between the transmission intensities of the nucleus and cytoplasm of a single cell, with the use of QDLEDs fabricated using the modified structure. As we have already shown in chapter 4, a higher intensity was achieved using the modified QDLED design and hence the results achieved from the cell imaging were consistent with expected results. In figure 6.7 we show results obtained by using QDLEDs with emission wavelength of 580nm.

From the imaging results shown so far, one constraint that our QDLEDs face as light sources for cell imaging is low intensity. Due to this we were unable to acquire images of greater magnification with good signal to noise ratio. All images acquired with these QDLEDs were at a maximum magnification of 10X and a long exposure time of 300 seconds was used. To acquire high quality images at higher magnifications, an increase in light source intensity is required.

As shown in chapter 5, we improved the intensity of light extracted from the modified design of our QDLEDs by integrating a plasmonic grating structure with the metal cathode of our device. We used the increased electroluminescence intensity from our device with the integrated plasmonic grating structure to image the same cells stained with HEMA 3 dye. The results from this imaging are shown in figure 6.8. The increased intensity also allowed for imaging at a higher magnification of 20X with 300s exposure time, using the RGB CCD. We also show a better contrast between the cytoplasm and nucleus which indicates a better signal to noise ratio and thus an increased efficiency of the applicability of our devices as light sources for cell imaging. Figure 6.8 (a) shows the intensity profile of a cell images at 10X magnification and 300s exposure time and (b) shows the intensity profile of a cell images at 20X magnification and 300s exposure time.

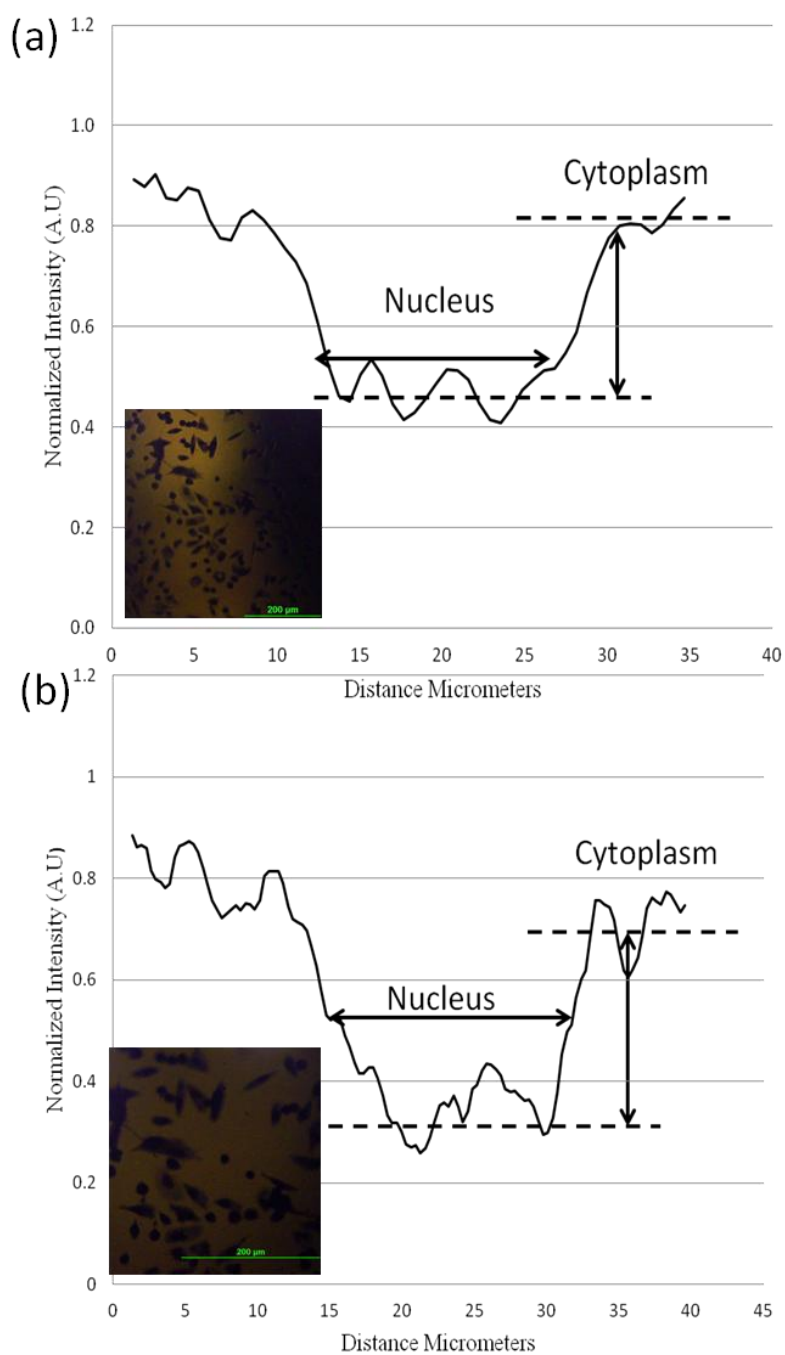


Figure 6.8: Intensity profiles of a cell imaged with electroluminescence from QDLED with plasmonic structure (a) Cell imaged at 10X magnification and 300s exposure time (b) Cell imaged at 10X magnification and 300s exposure time. Insets show images with RGB CCD at specified magnifications

Another advantage with imaging at a higher magnification is that we can image cell structures that cannot be distinguished at a lower magnification and intensity. Figure 6.9 shows examples of cells imaged both at 10X and 20X magnifications where a greater detail can be observed from the 20X images

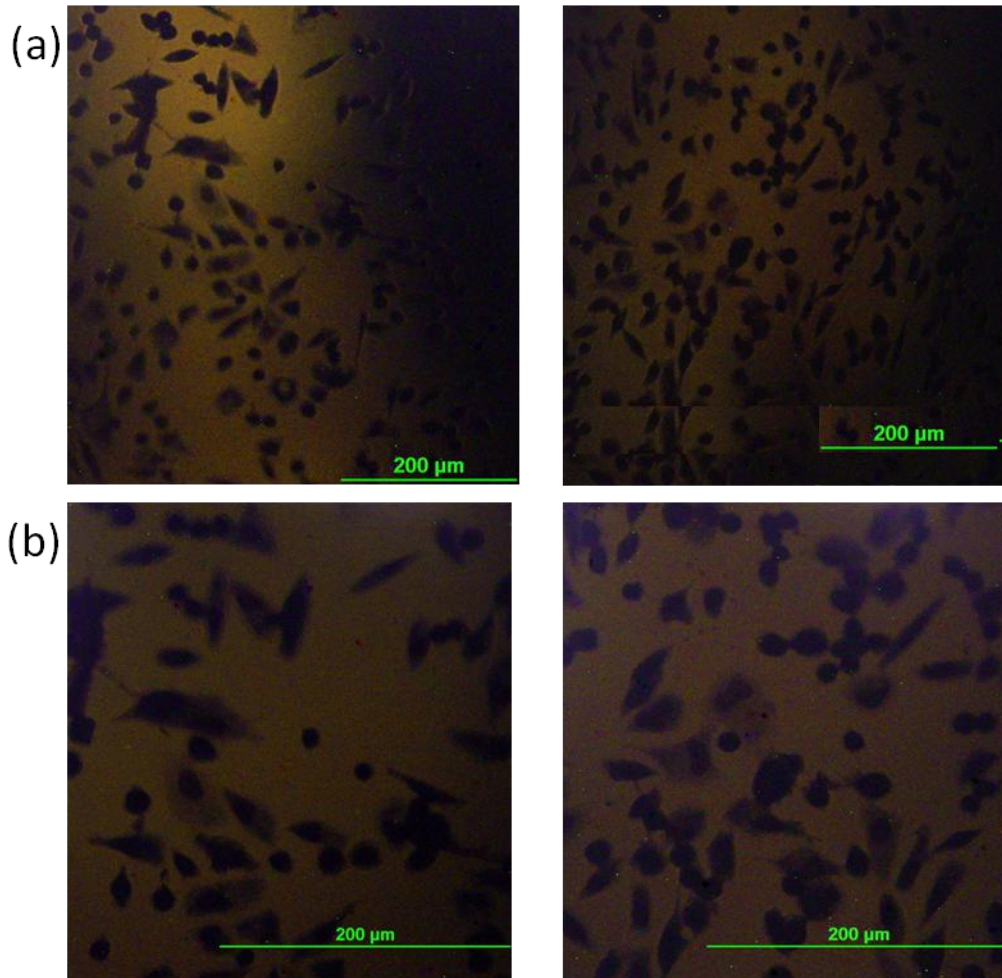


Figure 6.9: Electroluminescence Images of cells using QDLED with integrated plasmonic structure at 580nm, and 300s exposure time (a) 10X magnification, (b) 20X magnification

6.4 SUMMARY

In this chapter we discussed the applicability of our fabricated QDLED devices as light sources for imaging of stained cell samples. We showed preliminary results to demonstrate the use of our devices as single emission wavelength devices and showed the advantages that the modified structure device designs offer to the use of our devices in our target application. We discussed parameters which were used to quantify the improvements in the applicability of our devices and compared the imaging results obtained by imaging the same cells using our different device designs. We showed that the multiple emission wavelengths can be advantageous in the imaging of stained cells. Finally we show the advantages of fabricating multicolor light sources on a single substrate.

CHAPTER 7: CONCLUSIONS AND FUTURE WORK

7.1 CONCLUSIONS

In this thesis we have discussed the fabrication of colloidal quantum dot based light emitting diodes for applications in cellular imaging. We demonstrated the capability of fabricating multicolor quantum dot based patterned devices on a single substrate. Fabrication of compact, planar, patterned and individually addressable devices on a single substrate can be easily integrated with lab-on chip imaging systems and micro total analysis systems.

We first created QDLEDs with inorganic charge transport layers on a glass substrate. For the fabrication of these devices we used the basic design discussed in some seminal papers on this topic. The design was modified to suit our multicolor patterning requirement by using micro-contact printing to deposit the emissive QD layer on the substrate. These devices were fabricated using sputtering of charge transport layer below and over the emissive QD layers. Electroluminescence was achieved from this basic QDLED device and various operating parameters were analyzed to devise changes in the design to improve the performance of the inorganic based QDLEDs.

Upon analysis of the performance characteristics achieved from the basic QDLED design, we found two main areas of possible improvements. One was the working lifetime of the device that could be achieved and the second was the maximum intensity output obtained from the QDLEDs. Our approach to improving these performance characteristics was to make changes in the materials used and fabrication techniques applied to target specific drawbacks of the initial device.

We initially focused on improving the lifetime of the device. We demonstrated a technique of fabricating completely solution processed charge transport layers. We used a spin coated NiO hole transporting layer below the QD layer and a solution processed ZnO nanoparticles electron transporting layer overlying the emissive QD layer. The ZnO layer with low energy levels facilitated the transport of electrons while suppressing the hole leakage current from the HTL to the ETL. ZnO nanoparticles showed low quenching of excitons formed in the QD layer as compared to the quenching observed when using other metal oxides formed using sputter or thermal annealing.

Solution processing of the charge transport layers allowed for simpler fabrication process and more robust film as compared to films formed by sputtering. The robust spin-coated NiO layer in addition to an aluminum oxide insulating layer between the anode and the HTL improved the stability of the structure increasing the lifetime of the QDLEDs. We showed electroluminescence from these devices and an improvement in the stability of the devices due to the use of a more robust charge transport layers and the use of an aluminum oxide layer as an insulating layer. We showed a continuous working lifetime of more than 12h and a shelf life of more than 240 days upon testing of unencapsulated devices stored and tested at room condition. The average lifetime for devices with sputtered charge transport layers is shown to be less than 10h of continuous emission and a shelf life of less than 5 days was observed for both structures with sputtered metal oxide layers as well as structures with organic charge transport layers. We thus achieved a more than threefold increase in the total lifetime of the QDLEDs, increasing its applicability for long term use as light sources integrated with lab-on-chip systems.

Our next goal was on increasing the extraction of light intensity from our QDLEDs. Although modifications in device design applied for improvement to device

lifetime resulted in a marginal improvement in device intensity, we applied the technique of electrode surface patterning to achieve additional improvements in emission intensity from device. From the analysis of the original device design, we observed that a part of the emission from our QDLED structure was lost in the form of surface Plasmon waves travelling along the surface of the plain metal electrode which lies in the direction perpendicular to our direction of observation. We designed a plasmonic grating structure to achieve resonant suppression of transmission waves along the metal surface causing reflection of the surface plasmons resulting in higher observed intensity in the direction of observation. The pitch period of the designed grating structure defined the wavelength bandgap for which resonant suppression occurred.

We designed the structure with parameters compatible with the emission wavelength of interest to us (580nm) and performed simulations to study the expected increase in emission intensity. From the simulation results, we expected ~40% increase in emission intensity in the direction of observation.

We integrated this pattern with our fabricated QDLEDs and performed experiments with both photoluminescence and electroluminescence. In summary, we have experimentally demonstrated that the integration of plasmonic grating patterns with QDLEDs can increase the intensity of emissions obtained from the QDLED by scattering the surface plasmons coupled with the metal electrode of the QDLED. We found an increase of 34.72% in the intensity of electroluminescence and an increase of 32.63% in the photoluminescence intensity from QDs.

To show the potential application of our device as a light source for imaging of biological samples, we imaged HEMA3 stained breast cancer cells. We performed imaging of these cells using electroluminescence from QDLEDs with both 580nm and 600nm emission wavelengths. Images were acquired using both device designs and

QDLEDs with integrated plasmonic grating structures. We showed the feasibility of using QDLEDs as light sources in lab-on-chip imaging systems and from comparisons of various device structures proved the value added to the QDLEDs as light sources for our target application by the modifications introduced in the QDLED structure.

7.2 FUTURE WORK

The results in this dissertation provide insights to several key directions in which this research can move forward. One area of further research includes further improvements in the device design. These can include the use of a combination of organic and inorganic charge transport layers with additional layers for hole and electron suppression to avoid charge carrier leakage, thus improving the device performance. Other improvements can be the use of flexible substrates to increase the applicability of the devices. Integration of plasmonic structures can also be further researched to achieve directional beaming and further improvements in device intensities. Many methods of patterning of QDs are also currently being researched which can be implemented in our device structure to achieve better uniformity of emission.

Another application of our QDLEDs that can be explored is hyperspectral microscopy. Gold nanoparticles with specific spectral signatures can be used for labeling of cells. QDLEDs with specific emission wavelengths can be used as the source. Absorption of each wavelength can be measured to plot spectrum observed from samples to identify the existence of nanoparticles labeled biological samples. Thus a chip-based hyperspectral imaging system can be investigated.

References

- [1] X. Cui, X. Heng, C. Yang, "Optofluidic Microscope - A Complete On-Chip Imaging Device", *Imaging, Manipulation, and Analysis of Biomolecules, Cells, and Tissues VI*, Vol. 6859, 68590Y, (2008).
- [2] M. Adams, M. Enzelberger, S. Quake, A. Scherer, "Microfluidic integration on detector arrays for absorption and fluorescence micro-spectrometers", *Sensors and Actuators A*, 104 (2003) 25-31.
- [3] Atakan Gurkan, S. Moon, H.Gecki, F. Xu, S.Wang, T. Jian Lu and U.Demirci, "Miniaturized lensless imaging systems for cell and microorganism visualization in point-of-care testing", *Biotechnol. J.* 2011, 6, 138–149.
- [4] C. D. Chin, V. Linder and S. K. Sia, "Lab-on-a-chip devices for global health: Past studies and future opportunities", *Lab Chip*, 2007, 7, 41–57.
- [5] G. Stybayeva, O. Mudanyali, S. Seo et. al., "Lensfree Holographic Imaging of Antibody Microarrays for High-Throughput Detection of Leukocyte Numbers and Function", *Anal. Chem.* 2010, 82, 3736–3744.
- [6] A. Ozcan And U. Demirci, "Ultra Wide-Field Lens-Free Monitoring Of Cells On-Chip", *Lab Chip*, 2008, 8, 98–106.
- [7] A. Coskun, T-W. Su And A. Ozcan, "Wide Field-Of-View Lens-Free Fluorescent Imaging On A Chip", *Lab Chip*, 2010, 10, 824–827.
- [8] W. Bishara, T-W. Su, A. F. Coskun, And A. Ozcan, "Lensfree On-Chip Microscopy Over A Wide Fieldof-View Using Pixel Super-Resolution", *Optics Express*, Vol. 18, No. 11 (2010).
- [9] G. M. Whitesides, "The Origins And The Future Of Microfluidics," *Nature* 442, 368-373 (2006).
- [10] J. El-Ali, P. K. Sorger, And K. F. Jensen, "Cells On Chips," *Nature* 442, 403-411 (2006).
- [11] X. Heng, D. Erickson, L. R. Baugh, Z. Yaqoob, P. W. Sternberg, D. Psaltis, And C. H. Yang, "Optofluidic Microscopy - A Method For Implementing A High Resolution Optical Microscope On A Chip," *Lab On A Chip* 6, 1274-1276 (2006).
- [12] W. Bishara, S. O. Isikman, And A. Ozcan, "Lensfree Optofluidic Microscopy And Tomography", *Annals Of Biomedical Engineering*, Vol. 40, No. 2, February 2012 (_ 2011) Pp. 251–262.
- [13] Caruge, J.-M., Halpert, J. E., Bulovic', V. & Bawendi, M. G. "Nio As An Inorganic Hole-Transporting Layer In Quantum-Dot Light Emitting Devices", *Nano Lett.* 6, 2991–2994 (2006).
- [14] Coe-Sullivan, S., Woo, W. K., Steckel, J. S., Bawendi, M. G. & Bulovic', V. "Tuning The Performance Of Hybrid Organic/Inorganic Quantum Dot Light-Emitting Devices". *Organic Electron.* 4, 123–130 (2003).
- [15] Zhao, J. Et Al. "Efficient Cdse/Cds Quantum Dot Light-Emitting Diodes Using A Thermally Polymerized Hole Transport Layer". *Nano Lett.* 6, 463–467 (2006).

- [16] Mueller, A. H. Et Al. "Multicolor Light-Emitting Diodes Based On Semiconductor Nanocrystals Encapsulated In Gan Charge Injection Layers". *Nano Lett.* 5, 1039–1044 (2005).
- [17] Colvin, V. L., Schlamp, M. C. & Alivisatos, A. P. "Light-Emitting Diodes Made From Cadmium Selenide Nanocrystals And A Semiconducting Polymer". *Nature* 370, 354–357 (1994).
- [18] Hikmet, R. A. M., Talapin, D. V. & Weller, H. "Study Of Conduction Mechanism And Electroluminescence In Cdse/Zns Quantum Dot Composites". *J. Appl. Phys.* 93, 3509–3514 (2003).
- [19] L. A. Kim, P. O. Anikeeva, S. A. Coe-Sullivan, J. S. Steckel, M. G. Bawendi, And V. Bulovic, "Contact Printing Of Quantum Dot Light-Emitting Devices," *Nano Letters*, Vol. 8, Pp. 4513-4517, 2008
- [20] A. Gopal, K. Hoshino, S. Kim, And X. Zhang, "Multi-Color Colloidal Quantum Dot Based Light Emitting Diodes Micropatterned On Silicon Hole Transporting Layers," *Nanotechnology*, Vol. 20, P. 235201, 2009.
- [21] A. Gopal, K. Hoshino, And X. Zhang, "Photolithographic Patterning Of Subwavelength Top Emitting Colloidal Quantum Dot Based Inorganic Light Emitting Diodes On Silicon," *Applied Physics Letters*, Vol. 96, P. 131109, 2010.
- [22] P. Fenter, F. Schreiber, V. Bulovic, And S. R. Forrest, "Thermally Induced Failure Mechanisms Of Organic Light Emitting Device Structures Probed By X-Ray Specular Reflectivity," *Chemical Physics Letters*, Vol. 277, Pp. 521-526, 1997.
- [23] V. L. Colvin, M. C. Schlamp, And A. P. Alivisatos, "Light-Emitting Diodes Made From Cadmium Selenide Nanocrystals And A Semiconducting Polymer," *Nature*, Vol. 370, Pp. 354-357, 1994.
- [24] Caruge, J.-M., Halpert, J. E., Bulovic', V. & Bawendi, M. G. "Nio As An Inorganic Hole-Transporting Layer In Quantum-Dot Light Emitting Devices", *Nano Lett.* 6, 2991–2994 (2006).
- [25] Coe-Sullivan, S., Woo, W. K., Steckel, J. S., Bawendi, M. G. & Bulovic', V. "Tuning The Performance Of Hybrid Organic/Inorganic Quantum Dot Light-Emitting Devices". *Organic Electron.* 4, 123–130 (2003).
- [26] Zhao, J. Et Al. "Efficient Cdse/Cds Quantum Dot Light-Emitting Diodes Using A Thermally Polymerized Hole Transport Layer". *Nano Lett.* 6, 463–467 (2006).
- [27] Mueller, A. H. Et Al. "Multicolor Light-Emitting Diodes Based On Semiconductor Nanocrystals Encapsulated In Gan Charge Injection Layers". *Nano Lett.* 5, 1039–1044 (2005).
- [28] Colvin, V. L., Schlamp, M. C. & Alivisatos, A. P. "Light-Emitting Diodes Made From Cadmium Selenide Nanocrystals And A Semiconducting Polymer". *Nature* 370, 354–357 (1994).

- [29] Hikmet, R. A. M., Talapin, D. V. & Weller, H. "Study Of Conduction Mechanism And Electroluminescence In Cdse/Zns Quantum Dot Composites". *J. Appl. Phys.* 93, 3509–3514 (2003).
- [30] Caruge, J.M., Halpert, J.E., Wood, V., Bulovic, V., And Bawendi, M.G., Colloidal Quantum-Dot Light-Emitting Diodes With Metal Oxide Charge Transport Layers," *Nature Photonics*, Vol 2, April 2008.
- [31] K. S. Shin, Y. H. Kim, K. K. Paek, J. H. Park, E. G. Yang, T. S. Kim, J. Y. Kang, And B. K. Ju, "Characterization Of An Integrated Fluorescence-Detection Hybrid Device With Photodiode And Organic Light-Emitting Diode," *Ieee Electron Device Letters*, Vol. 27, Pp. 746-748, 2006.
- [32] S. Khalfallah, C. Gorecki, J. Podlecki, M. Nishioka, H. Kawakatsu, And Y. Arakawa, "Wet-Etching Fabrication Of Multilayer Gaalas/Gaas Microtips For Scanning Near-Field Optical Microscopy," *Applied Physics A: Materials Science & Processing*, Vol. 71, Pp. 223-225, 2000.
- [33] O. Hofmann, X. Wang, A. Cornwell, S. Beecher, A. Raja, D. D. C. Bradley, A. J. Demello, And J. C. Demello, "Monolithically Integrated Dye-Doped Pdms Longpass Filters For Disposable On-Chip Fluorescence Detection," *Lab On A Chip*, Vol. 6, Pp. 981-987, 2006.
- [34] M. F. Garcia-Parajo, J. A. Veerman, S. J. T. Van Noort, B. G. De Grooth, J. Greve, And N. F. Van Hulst, "Near-Field Optical Microscopy For Dna Studies At The Single Molecular Level," *Bioimaging*, Vol. 6, Pp. 43-53, 1998.
- [35] B. Yao, G. Luo, L. Wang, Y. Gao, G. Lei, K. Ren, L. Chen, Y. Wang, Y. Hu, And Y. Qiu, "A Microfluidic Device Using A Green Organic Light Emitting Diode As An Integrated Excitation Source," *Lab On A Chip*, Vol. 5, Pp. 1041-1047, 2005.
- [36] V. Savvate'Ev, Z. Chen-Esterlit, J. W. Aylott, B. Choudhury, C. H. Kim, L. Zou, J. H. Friedl, R. Shinar, J. Shinar, And R. Kopelman, "Integrated Organic Light Emitting Device/Fluorescence-Based Chemical Sensors," *Applied Physics Letters*, Vol. 81, P. 4652, 2002.
- [37] S. Camou, M. Kitamura, G. Jean-Philippe, F. Hiroyuki, A. Yasuhiko, And F. Teruo, "Organic Light Emitting Device As A Fluorescence Spectroscopy'S Light Source : One Step Towards The Lab-On-A-Chip Device," 2003.
- [38] M. Agathocleous, W. A. Harris, "Metabolism In Physiological Cell Proliferation And Differentiation", *Trends In Cell Biology*, 484-492, 05 June 2013.
- [39] N. Guo, L. Zeng., L. Wu," A Method Based On Multispectral Imaging Technique For White Blood Cell Segmentation", *Computers In Biology And Medicine* 37 (2006) 70 – 76
- [40] Schubert, E. F., Gessmann, T. And Kim, J. K. 2005. Light Emitting Diodes. *Kirk-Othmer Encyclopedia Of Chemical Technology*.
- [41] A.Gopal, "Multicolor Colloidal Quantum Dot Based Inorganic Light Emitting Diode on Silicon: Design, Fabrication and Biomedical Applications" University of Texas, Austin, Dec. 2010.

- [42] H. H. Kim, T. M. Miller, E. H. Westerwick, Y. O. Kim, E. W. Kwock, M. D. Morris, And M. Cerullo, "Silicon Compatible Organic Light Emitting Diode," *Journal Of Lightwave Technology*, Vol. 12, Pp. 2107-2113, 1994.
- [43] [Http://En.Wikipedia.Org/Wiki/Oleds](http://en.wikipedia.org/wiki/OLEDs).
- [44] A. P. Alivisatos, "Semiconductor Clusters, Nanocrystals, And Quantum Dots," *Science*, Vol. 271, P. 933, 1996
- [45] K. Hoshino, A. Gopal, D. Ostrowski, L. Rozanski, R. Patel, A. Heitsch, B.Korgel, D. Vandebout, And X. J. Zhang, "Single Monolayer Nanocrystal Led On Probe Tip For Near-Field Molecular Imaging And Patterning," Presented At International Conference On Micro-Electro-Mechanical Systems (Mems '08), Arizona, Usa, 2008.
- [46] D. Bimberg, M. Grundmann, And N. N. Ledentsov, *Quantum Dot Heterostructures*: Wiley, 1999.
- [47] B. O. Dabbousi, J. Rodriguez-Viejo, F. V. Mikulec, J. R. Heine, H. Mattoussi, R. Ober, K. F. Jensen, And M. G. Bawendi, "(Cdse) Zns Core-Shell Quantum Dots: Synthesis And Characterization Of A Size Series Of Highly Luminescent Nanocrystallites," *Journal Of Physical Chemistry B*, Vol. 101, Pp. 9463-9475, 1997.
- [48] S. Coe-Sullivan, J. S. Steckel, W. K. Woo, M. G. Bawendi, And V. Bulovic, "Large-Area Ordered Quantum-Dot Monolayers Via Phase Separation During Spincasting," *Advanced Functional Materials*, Vol. 15, Pp. 1117-1124, 2005.
- [49] J. Zhao, J. A. Bardecker, A. M. Munro, M. S. Liu, Y. Niu, I. K. Ding, J. Luo, B. Chen, K. Y. J. Alex, And D. S. Ginger, "Efficient Cdse/Cds Quantum Dot Lightemitting Diodes Using A Thermally Polymerized Hole Transport Layer," *Nano Letters*, Vol. 6, Pp. 463-467, 2006.
- [50] M. Achermann, M. A. Petruska, D. D. Koleske, M. H. Crawford, And V. I. Klimov, "Nanocrystal-Based Light-Emitting Diodes Utilizing High-Efficiency Nonradiative Energy Transfer For Color Conversion," *Nano Letters*, Vol. 6, Pp. 1396-1400, 2006.
- [51] V. Santhanam And R. P. Andres, "Microcontact Printing Of Uniform Nanoparticle Arrays," *Nano Letters*, Vol. 4, Pp. 41-44, 2004.
- [52] V. Santhanam, J. Liu, R. Agarwal, And R. P. Andres, "Self-Assembly Of Uniform Monolayer Arrays Of Nanoparticles," *Langmuir*, Vol. 19, Pp. 7881-7887, 2003.
- [53] J. S. Steckel, P. Snee, S. Coe-Sullivan, J. P. Zimmer, J. E. Halpert, P. Anikeeva, L. A. Kim, V. Bulovic, And M. G. Bawendi, "Color-Saturated Green-Emitting Qdleds," *Angewandte Chemie*, Vol. 118, Pp. 5928-5931, 2006.
- [54] A. Rizzo, M. Mazzeo, M. Palumbo, G. Lerario, S. D'Amone, R. Cingolani, And G. Gigli, "Hybrid Light-Emitting Diodes From Microcontact-Printing Double-Transfer Of Colloidal Semiconductor Cdse/Zns Quantum Dots Onto Organic Layers," *Advanced Materials*, Vol. 20, Pp. 1886-1891, 2008.

- [55] J. Yu, J. Chen, H. Huang, M. Bawendi, And V. Bulovic, "Microcontact Printing Of Quantum-Dot Leds Using An Inkjet-Assisted Patterning Method."
- [56] C. Y. Kuan, J. M. Chou, C. Leu, And M. H. Hon, "Sol–Gel-Derived ZnO Coating With Nanopatterns Fabricated By Nanoimprinting," *Journal Of The American Ceramic Society*, Vol. 91, Pp. 3160-3166, 2008.
- [57] J.-M. Caruge, J. E. Halpert, V. Bulovic & M. G. Bawendi, "NiO As An Inorganic Hole-Transporting Layer In Quantum-Dot Light Emitting Devices", *Nano Lett.* 6, 2991–2994 (2006).
- [58] M. Gulen, G. Yildirim, S. Bal, A. Varilci, I. Belenli, M. Oz, "Role Of Annealing Temperature On Microstructural And Electro-Optical Properties Of ITO Films Produced By Sputtering", *J Mater Sci: Mater Electron*, Doi 10.1007/S10854-012-0768-8
- [59] G. Chumanov, K. Sokolov, B. W. Gregory, And T. M. Cotton, "Colloidal Metal Films As A Substrate For Surface-Enhanced Spectroscopy," *The Journal Of Physical Chemistry*, Vol. 99, Pp. 9466-9471, 1995.
- [60] H. O. Finklea, "Of Thiols And Related Molecules On Electrodes," *Electroanalytical Chemistry: A Series Of Advances: Volume 19*, P. 109, 1996.
- [61] T. P. Bigioni, X. M. Lin, T. T. Nguyen, E. I. Corwin, T. A. Witten, And H. M. Jaeger, "Kinetically Driven Self Assembly Of Highly Ordered Nanoparticle Monolayers," *Nature Materials*, Vol. 5, Pp. 265-270, 2006.
- [62] Y. Cui, Q. Wei, H. Park, And C. M. Lieber, "Nanowire Nanosensors For Highly Sensitive And Selective Detection Of Biological And Chemical Species," *Science*, Vol.293, P. 1289, 2001.
- [63] <http://www.dowcorning.com/>
- [64] J. R. Anderson, D. T. Chiu, R. J. Jackman, O. Cherniavskaya, J. C. McDonald, H. Wu, S. H. Whitesides, And G. M. Whitesides, "Fabrication Of Topologically Complex Three-Dimensional Microfluidic Systems In PDMS By Rapid Prototyping," *Anal. Chem*, Vol. 72, Pp. 3158-3164, 2000.
- [65] A.A. Al-Ghamdia, W.E. Mahmouda, S.J. Yaghmoura, F.M. Al-Marzoukia, "Structure and optical properties of nanocrystalline NiO thin film synthesized by sol–gel spin-coating method", *J. Alloys and Compounds*, Volume 486, Issues 1–2, Pages 9–13, 3 November 2009
- [66] Kwak, J., Bae, W.K., Lee, D., Park, I., Lim, J., Et. Al. "Bright And Efficient Full-Color Colloidal Quantum Dot Light-Emitting Diodes Using An Inverted Device Structure", *Nano Lett.* 2012, 12, 2362-2366.
- [67] A.I. Zhmakin, "Enhancement Of Light Extraction From Light Emitting Diodes", *Physics Reports* 498 (2011) 189–241
- [68] R. W. Wood, "On A Remarkable Case Of Uneven Distribution Of Light In A Diffraction Grating Spectrum," *Proceedings Of The Physical Society Of London* 18 (1), 269 (1902).

- [69] L. Rayleigh, "Iii. Note On The Remarkable Case Of Diffraction Spectra Described By Prof. Wood," *Philosophical Magazine Series 6* 14 (79), 60-65 (1907).
- [70] L. Rayleigh, "On The Dynamical Theory Of Gratings," *Proceedings Of The Royal Society Of London. Series A, Containing Papers Of A Mathematical And Physical Character* 79 (532), 399-416 (1907).
- [71] U. Fano, "The Theory Of Anomalous Diffraction Gratings And Of Quasi-Stationary Waves On Metallic Surfaces (Sommerfeld'S Waves)," *J. Opt. Soc. Am.* 31 (3), 213-222 (1941).
- [72] A. Hessel And A. A. Oliner, "A New Theory Of Wood'S Anomalies On Optical Gratings," *Appl. Opt.* 4 (10), 1275-1297 (1965).
- [73] M. Neviere, R. Petit, And M. Cadilhac, "About The Theory Of Optical Grating Coupler-Waveguide Systems," *Opt. Commun.* 8 (2), 113-117 (1973).
- [74] S. Peng And G. M. Morris, "Resonant Scattering From Two-Dimensional Gratings," *J. Opt. Soc. Am. A* 13 (5), 993-1005 (1996).
- [75] R. Taubert, D. Dregely, T. Stroucken, A. Christ, And H. Giessen, "Octave-Wide Photonic Band Gap In Three-Dimensional Plasmonic Bragg Structures And Limitations Of Radiative Coupling," *Nat. Commun.* 3, 691 (2012).
- [76] W. Zhou And T. W. Odom, "Tunable Subradiant Lattice Plasmons By Out-Of-Plane Dipolar Interactions," *Nat. Nano.* 6 (7), 423-427 (2011).
- [77] B. Augu   And W. L. Barnes, "Collective Resonances In Gold Nanoparticle Arrays," *Phy. Rev. Lett.* 101 (14), 143902 (2008).
- [78] V. G. Kravets, F. Schedin, And A. N. Grigorenko, "Extremely Narrow Plasmon Resonances Based On Diffraction Coupling Of Localized Plasmons In Arrays Of Metallic Nanoparticles," *Physical Review Letters* 101 (8), 087403 (2008).
- [79] R. Adato, A. A. Yanik, C.-H. Wu, G. Shvets, And H. Altug, "Radiative Engineering Of Plasmon Lifetimes In Embedded Nanoantenna Arrays," *Opt. Express* 18 (5), 4526-4537 (2010).
- [80] R. Cailleau, M. Oliv  , And Q. V. J. Cruciger, "Long-Term Human Breast Carcinoma Cell Lines Of Metastatic Origin: Preliminary Characterization," *In Vitro Cellular & Developmental Biology-Plant*, Vol. 14, Pp. 911-915, 1978.
- [81] J. E. Price, "Metastasis From Human Breast Cancer Cell Lines," *Breast Cancer Research And Treatment*, Vol. 39, Pp. 93-102, 1996.
- [82] J. E. Price, A. Polyzos, R. Dan Zhang, And L. M. Daniels, "Tumorigenicity And Metastasis Of Human Breast Carcinoma Cell Lines In Nude Mice," *Cancer Research*, Vol. 50, P. 717, 1990.
- [83] J. E. Price And R. D. Zhang, "Studies Of Human Breast Cancer Metastasis Using Nude Mice," *Cancer And Metastasis Reviews*, Vol. 8, Pp. 285-297, 1990.
- [84] J. V. Dacie, *The Haemolytic Anaemias*: Churchill Livingstone Edinburgh, 1992.